

Chapter III

Molecule-Like Structures in Nuclear System

Hisashi HORIUCHI, Kiyomi IKEDA* and Yasuyuki SUZUKI*

*Research Institute for Fundamental Physics, Kyoto University*** Department of Physics, Niigata University*

(Received December 15, 1972)

Contents

- §1 Introduction—*Development of the molecular viewpoint*—
- §2 Confirmation of the di-molecule-like structures of α - ^{12}C and α - ^{16}O through their decay widths
 - 2.1 Di-molecule-like structure and decay width
 - 2.2 The reduced width and its evaluational method
 - 2.3 The reduced widths obtained from the various kinds of model wave functions
 - 2.4 Comparison with experiments and summary
- §3 Inversion doublet and the structure of $K=0^+$ band in ^{16}O and ^{20}Ne
 - 3.1 The indication of the experimental gap energies
 - 3.2 The estimation of the gap energy with the molecular model
 - 3.3 Microscopic studies on the gap energy
 - 3.4 Summary and further problem
- §4 Alpha-chain structures in nuclei
 - 4.1 Characteristic properties of the noted levels in ^{12}C and ^{16}O
 - (A) The two anomalous levels in ^{12}C
 - (B) The anomalous rotational band in ^{16}O
 - 4.2 Study of the energetic properties with the alpha-particle model
 - 4.3 $n\alpha$ -chain structures
- §5 Multi-molecular structures with the linear chain configuration
 - 5.1 The interactions between an alpha-particle and a residual core in the contact region
 - 5.2 The energies of the three-and four-body linear chain structures
 - 5.3 The stabilities of the linear chain structures
 - 5.4 Prolongation of the linear molecule-like structure due to the Coulomb interaction
- §6 Summary on the molecule-like structures

Appendices

1. Computational method of the matrix elements necessary for the evaluation of the reduced width from the model wave function
2. Correction factor for the normalization constant

§1. Introduction

—Development of the molecular viewpoint—

The nuclei composed of protons and neutrons are the bound or quasi-bound system with the various aspects of the structures. In such a complex nuclear system, there is a group of the states with the structure polarized strongly into subunit nuclear clusters which can be defined as molecule-like structures. A typical example of such structures can be found in the nucleus of ${}^8\text{Be}$ as of two alpha-particles, which is almost only one example realized in the ground states of nuclei. Naturally the studies of the molecule-like structures in nuclei were initiated from this nucleus of ${}^8\text{Be}$, (as summarized in Chap. II) and then the studies of ${}^8\text{Be}$ gave the basis for the developments of the researches concerning the other complex molecule-like structures in nuclear system.

As mentioned in the previous chapter, the direct empirical evidences by which the ground rotational band of ${}^8\text{Be}$ can be understood to have the molecule-like intrinsic structure of two alpha-particles are briefly summarized as follows:

- i) There appears the rotational spectrum upon the ground state ($I=0^+$, 2^+ , 4^+ , (6^+) , (8^+) , ...) and this band has a large moment of inertia expected from the well separated two alpha particles with the mean inter- α distance about 4 fm.
- ii) The alpha decay widths from these levels are large enough to indicate that there are two alpha-particles in these quasi-bound states for almost whole lifetime.

To form such a molecule-like structure in nuclear system as in ${}^8\text{Be}$ two conditions are necessary at least. First one is that the constituent such as an alpha-particle is strongly bound in the isolated system. The other is that the interactions between subunit nuclei are weak enough. For ${}^8\text{Be}$, the constituents (alpha-particles) have a large binding energy and are so stiff as to show no intrinsic excitations in the energy region up to about 20 MeV. The large binding and the stiffness of the alpha-particle are known to come from the character of original nuclear interactions, that is, nuclear forces favour the highest orbital symmetry due to the strong attractive force in the relative 1S and 3S states. (For the latter the contribution of the strong tensor forces is very large.) The effective interaction between alpha-particles as the composite systems has been also shown to be understood

theoretically on the bases of the two-body nuclear interactions and the Pauli principle. It can be described by an energy independent potential with innre strong repulsive core, outer weak attractive part (about 10 MeV) with the angular momentum dependence and the tail of Coulomb potential. Such a kind of potential with the similar form to the Morse potential has been known to reproduce the phase shifts of the elastic scattering between alpha-particles up to about 60 MeV (C. M.). Therefore we can understand that the two important factors to form the molecule-like structure in nuclei are derived as the natural consequences of the action of the two-body nuclear forces and the Pauli principle in the system of ${}^8\text{Be}$.

The deep understanding of ${}^8\text{Be}$ as α - α led to the thought^{1),2)} that the molecule-like structure of α - α is not an exception but only one of typical examples in nuclear system. Actually the other typical examples appeared in the levels belonging to the rotational bands with $K=0^-$ in ${}^{16}\text{O}$ and ${}^{20}\text{Ne}$, which are based upon the 1^- states at 9.60 MeV in ${}^{16}\text{O}$ and at 5.79 MeV in ${}^{20}\text{Ne}$. The levels of these bands are known up to 7^- and their decay properties are also well known.^{3),4),5)} The most characteristic property of these levels shows up in the alpha decay widths from which the probability of a separated alpha-particle in surface region is known to be commonly about unity. Then we can naturally understand the intrinsic structure of these rotational bands as α -C for ${}^{16}\text{O}$ and α -O for ${}^{20}\text{Ne}$ and that an alpha-particle moves grazing around the core with the corresponding angular momentum of the level. The moments of inertia of these rotational bands have the magnitude of the rigid di-molecular case that an alpha-particle contacts with the corresponding core particle (C or O) at the surface. Therefore we can understand consistently the magnitudes of the alpha decay width and the moments of inertia from the molecular point of view.

Existence of the negative parity band with the intrinsic structure composed of the different subunit nuclei (α -C and α -O) suggests the possible existence of the positive parity rotational band with the similar intrinsic structure in ${}^{16}\text{O}$ and ${}^{20}\text{Ne}$. If there is such a positive rotational band, both rotational bands with $K=0^\pm$ can be understood as the so-called "inversion doublet"¹¹⁾ with the same intrinsic structure and then the positive parity band is expected to appear below the negative rotational band by the small gap energy. Really the rotational band upon the "mysterious zero plus state" at 6.06 MeV in ${}^{16}\text{O}$ corresponds to such a kind of positive parity rotational band and the ground rotational band in ${}^{20}\text{Ne}$ is considered to correspond to it. For the positive parity band in ${}^{16}\text{O}$, the interpretation as the "inversion doublet" is also supported from the successful understanding of the level structures by the weak coupling model.⁶⁾

Recognition of the di-molecule-like structures of α -C and α -O next to the structure of α - α stimulated to establish the general viewpoint of the molecule-like structures in the nuclear system, especially of the self-conjugate

$4n$ -nuclei. An aid of such a systematical point of view was brought by the considerations about the alpha-chain structures. At very early time, Morinaga⁷⁾ proposed the idea of such structures in attempt to give a general account for the characteristic excited 0^+ levels and closely excited 2^+ levels, pointing out that the structure with highly deformed configuration or the alpha-chain-like configuration might arise after the rearrangements of the whole nucleus, when so many particles as four particles are excited from the closed core. The idea was afterward applied to the interpretation of the second excited zero plus state at 7.66 MeV and a broad structure with 2^+ around 10 MeV in ^{12}C .⁸⁾ Five years ago an important experimental result concerning the four alpha-chain structure in ^{16}O was reported by Chevallier et al.⁹⁾ that an anomalous rotational band with a **very** large moment of inertia, which is just expected from the 4α -chain configuration, has been found in the higher excited energy region (about 17 MeV) than considered before.⁷⁾ The analysis of the decay widths of these levels in ^{12}C and ^{16}O has given the conclusions¹⁰⁾ that the levels in ^{12}C are characterized by the aggregation of alpha-particles with no definite configuration (not linear one) and that the levels in ^{16}O are possibly characterized by the linear chain structure.

Although only a few examples of the molecule-like structures were known before 1967, it was noted as a common fact of all these examples in the self-conjugate $4n$ -nuclei that the levels with the molecule-like structures are observed above the threshold energy^{†)} of the fission into the constituent subunit nuclei. The deviation energies of the band head from the threshold are listed up as 0.09 MeV for α - α of ^8Be , 2.0 MeV and 0.7 MeV for the negative parity bands of $^{16}\text{O}^*$ (α -C) and $^{20}\text{Ne}^*$ (α -O) and 0.37 MeV and 2.3 MeV for $^{12}\text{C}^*$ and for the anomalous rotational band in ^{16}O , respectively. From the dynamical point of view of the structure change, this common fact was pointed out to be one of the most important necessary conditions for the formation of the molecule-like structure in the nuclear system. This empirical rule has been, therefore, recognized as "*the threshold energy rule for the formation of the molecule-like structures in light nuclei.*"²⁾ In the following we recapitulate the physical meanings of this threshold rule as was discussed in Ref. 2).

The molecular structure in nuclear system has intrinsically the meaning as a relative concept, since the interactions between the subunit nuclei are the same nuclear interactions as those acting between the nucleons in a subunit nucleus. However, the complex character of the nuclear interactions causes the varieties of their actions in the two kinds of Fermion system, which bring about the possibility of the special existing style like the molecular structure which is distinctly deviated from the shell model aspect.

^{†)} The clustering levels in light nuclei have been often observed also near the threshold energy for decays.^{11),12)}

If the molecule-like structure is formed, the actions of the nuclear interactions are dominated by internally strong but externally (relatively) weak character. But when the structure is changed into the other structure (shell-like one), the actions become different. The meaning of the threshold energy rule has to be sought in such a linked character between the structure and the actions of the interactions in the self-sustained nuclear system.

To consider the meaning of the threshold energy rule we assume at first that the molecule-like structure exists only near or at a little higher energy than the threshold energy for the fission into the relevant subunit nuclei. This assumption includes automatically the weakness of the interactions between the subunit nuclei. Simultaneously it means that the wave function for the relative motions stretches largely in the outside region where the Pauli principle between nucleons belonging to the different subunits plays no role effectively, and then the interplay between the molecule-like structure and other structures is expected to be small. If the interplay with different structures are not so weak, the cooperative action of the interactions and the Pauli principle between the subunit nuclei can easily induce the rearrangement from or to the molecule-like structure. In other words, if the interactions between the subunit nuclei were not so weak, they would not be tightly bound with each other conserving their identity but the rearrangement would rather take place. If not so, there arises the contradiction in the actual situation; for example, the ground state of ^{16}O which has the typical closed shell character would consist of an alpha-particle and a Carbon. Thus "*the threshold energy rule*" means that the molecule-like structure is realized only for the case that the nuclear system satisfies the optimum condition^{*)} to avoid the collapse of the subunit nuclei. Once the molecule-like structure is formed, the weak attractive interactions between the subunit nuclei play the role mainly to keep them in a quasi-bound state, together with the outside Coulomb force and centrifugal potential, and also the Pauli principle, as was discussed in Chap. II, bears the role as if to act against the dissolution in the inside region.

As the natural consequence of the threshold energy rule, the deviation energy of the noted levels from the threshold is considered to reflect the degree of the polarization into the relevant molecule-like structure. Actually the ground rotational band of ^8Be , the negative parity bands in ^{16}O and ^{20}Ne and also the anomalous rotational band which is considered to have the

^{*)} Since we have so far considered the molecule-like structures in light nuclei, we have not taken into account explicitly the effects of the Coulomb (and centrifugal) forces on the consideration of the threshold energy rule. When the heavy elements appear in the molecule-like structures as the subunit nuclei, it should be meant by the threshold energy rule that the molecule-like structure would be realized near the top of Coulomb (plus centrifugal) barrier for the fission into the relevant subunit nuclei. We know that the molecular resonances,^{46),48)} observed by C+C and O+O scatterings accord with this rule.

4α -chain structure are the cases with the well-grown molecule-like structures, all of which are the quasi-bound states with the larger excitation energy than the threshold energy for the decays into the relevant subunit nuclei. The positive parity bands in ^{16}O and ^{20}Ne are the cases with the smaller energy than the threshold energy. For the case of ^{16}O , the deviation of the excitation energy, $\delta E_0 (=E_0 - E_{\text{th}})$, is about -1.1 MeV and for the case of ^{20}Ne about -4.7 MeV. When we compare these deviations with the separation energy of an alpha-particle from the ground states with the shell structure (about 7 MeV), the deviation for ^{16}O is not considered to be so large but the deviation for ^{20}Ne to be appreciably large. Thus it has been pointed out that the structure in the ground band of ^{20}Ne has a certain transient character from a di-molecular structure (α -O) to a shell-like structure.

The other observable quantity which has the strong correlation with the degree of the polarization or of the dissolution has been pointed out to be the gap energy between two band heads with the negative and positive parities: when the gap energy is small the molecule-like structure is very

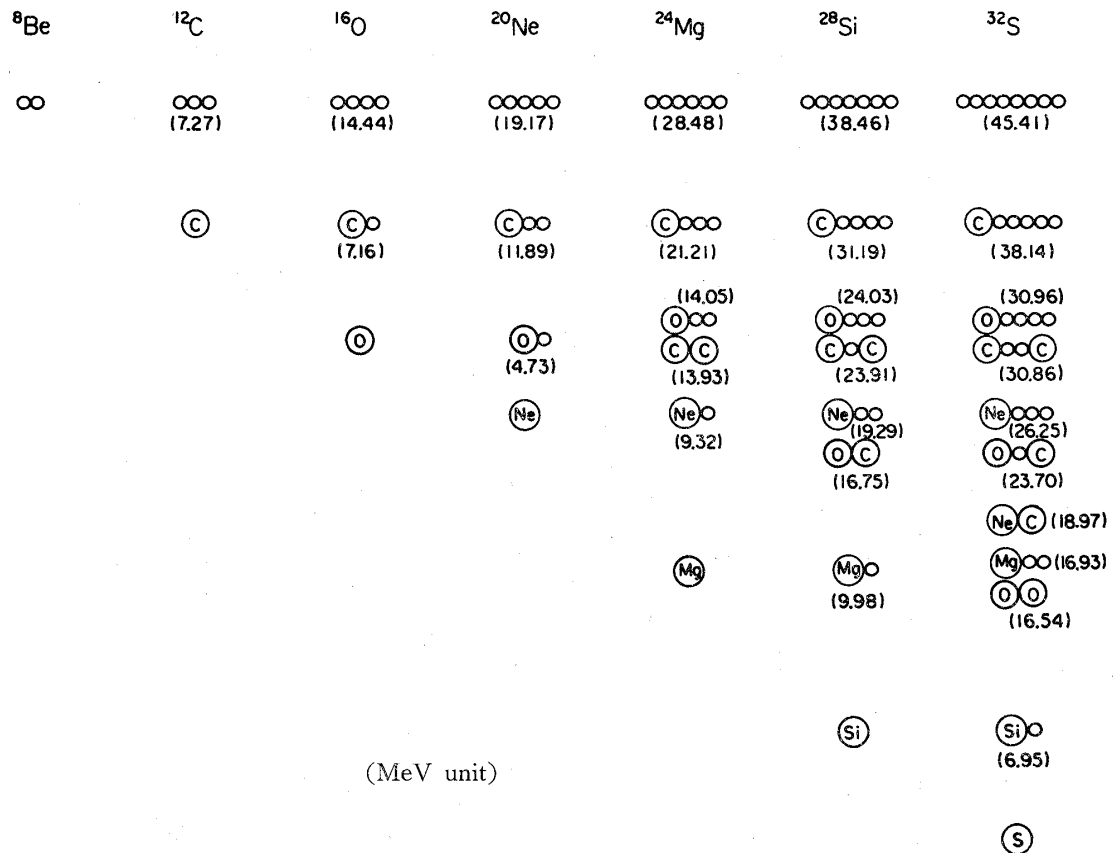


Fig. 1-1. Diagram of the subunit of the possible molecule-like structures as the function of the energy and the mass number, where the threshold energy for the decay into subunit nuclei is written in the parentheses. (The energies of the multi-molecular structures with the linear configuration are predicted in §§4 and 5 for some cases listed in this figure.)

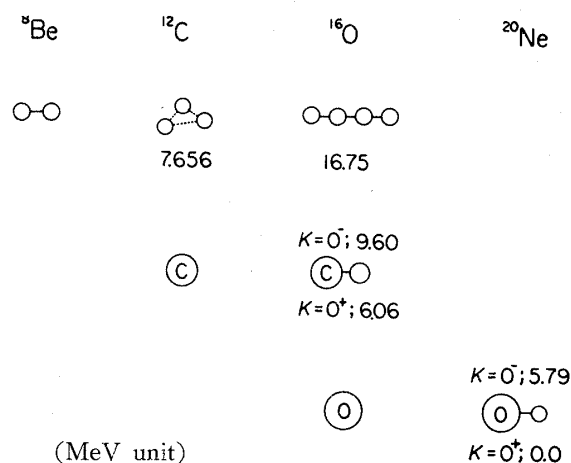


Fig. 1.2. Experimental systematics of the states with the molecule-like structures, which will be discussed in the later sections.

clear and when it is large the molecule-like structure is not clear. The experimental values of the gap energy are 3.4 MeV for the case of ${}^{16}\text{O}$ and 5.2 MeV for ${}^{20}\text{Ne}$. Therefore the difference in these values for two cases shows the consistency with the conclusion obtained from the deviation energy of δE_0 in the comparison of the case of ${}^{16}\text{O}$ with the case of ${}^{20}\text{Ne}$.

As summarized in the threshold energy rule the molecule-like structures are realized systematically near or above the threshold energy for the decay into the relevant subunit nuclei, e. g., $\alpha\text{-}\alpha$, $\alpha\text{-C}$, $\alpha\text{-O}$ and $\alpha\text{-chain-like}$ structures. To show such systematics clearly, the possible set of the subunits of molecule-like structures were represented in a figure as the function of the excitation energy and mass number.²⁾ This diagram for the molecule-like structures shown in Fig. 1.1 (which is referred to as the Ikeda diagram in the other chapters) has been very useful not only to know the systematics for the observed ones (which are shown in Fig. 1.2) but also to suppose the possible existence of the unobserved ones.

In the self-conjugate $4n$ -nuclei, the alpha-particle is the fundamental unit for the molecule-like structures. Then the molecule-like structures consisting of n -alpha-particles give the energetically upper limit in the diagram. The lower limit is of course the "ground-state series" with the familiar shell-like structures which may be called the zeroth order molecule-like structure. From the molecular point of view, the series of the alpha-particle aggregation in the upper limit can be taken as a good standard from which the various kinds of molecule-like structures can be generated. Then the diagram can be also read as the processes of the alpha-particle dissolutions from the higher order molecule-like structures to the lower order ones. Inversely the changes from the lower limit of the ground state series to the upper limit correspond to the processes of the alpha-particle release or the other $4n$ -subunit nucleus release. The paths of the dissolution or the particle release

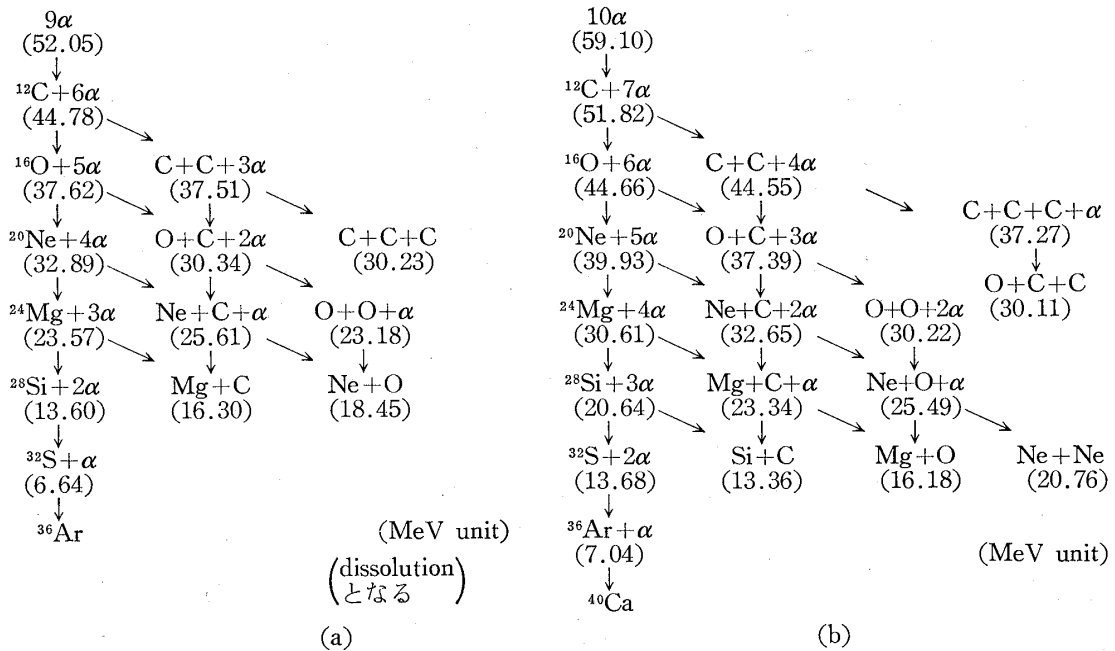


Fig. 1.3. The paths of the alpha-particle dissolution in the case of the systems of $A=36$ (a) and 40 (b) along which all the kinds of possible molecule-like structures are generated.

have many branches along which the various kinds of molecule-like structures are hypothetically considered. We illustrate in Fig. 1.3 the path of the dissolution for the cases of 9α and 10α . This figure should be noted to show also the relation between the different kinds of molecule-like structures. The energies listed in the figures are the values necessary for the separation into the constituent subunits from the ground state, which are the same as the threshold energy for the fission into the subunits.

For the cases of the di-molecular structure the loosely bound structures of the two subunits are automatically of the linear chain configuration. However, for the cases of the multi-molecular structure, the loosely bound structures do not necessarily mean the structures with the linear chain configuration. It should be noted for such cases that the linear chain configuration means to put a restriction on the configuration. We often give, however, the special attention to the linear chain configuration, because the Coulomb and centrifugal forces favour this configuration and the interplay between the linear chain structure and the other structures is considered to be the smallest.

All kinds of molecule-like structures in the region of $8 \leq A \leq 20$ have been already recognized as shown in Fig. 1.2. Such an actual situation has led us to establish the strategy for the understanding about the molecule-like structures in the complex nuclear system. The first step of the strategy is to obtain a deeper understanding of the observed phenomena from which the common fundamental features are drawn. The second step is to develop the studies on more rich phenomena indicating the molecule-like structures

on the basis obtained in the first step. The development in the second step will further extend the domain for the studies of the first step and then the development in the second step will be stimulated. Such cyclic processes of the studies will further develop the recognition concerning "the molecular aspect" in the complex nuclear system. The results at the present stage of the studies according to the above strategy are summarized in this chapter. The first half of this chapter (§§2 and 3) is devoted to the deep understanding of the experimental results which have driven us to the considerations of the molecule-like structures. The second half (§§4 and 5) is devoted to further developments of the theoretical studies about the multi-molecule-like structures.

In §2, the quantitative analyses of the decay widths from the levels with the di-molecule-like intrinsic structures are given, by assuming the various kinds of model wave functions for the intrinsic states, in order to confirm that the molecular point of view stands on the firm basis. In §3, we examine the intrinsic structures of the positive parity rotational band which are interpreted as a part of the inversion doublet from the molecular viewpoint. The positive parity rotational bands involve the information about the transient character from the di-molecule-like structure to the shell-like structure. Such an interpretation of the transient characters is discussed qualitatively by using the semi-classical model and the microscopic model.

In §4, the studies of the alpha-chain series are developed on the basis of the alpha-particle model where we use the parameters determined by the properties of the nucleus, ^8Be . First part of §4 gives the summary of the studies for the levels with the 3α - and 4α -chain-like configurations: The contents are i) the theoretical analysis of the decay widths from the noted levels (§4.1) and ii) the interpretations of their structures with use of the alpha-particle model (§4.2). In these studies, the basic understanding has been obtained for the properties of these levels. In the second part (§4.3), the studies for the general case of the $n\alpha$ -chain structures ($n \geq 5$) are developed with the same assumptions as in §4.2 and the excitation energies of the $n\alpha$ -chain configurations are predicted.

The studies on the di-molecule-like structures (α -C and α -O) and on the $n\alpha$ -chain structures lead us to the problems of the more general multi-molecule-like structures with the linear chain configurations. In §5, we try to discuss about the molecule-like structures in which the heavy elements (C or O) are connected by an alpha-particle or alpha-chains.

In the last section (§6), the summarized discussions are given together with the discussions of the further problems on the molecule-like structures.

§2. Confirmation of the di-molecule-like structures of α - ^{12}C and α - ^{16}O through their decay widths

2.1 Di-molecule-like structure and decay width

It has been considered that the decay width is one of the most important physical quantities to identify the molecule-like structure, especially di-molecular one, because the value of the decay width directly reflects the probability of finding out the fragment clusters in the surface region of the parent nucleus. In fact, all the ground band levels of ^8Be are quasi-bound and have large α reduced widths, by which the di-molecular structure of two α -particles is strongly supported. (See Chapter II.)

In the nuclei of ^{16}O and ^{20}Ne , the rotational band with $K=0^-$ is known to exist at a little above the each threshold energy of α decay. All the levels of these two rotational bands have the very large α decay reduced widths which can be obtained by taking the picture that an α -particle grazes around the residual core. We have therefore understood that these negative parity bands have the molecule-like intrinsic structures of α - ^{12}C and α - ^{16}O . These molecule-like structures are clearly different from the usual shell structure. It has been, however, generally prevailing that these levels of peculiar character can be interpreted in the framework of the SU_3 model. Especially, the theoretical result that some type of simple cluster model wave function is an alternative description of the SU_3 model wave function¹³⁾, has been regarded as one of the important reasonings for the interpretations with the SU_3 model.

Our task of this section is therefore to confirm that the difference between the di-molecule-like structure and the shell-like structure is distinctly reflected into the magnitude of the decay width and that such large reduced widths as in ^8Be , ^{16}O and ^{20}Ne can be duely understood only when we assume the molecule-like structures for these rotational levels.

To do the task, the decay widths are quantitatively studied by adopting the several kinds of model wave functions as the representatives of the molecule-like structure and of the shell-like structure. The model wave functions which are worked out for the structural analysis have usually the bad tails. It is necessary therefore to amend these ill tails in order to obtain the theoretical values of the α widths. In the evaluations of the α widths in this section we have utilized the devices which have been developed for the improvement of the tail of the radial form factor of the direct reaction such as stripping or pick-up. Thus we have become able to compare the experimental reduced widths with the theoretical ones, and to understand the quantitative difference of the reduced widths between the two kinds of structures.

In the following subsections we summarize the results of the theoretical

analyses¹⁴⁾ done for the ground band levels of ^8Be as well as for the $K=0^-$ band levels of ^{16}O and ^{20}Ne . From these results we confirm that the molecule-like structures of α - ^{12}C and α - ^{16}O are surely realized as the actual intrinsic structure of the negative parity bands in ^{16}O and ^{20}Ne , respectively. Then it is known that the molecular aspect can be developed on the firm basis.

2.2 The reduced width and its evaluational method

We show first of all in Table II-1 the experimental values of the α decay widths of the above cited levels of ^8Be , ^{16}O and ^{20}Ne . The quantity of θ_L^2 in the Table is defined as the ratios of the reduced widths, $\gamma_L^2(a)$, to the Wigner limit value $\gamma_W^2(a)$. Then the reduced width in unit of the Wigner limit value, θ_L^2 , is derived from the experimental decay width of Γ_L according to the following formulae;

$$\begin{aligned}\Gamma_L &= 2P_L(a)\gamma_L^2(a), \\ P_L(a) &= \frac{ka}{F_L^2(ka) + G_L^2(ka)}, \\ \gamma_L^2(a) &= \theta_L^2(a)\gamma_W^2(a), \\ \gamma_W^2(a) &= \frac{3\hbar^2}{2\mu a^2},\end{aligned}\tag{2.1}$$

Table II-1. Experimental α -particle decay widths Γ_α and their reduced widths θ_α^2 for suitable channel radii (a).

(a) ^8Be

J^π	Ex (MeV)	$\Gamma_\alpha(\text{MeV})$	θ_α^2	$a(\text{fm})$	Ref
0^+	0	$6.8 \pm 0.6 (4.5 \pm 3) \times 10^{-6}$	$0.20 (0.15 \pm 0.1)$	5.7	19(21)
2^+	2.90 ± 0.03	$1.45 \pm 0.06 (2)$	$0.52 (0.70)$	5.0	19(21)
4^+	11.4 ± 0.3	$\sim 7.0 (6.7)$	$1.07 (0.95)$	4.5	19(21)

(b) ^{16}O

J^π	Ex (MeV)	$\Gamma_\alpha(\text{keV})$	θ_α^2	$a(\text{fm})$	Ref
1^-	9.60	510 ± 60	0.83	5.0	22
3^-	11.63	1200	1.03	5.0	22
5^-	16.9	700	0.25	5.0	22
7^-	21.01	750	0.36	5.0	22

(c) ^{20}Ne

J^π	Ex (MeV)	$\Gamma_\alpha(\text{keV})$	θ_α^2	$a(\text{fm})$	Ref
1^-	5.79	$> 13 \times 10^{-3}$	> 0.54	5.0	5
3^-	7.17	8	0.89	5.0	5
5^-	10.30	150	1.06	5.0	5
7^-	15.43	376	0.79	5.0	4

where k , a and μ are the wave number of the relative motion, the channel radius and the reduced mass, respectively, and F_L and G_L are the regular and irregular Coulomb wave functions, respectively.

The reduced width of θ_L^2 is related with the wave function ϕ_L of the parent nucleus as follows:

$$\theta_L^2(a) = (a^3/3) \cdot y_L^2(a),$$

$$y_L(a) = \frac{1}{\sqrt{1 + \delta_{A-4,4}}} \sqrt{\left(\frac{A}{4}\right)} \langle Y_{L0}(\Omega_r) \phi_0(C) \phi_0(\alpha) | \phi_L \rangle_{r=a}, \quad (2.2)$$

where A is the mass number of the parent nucleus, $\phi_0(C)$ the wave function of the residual core and r and Ω_r the length and the angles of the relative coordinate \mathbf{r} between α and the core.

Therefore our task is to obtain theoretically the reduced width defined in Eq. (2.2) and to compare the theoretical value with the experimental one of Eq. (2.1)

As is seen in the above expression of Eq. (2.2), the calculation of the width requires the knowledge of the wave function in the surface region of the decay channel, core + α . In the usual cases the model wave functions worked out for the structural calculations have a bad behaviour in tails. We are thus forced to improve the tail behaviour of $y_L(a)$ of a given model wave function ϕ_L . When we modify the tail behaviour, we put the demand that the modified tail of $y_L(r)$ should be smoothly connected with the inner part of y_L calculated directly from the model wave function by Eq. (2.2), since the model wave function is assumed to be reliable at least in the inner region.

One of the simplest devices to get the modified tail is to connect smoothly the resonance tail of $G_L(kr)$ with $y_L(r)$ at some point outside the final peak¹⁵⁾ of $y_L(r)$. We call this treatment a separation energy method (hereafter abbreviated as SEM). It should be noticed that this SEM in which the original model wave function is used in the inner region is different from the method which replaces directly the function $y_L(r)$ by the Woods-Saxon wave function with the correct separation (or release) energy.

Another device we adopt here is a Green's function method (GFM) which was developed by Kawai and Yazaki for the calculations of the radial form factor of the stripping or pick-up reactions.¹⁶⁾ According to GFM, $y_L(r)$ is calculated by the following formulae;

$$y_L(r) = \int_0^\infty ds \cdot s^2 \mathcal{G}_L(r, s) Z_L(s),$$

$$Z_L(s) = \frac{1}{\sqrt{1 + \delta_{A-4,4}}} \sqrt{\left(\frac{A}{4}\right)} \langle Y_{L0}(\Omega_r) \phi_0(C) \phi_0(\alpha) | \left(\sum_{\substack{i=1 \sim 4 \\ j=5 \sim A}} V_{ij} - U(r) \right) | \phi_L \rangle_{r=s},$$

$$\mathcal{G}_L(r, s) = -\frac{2\mu k}{\hbar^2} \frac{\hat{F}_L(kr_<)}{kr_<} \frac{u_L^{(+)}(kr_>)}{kr_>},$$

$$u_L^{(+)}(kr) = i\hat{F}_L(kr) + \hat{G}_L(kr), \quad (2.3)$$

where the potential of $U(r)$ between α and the core contains at least the Coulomb potential in the outer region so as to cancel the effect of $\sum V_{ij}$ in this region, while in the inner region it can be chosen arbitrarily in principle. Here the functions of \hat{F}_L and \hat{G}_L are the regular and irregular solutions of the Schrödinger equation with this potential of $U(r)$ with asymptotic forms of $\sin(kr - n \log 2kr - L\pi/2 + \eta_L + \delta_L)$ and $\cos(kr - n \log 2kr - L\pi/2 + \eta_L + \delta_L)$, respectively, where n is the Sommerfeld parameter, η_L the Coulomb phase shift and δ_L the so-called nuclear phase shift due to the nuclear interaction part of $U(r)$. As is seen in Eq. (2.3) only the inner part information of ϕ_L is necessary for the evaluation of $y_L(r)$ due to the short range character of $\sum V_{ij} - U(r)$. The asymptotic form of $y_L(r)$ is clearly ensured by the Green function of \mathcal{Q}_L .*) When y_L is calculated by GFM, we have to impose the condition, as mentioned before, that the obtained y_L nearly agrees in the inner region with the function of Eq. (2.2) which is directly derived by using the original model wave function. This condition is expected to be satisfied if we choose the suitable potential of U in the inner region or we may choose the two-body nuclear interaction part in $\sum V_{ij}$ somewhat arbitrarily in a suitable range so as to satisfy this condition. For, our present purpose is limited to find the modified tail by the reasonable device under the premise that the adopted model gives the inner behaviour of $ry_L(r)$ correctly. As will be seen, the tail obtained by GFM is similar to that by SEM and so we regard that the simple device of SEM is justified by GFM.

2.3 The reduced widths obtained from the various kinds of model wave functions

Using the methods (SEM and GFM), we now study how much difference is there among the reduced widths of the different kinds of models: that is SU_3 , deformed oscillator and cluster models.

First we evaluate the reduced widths of the SU_3 model as a representative**) of the spherical shell model.

The wave functions with (40),^{13),17)} (94) and (90)¹⁸⁾ representations are adopted here for ^8Be , ^{16}O and ^{20}Ne , respectively;

) As is shown in Eq. (2.3), we choose the outgoing wave boundary condition for the Green's function of \mathcal{Q}_L . In our cases the magnitude of F_L/G_L is negligibly very small in the channel radius region. Therefore the functional form of the tail of $y_L(r)$ is practically the same as G_L . When F_L is neglected, the imaginary part of $u_L^{()}$ appears only through $e^{i\delta_L}$ factor. However, since the potential of $U(r)$ can be taken so as to make the phase shift of δ_L small, we can practically neglect the imaginary part of \mathcal{Q}_L .

**) When the oscillator parameters of the two fragment nuclei (α and residual core) are chosen to be the same as that of the parent nucleus, the SU_3 model wave functions (40) and (90) give the largest reduced widths among all the configurations with the same number of total oscillator quanta.

$$\begin{aligned}
\psi_L((40)) &= N_L P_L (000)^4 (001)^4, \\
\psi_L((94)) &= N'_L P_L \left\{ \frac{\sqrt{3}}{2} [a^+(101)a(100)]_{[4]} - \frac{1}{2} [a^+(003)a(002)]_{[4]} \right\} \\
&\quad \times (000)^4 (100)^4 (001)^4 (002)^4, \\
\psi_L((90)) &= N''_L P_L \sqrt{\frac{2}{5}} \{ [a^+(003)a(002)]_{[4]} - \frac{\sqrt{3}}{2} [a^+(101)a(100)]_{[4]} \\
&\quad - \frac{\sqrt{3}}{2} [a^+(011)a(010)]_{[4]} \} (000)^4 (100)^4 (010)^4 (001)^4 (002)^4,
\end{aligned} \tag{2.4}$$

where P_L is the projection operator onto the space of angular momentum (L), N_L , N'_L and N''_L the normalization constants and $[a^+(j)a(k)]_{[4]}$ means to make the $1p$ - $1h$ configuration with a particle of j orbit and a hole of k orbit coupled to zero isospin and zero intrinsic spin.

These wave functions of ψ_L are related to ϕ_L which appear in Eqs. (2.2) and (2.3) as follows:

$$\psi_L((\lambda\mu)) = \left(\frac{2A\nu}{\pi} \right)^{3/4} e^{-A\nu X^2} \phi_L((\lambda\mu)), \tag{2.5}^*)$$

Table II-2. Spectroscopic factors S_{α^2} for the SU_3 model wave functions whose $(\lambda\mu)$ are (40), (94) and (90) for ${}^8\text{Be}$, ${}^{16}\text{O}$ and ${}^{20}\text{Ne}$, respectively. (See Eq. (2.4).) Tables (a) and (b) show the S_{α^2} value for the cases where the oscillator parameters of fragment nuclei are chosen to be the same and equal to that of the parent nuclei. In the ${}^{16}\text{O}$ case, the wave function of the fragment nucleus, ${}^{12}\text{C}$, is chosen to be the SU_3 wave function with (04) representation. Tables (c) and (d) show the S_{α^2} values when the oscillator parameters of two fragment nuclei (ν_α for α and ν_o for ${}^{16}\text{O}$) and that of the parent nucleus (ν) are chosen to be different. The case of ${}^8\text{Be}$ with $\nu_\alpha/\nu = \sqrt{2}$ is written in (c) and the case of ${}^{20}\text{Ne}$ with $\nu_o = \nu$, $\nu_\alpha/\nu = \sqrt{5}$ and with $\nu_o/\nu = \sqrt{5/4}$, $\nu_\alpha/\nu = \sqrt{5}$ are shown in (i) and (ii) of (d), respectively.

(a)	J^π	$S_{\alpha^2}(40)$
	0^+	0.75
	2^+	0.75
	4^+	0.75

(b)	J^π	$S_{\alpha^2}(94)$	$S_{\alpha^2}(90)$
	1^-	0.238	0.344
	3^-	0.223	0.344
	5^-	0.193	0.344
	7^-	0.145	0.344

(c)	J^π	$S_{\alpha^2}(40)$
	0^+	0.710
	2^+	0.696
	4^+	0.665

(d)	J^π	$S_{\alpha^2}(90)$	
		(i)	(ii)
	1^-	0.277	0.287
	3^-	0.273	0.280
	5^-	0.268	0.268
	7^-	0.260	0.249

^{*)} $\phi_L((40))$ and $\phi_L((90))$ are equivalent to the following single channel clustering wave functions,

$$\begin{aligned}
n_L \mathcal{A} \{ R_{4L}(r, 2\nu) Y_{L0}(\mathcal{Q}_r) \phi_0(\alpha) \phi_0(\alpha) \}, \\
n'_L \mathcal{A} \{ R_{9L}(r, 16/5\nu) Y_{L0}(\mathcal{Q}_r) \phi_0(\alpha) \phi_0({}^{16}\text{O}) \},
\end{aligned}$$

respectively, where n_L and n'_L are the normalization constants and $R_{NL}(r, \gamma)$ the radial harmonic oscillator wave function with N oscillator quanta and the oscillator constant γ .

where A is the mass number and \mathbf{X}_G the center-of-mass coordinate.

We give at first in Table II-2 the calculated values of the spectroscopic factors, S_L^2 , which is defined as

$$S_L^2 = \int_0^\infty dr \cdot r^2 y_L^2(r), \quad (2.6)$$

where $y_L(r)$ is directly calculated by using Eq. (2.2). (We give in Appendix 1 the explicit calculational procedure of $y_L(r)$.) From this Table the SU_3 model wave functions are known to contain rather large amount of the components of $\alpha + (\text{residual core})$ channel. It should be, however, noticed that the value of the width is determined by the behaviour of $y_L(r)$ in its tail region and is not directly related to the spectroscopic factor given by the integral value of $y_L^2(r)$. We therefore show at second in Fig. 2.1 the behaviour of $ry_L(r)$ and the modified tail of SEM. If the value of the modified tail at the channel radius, $[ry(r)]_{r=a}$, is equal to $(3/a)^{1/2}$, we can obtain the Wigner limit value of the reduced width. So we draw in Fig. 2.1 the function of $f(r) = (3/r)^{1/2}$ for the convenience of the comparison. It is easily seen from the figure that the obtained reduced widths are far smaller than the Wigner limit, although the values of S_L^2 are not so small as was stated above. (It is, therefore, dangerous to discuss quantitatively the theoretical prediction of the widths of the model wave function only from the spectroscopic factors.) In Fig. 2.1 we also show the calculated results of $ry_L(r)$ by GFM in the cases of ^8Be and ^{20}Ne . It is seen that two methods (SEM and GFM) yield nearly the same results. Then we know that the simple modification of the tail behaviour by SEM is fairly reliable for these cases. The calculated results in the figures clearly confirm that the alpha decay widths obtained with the SU_3 model are very small compared with the Wigner limit and then the SU_3 model wave functions cannot explain the experimental α widths.

From the studies for the SU_3 model, we understand that the experimental α decay width certainly requires fairly larger probability of the α -particle in the surface region than that obtained by the spherical shell model. Therefore it is necessary for getting the large widths that the position of the final peak of $ry_L(r)$ must be pushed out more outward than that of the $ry_L(r)$ of the SU_3 model, preserving its suitable height. If we adopt the cluster model in which the relative distance between two clusters is fairly large, these requirements can be easily known to be satisfied. To confirm these points quantitatively we study the alpha decay widths of the cluster model. Figure 2.2 shows the results of $ry_L(r)$ of the Bloch-Brink cluster model wave functions²⁰⁾ for ^8Be , ^{16}O and ^{20}Ne which are expressed as

$$\Psi_L = N_L P_L \mathcal{A} \{ \psi_0(C, \nu_p, \mathbf{R}_C) \psi_0(\alpha, \nu_\alpha, \mathbf{R}_\alpha) \}, \quad (2.7)$$

where \mathcal{A} is the antisymmetrizing operator and $\psi_0(\alpha, \nu_\alpha, \mathbf{R}_\alpha)$ and $\psi_0(C, \nu_p, \mathbf{R}_C)$

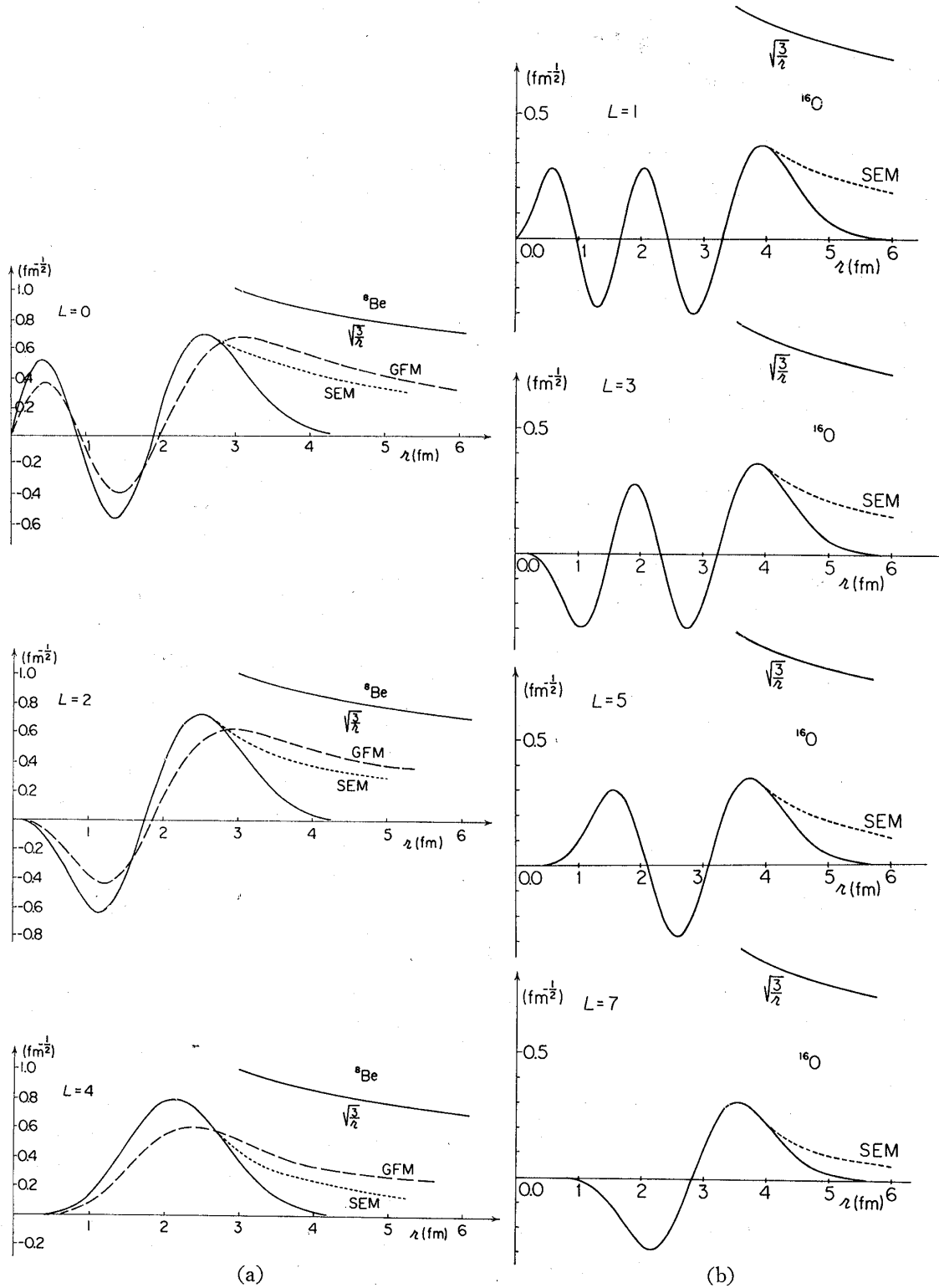
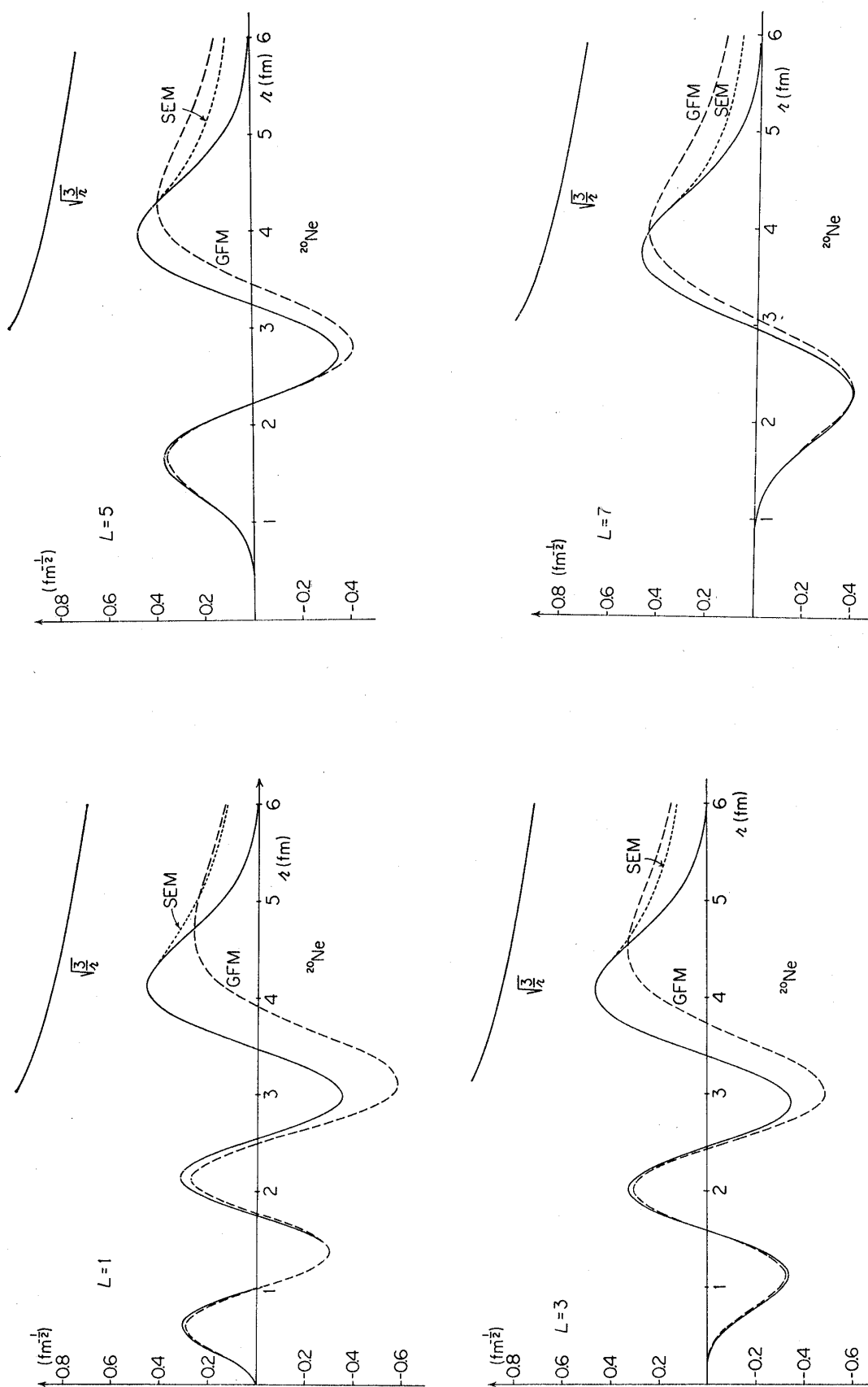


Fig. 2.1. Behaviour of $ry_L(r)$ for the SU_3 model wave functions. Here the SEM modified tails and in the case of ${}^8\text{Be}$ and ${}^{20}\text{Ne}$, $ry_L(r)$ by GFM are also drawn and compared with the curve $\sqrt{3}/r$. Oscillator parameters are for ${}^8\text{Be}$ $\nu=\nu_\alpha=0.287\text{ fm}^{-2}$, for ${}^{16}\text{O}$ $\nu=\nu_\alpha=0.179\text{ fm}^{-2}$ and for ${}^{20}\text{Ne}$ $\nu=\nu_\alpha=0.154\text{ fm}^{-2}$. In the calculation by GFM we used the two-body nuclear interaction of $60(0.4+0.6P_M) \times [\exp(-(r/1.01)^2) - \exp(-(r/1.80)^2)]$ (MeV) and as $U(r)$ we adopted for ${}^8\text{Be}$ $U(r)=(4e^2/2R_0)(3-r^2/R_0^2)$ ($r \leq R_0$), $U(r)=4e^2/r$ ($r \geq R_0$) with $R_0=3.0\text{ fm}$ and for ${}^{20}\text{Ne}$ $U(r)=16e^2/r$.



are the harmonic oscillator wave functions of the α and the residual core nucleus (when $C=^{12}\text{C}$, $p_{3/2}$ closed shell structure is adopted for $\psi_0(C)$) centered at \mathbf{R}_α and \mathbf{R}_c , respectively. In the case of ^{16}O , the spurious center-of-mass motion in Ψ_L is eliminated by the procedure $\int d\mathbf{S} \mathcal{A}\{\psi_0(^{12}\text{C}, \mathbf{R}_c + \mathbf{S})\psi_0(\alpha, \mathbf{R}_\alpha + \mathbf{S})\}$. It is seen from these figures that the experimental large widths are easily reproduced by this model when we take the appropriate values for the distance parameter $|\mathbf{R}_\alpha - \mathbf{R}_c|$ (which are consistent with the results of the variational calculations for the energy). From the comparison of Fig. 2.2 with Fig. 2.1 we clearly see the difference

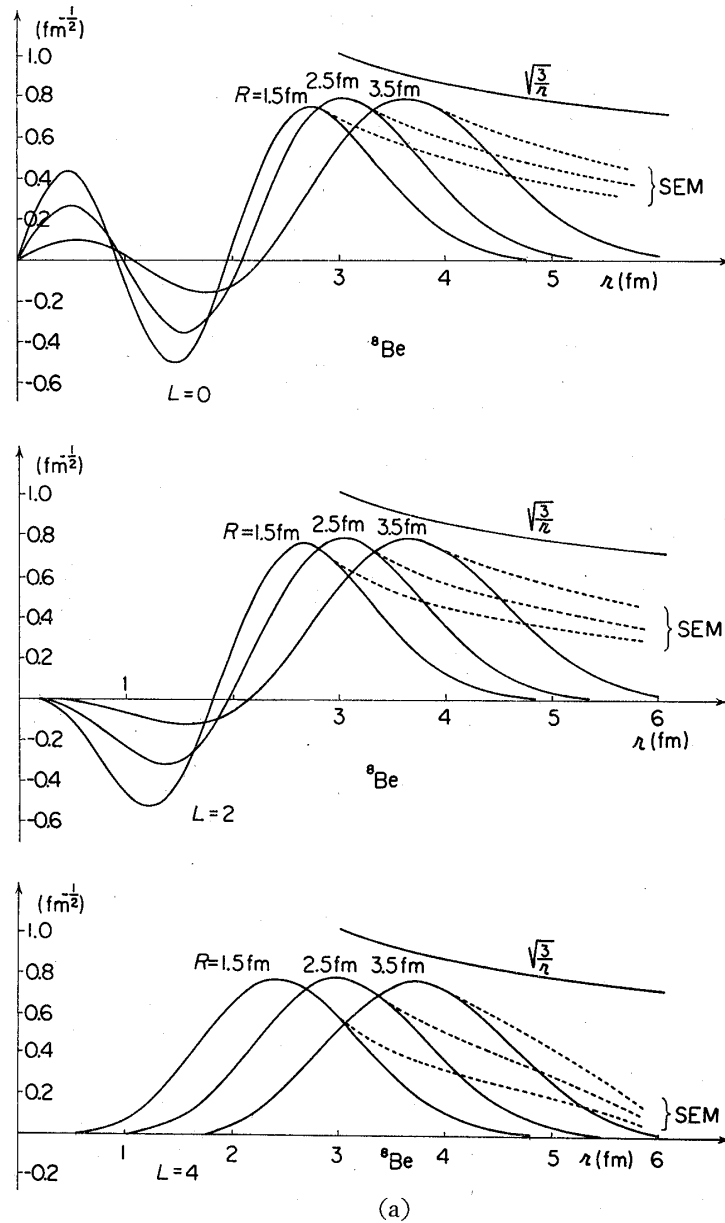
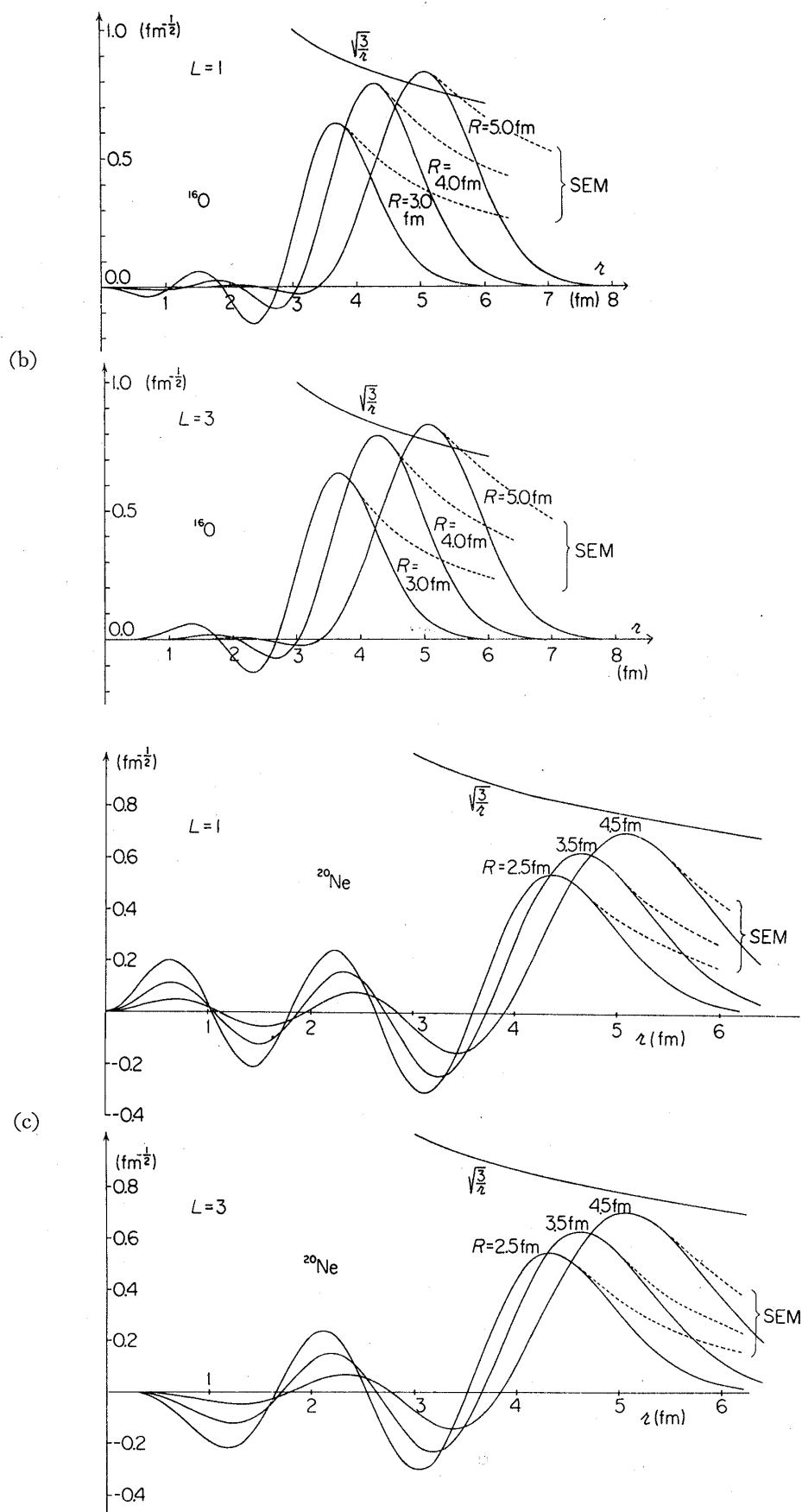


Fig. 2.2. The functions, $r y_L(r)$ of the Bloch-Brink wave functions and their modified tails by SEM. Here the oscillator parameters are for ^8Be $\nu = \nu_\alpha = 0.287 \text{ fm}^{-2}$, for ^{16}O $\nu_p = \nu_c = 0.193 \text{ fm}^{-2}$, $\nu_q = \nu_\alpha = 0.287 \text{ fm}^{-2}$ and for ^{20}Ne $\nu_p = \nu_q = \nu_o = \nu_\alpha = 0.154 \text{ fm}^{-2}$.



in the behaviour of $ry_L(r)$ between the two models; the final peaks by the Bloch-Brink model are pushed out fairly outwards and their heights are large compared with those of the SU_3 model (on the contrary the inner amplitudes of $ry_L(r)$ of the Bloch-Brink model are suppressed in comparison with the large inner amplitudes of SU_3 model). In the case of the cluster model the spectroscopic factors of S_L^2 are also larger than those of the SU_3 model. We show in Fig. 2.3 the calculated S_L^2 values of the Bloch-Brink model as a function of the distance parameter.

We have known that the large decay widths of the experiments can be obtained when the molecular character is assumed for these levels. It is interesting further to examine how large decay width can be obtained for the case of the major shell mixing deformed model, since it can also explain the rotational spectra and is based on the single particle field with a single center different from the cluster model. We here adopt the deformed oscillator model^{23)~26)} and study the behaviour of $ry_L(r)$ for this model wave function in the same manner as before. The wave functions of this model can be written with the same forms as Eq. (2.4) except that the different values are allowed for the oscillator parameters, ν_z and $\nu_1 = \nu_x = \nu_y$. In Fig. 2.4 we show $ry_L(r)$ for ^8Be and ^{20}Ne . We see that when the deformation with prolate shape is large (ν_1/ν_z large) the positions of the final peaks of $ry_L(r)$ are pushed out but the height of them becomes low. This lowering of the

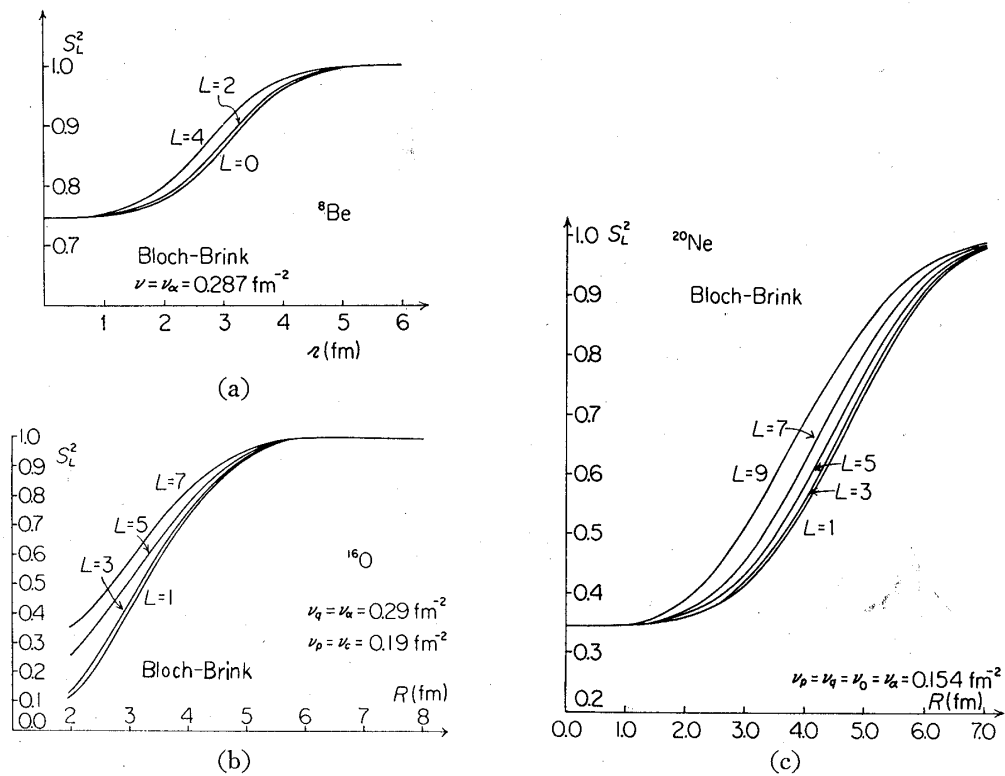


Fig. 2.3. Dependence of the S_L^2 values of the Bloch-Brink wave functions on the distance parameters.

height of the final peak of $ry_L(r)$, which is evident especially for ^{20}Ne case is due to the decrease of the probability of the wave function which belongs to the $\alpha + \text{core}$ channel space.*) The dependence of the probability of the

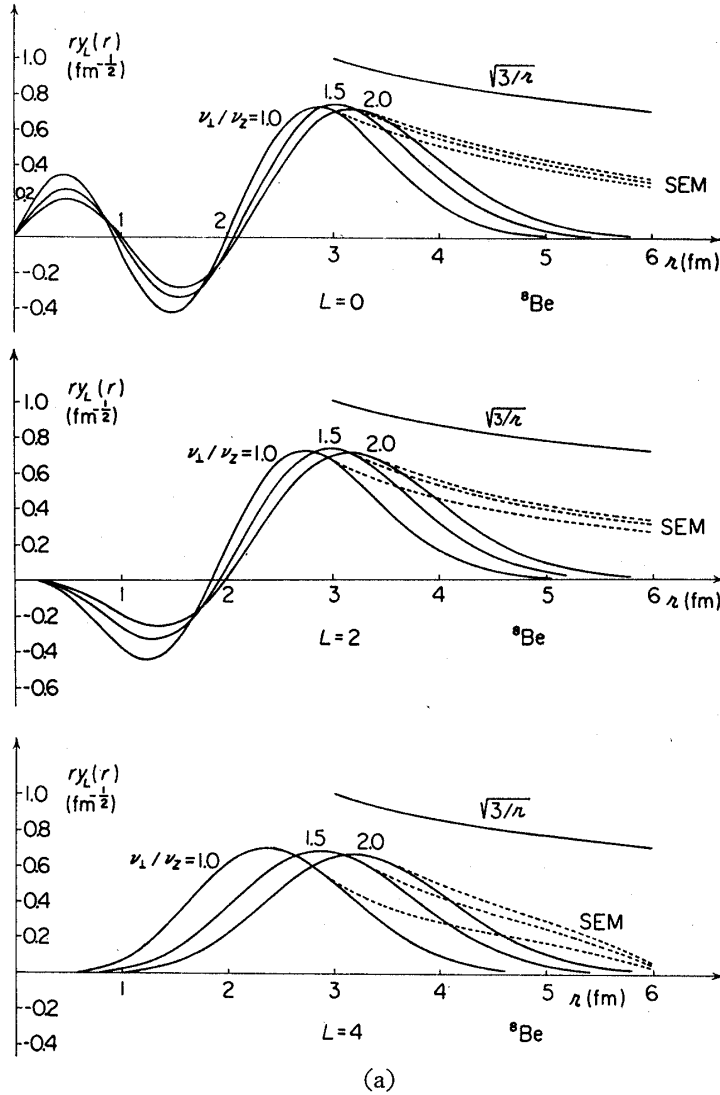
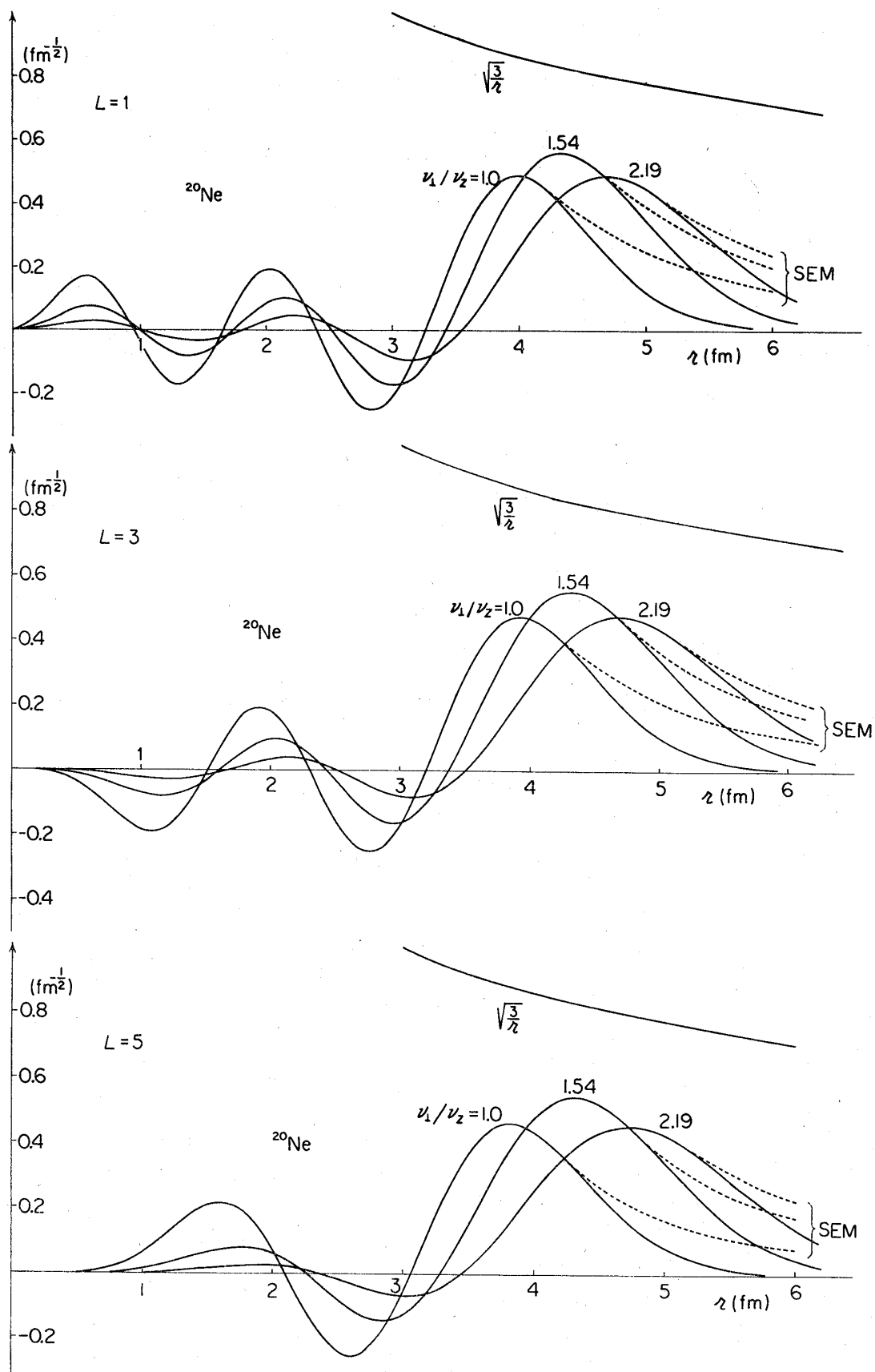


Fig. 2.4. The function, $ry_L(r)$ for the deformed oscillator model wave functions and their modified tails by SEM. Here the oscillator parameters are for ^8Be $(\nu_1^2\nu_2)^{1/3} = 0.205 \text{ fm}^{-2}$, $\nu_\alpha = 0.287 \text{ fm}^{-2}$ and for ^{20}Ne $(\nu_1^2\nu_2)^{1/3} = 0.154 \text{ fm}^{-2}$, $\nu_0 = 0.161 \text{ fm}^{-2}$, $\nu_\alpha = 0.287 \text{ fm}^{-2}$.

*) We define the $\alpha + \text{core}$ channel space by the functional space spanned by the wave functions of the form $\mathcal{A}\{X_L(r)Y_{L0}(\mathcal{Q}_r)\phi_0(C)\phi_0(\alpha)\}$ with arbitrary $X_L(r)$. Any wave function ϕ_L can be always decomposed into two mutually orthogonal parts as follows,

$$\phi_L = \mathcal{A}\{e_L(r)Y_{L0}(\mathcal{Q}_r)\phi_0(C)\phi_0(\alpha)\} + \phi_L^R,$$

where ϕ_L^R is the part of ϕ_L which does not belong to the $\alpha + \text{core}$ channel space and so is orthogonal to the first term of the r.h.s. of this equation. Because the part of ϕ_L which contributes to $y_L(r)$ is only the first term belonging to the $\alpha + \text{core}$ channel space due to the orthogonality of ϕ_L^R with the channel wave function $Y_{L0}(\mathcal{Q}_r)\phi_0(C)\phi_0(\alpha)$, the magnitude of the width is directly proportional to the squared norm of this first term.



(b)

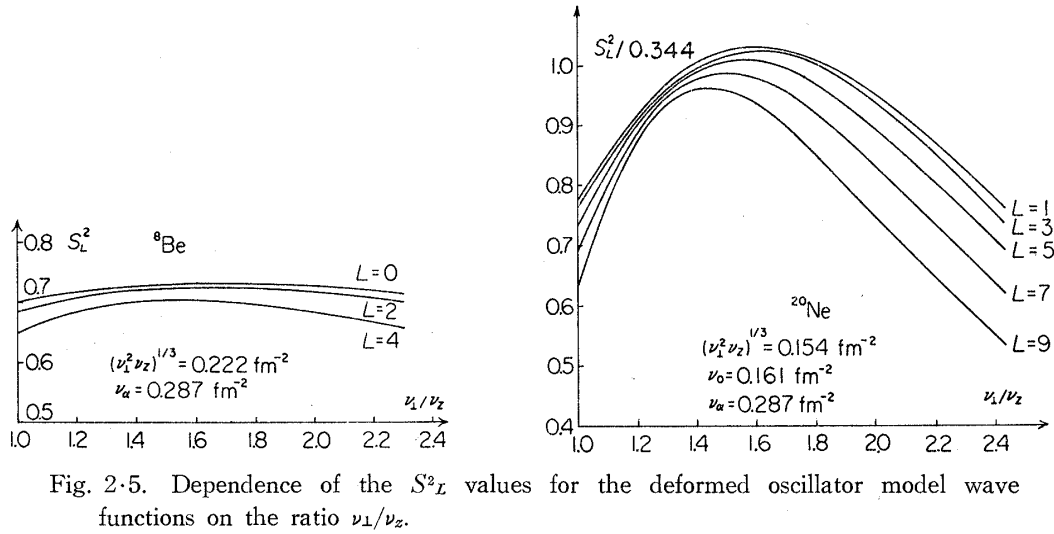


Fig. 2.5. Dependence of the S_L^2 values for the deformed oscillator model wave functions on the ratio ν_1/ν_z .

α +core channel part on the deformation parameter, (ν_1/ν_z) , is clearly reflected into the spectroscopic factor. Then we show the dependence of S_L^2 on ν_1/ν_z in Fig. 2.5, where the S_L^2 value is seen to decrease with the increase of ν_1/ν_z . Although the pushing out of the position of the final peak seems to make the reduced width of this model larger than that of the SU_3 model, the lowering effect of $ry_L(r)$ suppresses the value of the reduced width fairly. The resultant widths of the deformed oscillator model with large ν_1/ν_z are obtained to be not so larger than those of the SU_3 ($\nu_1/\nu_z=1$). Only for the case of the ground state of ${}^8\text{Be}$, the experimental value is seen to be reproduced if we take the value of $\nu_1/\nu_z \cong 2$.

2.4 Comparison with experiments and summary

We summarize in Table II-3 the calculated results of the widths by SU_3 , deformed oscillator and cluster models, together with the experimental values. In calculating $\theta_L^2(a)$ with use of modified tail, we have taken into account the correction factor which is necessary in order to preserve the normalization of the model wave function to unity, since the modification of the tail of $y_L(r)$ makes the normalization of the model wave function deviate from unity. We give in Appendix 2 the calculational formula for this correction factor.

As is seen in Table II-3 the calculated results by the molecular model agree well with experiments in every case of ${}^8\text{Be}$, ${}^{16}\text{O}$ and ${}^{20}\text{Ne}$, just as was expected. To assure the statement that the experimental large reduced width near the Wigner limit indicates clearly the formation of the nuclear di-molecule, we have also studied the reduced width of the SU_3 model (which can describe the rotational motion within the spherical shell model basis) and of the deformed oscillator model (where the single particle field is strongly deformed into prolate shape). It is only in the case of the

Table II-3. Calculated results of the α decay widths by the SU_3 , deformed oscillator and cluster model wave functions. Values in the parentheses are those by GFM.(a) ^8Be

(1) Bloch-Brink model.

J^π	θ_{exp}^2	$R(\text{fm}) (\nu=\nu_\alpha=0.287\text{fm}^{-2})$	
		2.5	3.5
0^+	0.15	0.18(0.26)	0.30(0.33)
2^+	0.70	0.25(0.40)	0.46(0.59)
4^+	0.95	0.22(0.41)	0.59(0.72)

(2) SU_3 and deformed oscillator model.

J^π	SU_3		Deformed Oscillator $\nu_\alpha=0.287\text{fm}^{-2} (\nu_1^2\nu_2)^{1/3}=0.222\text{fm}^{-2}$	
	$\nu=0.205\text{fm}^{-2}$ $\nu_\alpha=0.287\text{fm}^{-2}$	$\nu=\nu_\alpha=0.287\text{fm}^{-2}$	$\nu_1/\nu_2=1.50$	$\nu_1/\nu_2=2.00$
0^+	0.14(0.23)	0.10(0.17)	0.16	0.18
2^+	0.17(0.31)	0.11(0.22)	0.20	0.24
4^+	0.08(0.20)	0.05(0.13)	0.15	0.22

(b) ^{16}O

(1) Bloch-Brink model.

J^π	θ_{exp}^2	$R(\text{fm}) (\nu_p=\nu_c=0.193\text{fm}^{-2})$ $(\nu_q=\nu_\alpha=0.287\text{fm}^{-2})$	
		3.0	4.0
1^-	0.83	0.22	0.67
3^-	1.03	0.17	0.64
5^-	0.25	0.17	0.64
7^-	0.36	0.11	0.59

(2) SU_3 model.

J^π	$\nu=\nu_\alpha=\nu_c=0.179\text{fm}^{-2}$
1^-	0.10
3^-	0.07
5^-	0.05
7^-	0.01

(c) ^{20}Ne

(1) Bloch-Brink.

J^π	θ_{exp}^2	$R(\text{fm}) (\nu_q=\nu_p=\nu_\alpha=\nu_O=0.154\text{fm}^{-2})$	
		3.5	4.5
1^-	>0.54	0.56	1.27
3^-	0.89	0.56	1.27
5^-	1.06	0.56	1.27
7^-	0.79	0.56	1.27

(2) SU_3 and deformed oscillator models.

J^π	SU_3		Deformed Oscillator ($\nu_1^2\nu_2$) ^{1/3} =0.154 fm ⁻² ($\nu_\alpha=0.287\text{fm}^{-2}$ $\nu_o=0.161\text{fm}^{-2}$)	
	$\nu=0.154\text{fm}^{-2}$ $\nu_\alpha=0.287\text{fm}^{-2}$ $\nu_o=0.161\text{fm}^{-2}$	$\nu=\nu_\alpha=\nu_o$ =0.154 fm ⁻²	$\nu_1/\nu_2=1.54$	$\nu_1/\nu_2=2.19$
1 ⁻	0.10	0.10(0.10)	0.26	0.37
3 ⁻	0.07	0.09(0.13)	0.24	0.35
5 ⁻	0.05	0.07(0.14)	0.23	0.34
7 ⁻	0.02	0.04(0.11)	0.20	0.30

ground state of 8-body system that the calculated results by the SU_3 or the deformed oscillator model are comparably near the experimental value. And all the others are distinctly different from the values of the molecular model. The deformed model in the ^{20}Ne system yields the values which are less than 1/3 of those of the molecular model. As for the SU_3 model, the values of the spectroscopic factors are a little larger than those for the deformed oscillator model. But since the base of this model is spherical, the probability amplitude of the α -particle (which is expressed by the reduced width amplitude $y_L(a)$) rapidly decreases in the surface region. Thus the reduced widths of this model cannot but become very small compared with the molecular model.

We can conclude that it is impossible to understand systematically the experimental large reduced widths unless we use the intrinsic wave functions which represent the molecule-like structure faithfully and that the experimental large reduced widths indicate clearly the molecule-like intrinsic structures for the rotational bands with $K=0^-$ in ^{16}O and ^{20}Ne , together with the ground rotational band in ^8Be .

§3. Inversion doublet and the structure of $K=0^+$ band in ^{16}O and ^{20}Ne

3.1 The indication of the experimental gap energies

It was concluded in the previous section that the intrinsic structures of the negative parity rotational bands in ^{16}O and ^{20}Ne are the heteropolar di-molecule-like structures of α -C and α -O, respectively. The conclusion on the negative parity bands suggests the possible existence of the positive rotational bands with the similar intrinsic structure¹⁾ in ^{16}O and ^{20}Ne . If it is true, the situation in ^{16}O and ^{20}Ne can be considered to be very analogous to the inversion doublet²⁷⁾ in the atomic molecule like as NH_3 .

Since the constituent subunit nuclei α and $\text{C}(\text{O})$ are not assumed to be rigid in the nuclear system, we always have to take into account the effect that the configuration of α -C (α -O) is converted into its mirror image of

C- α (O- α) by the interactions. As the result of such an inversion vibration, the rotational band with $K=0$ splits into the positive and negative parity bands with the energy gap of ΔE_0 , where the positive parity band lies below the negative one due to the symmetry character.

In the actual cases of ^{16}O and ^{20}Ne , only one rotational band with $K=0^+$ can be found below the noted negative parity band; that is, the rotational band upon the "mysterious zero plus" state^{28)~32)} at 6.06 MeV in ^{16}O and the ground rotational band in ^{20}Ne . For these positive parity bands the alpha-clusterized intrinsic structure has been suggested by the successes of the weak coupling model⁶⁾ for ^{16}O and also from the good understanding of the ground rotational band by the alpha-Oxygen model.³³⁾ Recent experimental studies for such rotational levels by the four-particle transfer reaction^{34),35)} have also indicated that the intrinsic structures of the positive rotational bands have very strong alpha-like correlations. To display the characters of these rotational bands we regulate the rotational level structures with $K=0$ in ^{16}O and ^{20}Ne from the molecular point of view;

$$\begin{aligned} E_+(I) &= E_0 - \frac{\Delta E_0}{2} + \frac{\hbar^2}{2\mathcal{J}_+} I(I+1), \\ E_-(I) &= E_0 + \frac{\Delta E_0}{2} + \frac{\hbar^2}{2\mathcal{J}_-} I(I+1), \end{aligned} \quad (3.1)$$

where ΔE_0 is the gap energy between the two rotational bands with $K=0^\pm$, E_0 is defined to be the intrinsic energy of the molecule-like structure and \mathcal{J}_\pm are the moments of inertia of the two rotational bands. (These parameters obtained from the experimental levels are listed in Table III-1.)

Table III-1. Parameters in Eq. (3.1) which are determined to fit the experimental excitation energies.

	E_0	ΔE_0	$\hbar^2/2\mathcal{J}_+$	$\hbar^2/2\mathcal{J}_-$
^{16}O	7.36	3.39	0.25	0.22
^{20}Ne	2.81	5.18	0.19	0.17

(MeV unit)

The gap energy (ΔE_0) is the quantity related intimately to the rigidity of the subunit nuclei because it tends to zero in the extreme case of the perfect rigid bodies. Then the gap energy can be regarded as an important parameter for the degree of the dissolution of the subunit clusters in the nuclear molecule. If the positive parity band is assumed to have the same di-molecule-like structure as the negative parity band, the gap energy for $^{16}\text{O}(\alpha\text{-C})$ and $^{20}\text{Ne}(\alpha\text{-O})$ can be obtained as $1 \text{ MeV} \lesssim \Delta E_0 \lesssim 3 \text{ MeV}$ with the use of the schematic model which will be mentioned later in §3.2. On

the other hand, if the intrinsic structure would be described with the shell model (e. g., SU_3), the value of ΔE_0 might correspond to the frequency, $\hbar\omega_0$, of the collective vibrational mode which is expected to be $7 \text{ MeV} \lesssim \Delta E_0 < 15 \text{ MeV}$ in the region of ^{16}O .

When the actual value of ΔE_0 in ^{16}O and ^{20}Ne are compared with the above-mentioned values, the value of $\Delta E_0 = 3.39 \text{ MeV}$ in ^{16}O is known to be very close to the one for the di-molecule-like structure and the value of $\Delta E_0 = 5.18 \text{ MeV}$ in ^{20}Ne to be the intermediate one between two cases. Therefore, we can expect the di-molecule-like structure for the positive parity band in ^{16}O and expect the structure with the appreciable deviation from it for the ground band in ^{20}Ne . (The detailed discussions are given in the following subsections.) It should be noted here that the characteristics indicated by the gap energy are consistent with the conclusions obtained from the deviation energy of $\delta E_0 = E_0 - E_{\text{th}}$ for both cases, as mentioned in §1.

3.2 The estimation of the gap energy with the molecular model

To estimate the gap energy of the inversion doublet in the molecule-like structure, we adopt the schematic model which has the analogy to the case in the atomic molecule. In the atomic molecule, the path from a configuration to another configuration of its mirror image can be well defined as the displacements of its constituents. On the contrary, the path for the inversion in the nuclear molecule, which has a character of collective coordinate, is considered to be hardly defined as the function of particle coordinates. It is, however, necessary for the estimation of the gap energy to define the characters of the path for the inversion.

At first we assume that the intrinsic energy has a local minimum at the configuration of the heteropolar di-molecule-like structure. Then the mode corresponding to the relative motion between the subunits has its zero-point oscillation around the local minimum. Next we consider the inversion path and assume for the characters of the path that a symmetric configuration is realized just at middle in the path. Figure 3.1 shows such a character of the inversion path, where the two configurations on both sides are the mirror image of each other and the configuration at middle is symmetric with respect to the reflection.

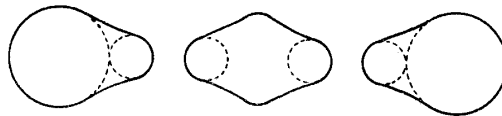


Fig. 3.1. Graphical picture of the path of the inversion motion.

If the motion along the path for the inversion is treated separately from other intrinsic motions with use of the adiabatic approximation, the wave functions localized around the two energy minima can be connected

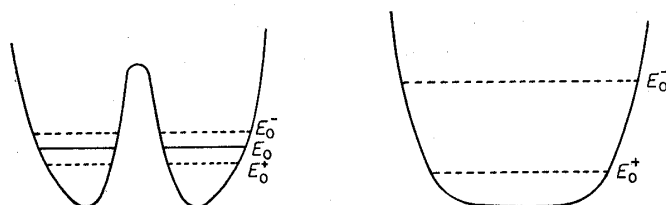


Fig. 3.2. Characteristic picture of the potential for the inversion motion.

with each other along the path for this inversion. We assume the adiabatic potential along the path which is necessary for the estimation of the gap energy. The two typical cases are illustrated in Fig. 3.2. The left-hand side is the case of the inversion potential with a strong barrier where the intrinsic energy for the symmetric configuration at the middle of the path is assumed to be higher than the intrinsic energy of the molecular configuration. In this case, the molecule-like configuration is very stable. The right-hand side in Fig. 3.2 corresponds to the case where the intrinsic states with the symmetric configuration and with the asymmetric molecular configuration are nearly degenerate energetically.

In the estimation of the gap energy according to the above-mentioned schematic model, we use the square type potential which is characterized by the parameters shown in Fig. 3.3, where E_0 is the zero-point energy for the molecule-like intrinsic structure, the distance of $(a_2 - a_1)/2$ indicates the spread of the zero-point oscillation for it, and the parameter of U_0 shows the height of the barrier along the inversion path from a_1 to $-a_1$. For the case of ${}^8\text{Be}$, the spread of the wave function for the relative motion between two α -particles has been known to be about 2.0 fm and then we assume the value of $a_2 - a_1 = 2.0$ fm for the present problems of $\alpha\text{-C}$ and of $\alpha\text{-O}$.

To define the length of the inversion path and the height of the central barrier, we assume the model which represents the inversion from a configuration to its mirror image by the dissolution of an alpha-particle into the larger subunit nucleus and the simultaneous creation of an alpha-particle from it as illustrated in Fig. 3.1.

According to this image, we represent the center-of-mass of the subunit

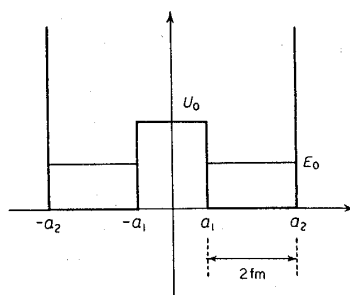


Fig. 3.3. Simple potential with square shape used to estimate the gap energy.

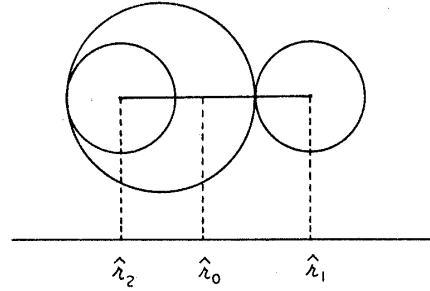


Fig. 3.4. Model picture for getting the quantitative values of the path length and of the inertial parameter along this path.

alpha-particle as \mathbf{r}_1 , of the virtual alpha-particle in the larger subunit nuclei as \mathbf{r}_2 , and of the residual part in the middle as \mathbf{r}_0 , as shown in Fig. 3.4. Then a set of internal coordinates are introduced as follows,

$$\begin{aligned}\mathbf{r}_\alpha &= \mathbf{r}_1 - \mathbf{r}_2, \\ \mathbf{r}_\beta &= \mathbf{r}_0 - (\mathbf{r}_1 + \mathbf{r}_2)/2.\end{aligned}\quad (3.2)$$

If the inversion vibration is assumed to be the relative motion between the residual part in the middle and the two alpha-particles, the coordinate of \mathbf{r}_β defined in Eq. (3.2) represents the inversion path, (where \mathbf{r}_α is fixed to be an appropriate value). In this model, the point of $\mathbf{r}_\beta = 0$ corresponds to the symmetric configuration and the point with a finite value $((a_1 + a_2)/2)$ corresponds to the molecular configuration. When the relative distance between two subunit nuclei of the di-molecule-like structure is given by the sum of their mean radii, $R = r_0(A_1^{1/3} + A_2^{1/3})$ with $A_1 = 4$ and $A_2 = 12$ or 16 , we can easily obtain the value of \mathbf{r}_β for the molecular configuration as

$$|\mathbf{r}_\beta| = (a_1 + a_2)/2 = r_0 A_1^{1/3} (1 - \nu^{2/3}) / (1 - \nu) \quad (3.3)$$

with $\nu = A_1/A_2$. According to this model, the effective mass of the motion along the path (\mathbf{r}_β) for inversion is obtained as

$$m_{\text{eff}} = \frac{2A_1(A_2 - A_1)}{2A_1 + (A_2 - A_1)} m_N, \quad (3.4)$$

where we assume for the simplicity of the model that the three parts in Fig. 3.4 move with the same inertia as of the free motion, (m_N nucleon mass).

Under the assumptions mentioned above the gap energy ($\Delta E_0 = E_0^- - E_0^+$) can be obtained from the solutions of the following equation;

$$\left\{ -\frac{\hbar^2}{2m_{\text{eff}}} \frac{d^2}{dr_\beta^2} + V(r_\beta) \right\} \psi_0^\pm = E_0^\pm \psi_0^\pm, \quad (3.5)$$

where $V(r_\beta)$ is the potential with the shape as shown in Fig. 3.3. The gap energies are estimated in the region of the parameter set ($U_0 - E_0$ and

$(a_1 + a_2)/2$) which includes the following typical cases:

Case (1) is that the both rotational bands with $K=0^\pm$ have the well-defined molecular intrinsic structure which corresponds to the case with the large central barrier and with the length parameter as given in Eq. (3.3).

Case (2) is that the asymmetric configuration with molecular structure remains still in the intrinsic state but the symmetric configurations are mixed strongly in it, where the value of $(a_1 + a_2)/2$ is not small like as in case (1) but the value of U_0 is very small.

Case (3) is that the molecular structure breaks down and the shell-like structure with the symmetric configuration has a majority, which is represented by the parameter set of $(a_1 + a_2)/2$ with small value and of $U_0 = 0$.

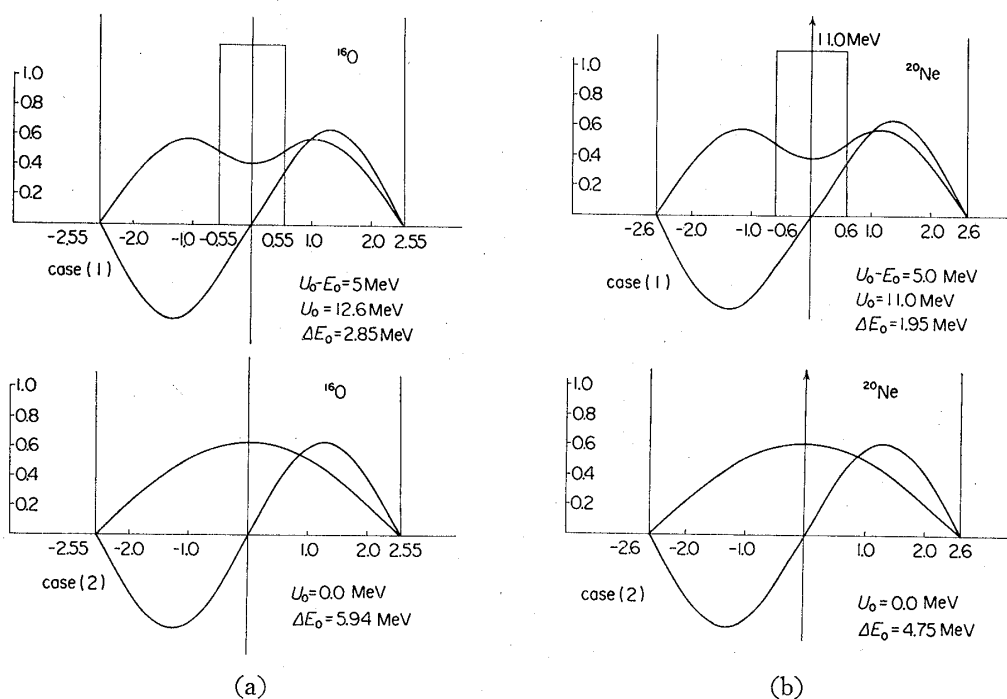


Fig. 3.5. Eigenenergies and wave functions for the cases (1) and (2).

The solutions of the equation, that is, the energy and the wave function are shown in Fig. 3.5 for the cases (1) and (2). We can see from the characteristic behaviors shown in Fig. 3.5 that the cases (1) and (2) correspond to the real situation of the negative parity band which has the well-defined molecule-like structure (but the case (3) is not). In the case (1) the probability of the wave function in the region of the central barrier is extremely small and in the case (2) the probability in that region is also small since the wave function always vanishes at the reflecting point of the symmetric configuration. We, therefore, understand that the molecular formation in the negative parity band depends essentially on the length parameter and that the dependence on the height of the central barrier is

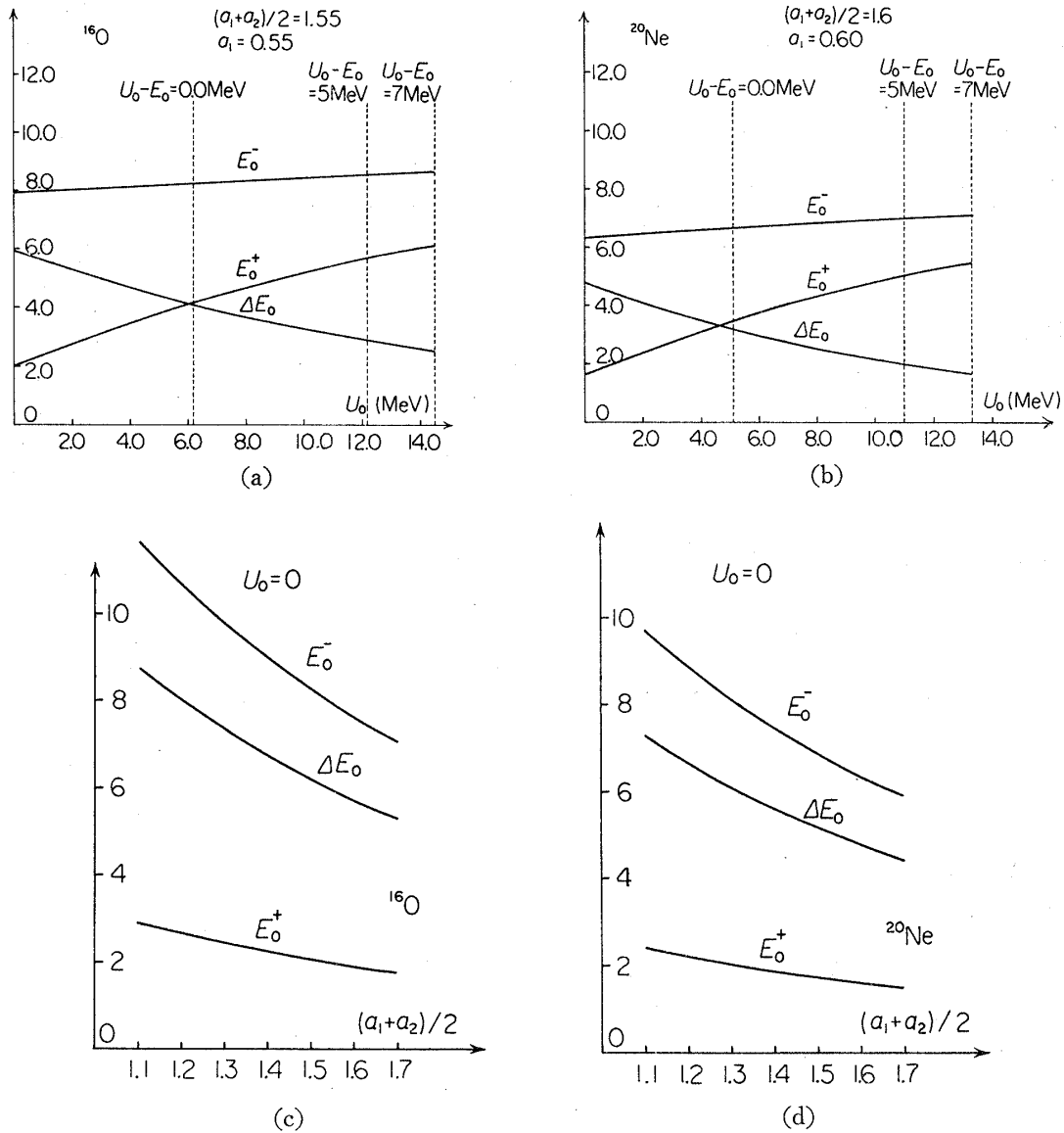


Fig. 3-6. Dependence of the gap energy on the parameters U_0 and $(a_1 + a_2)/2$.

not strong. On the contrary there appears the clear difference between the cases (1) and (2) for the positive parity band, as is seen in Fig. 3-5. To see the quantitative character we show in Fig. 3-6 the dependences of the gap energy on the parameters for the central barrier, i.e., U_0 and $(a_1 + a_2)/2$.

In the case (1) the gap energy is obtained as 2.85 MeV for $\alpha\text{-C}$ and as 1.95 MeV for $\alpha\text{-O}$ when we use the values of $(a_1 + a_2)/2$ given in Eq. (3-3) and of $U_0 - E_0 = 5.0 \text{ MeV}$.*) The gap energy for $\alpha\text{-O}$ is rather smaller than

*) As for the height $(U_0 - E_0)$ of the central barrier, the upper limit has been considered to be order of the separation energy of an alpha-particle from the larger subunit nucleus (about 7 MeV).

that for α -C because the magnitude of the mass-displacement¹⁾ ($a_1\sqrt{m_{\text{eff}}}$) for the former is larger than that for the latter. It should be noted that on the contrary the experimental value of the gap energy in ^{20}Ne is larger than that in ^{16}O .

Although for the case of ^{16}O , the experimental value of the gap energy (3.39 MeV) is about 1.2 times larger than that obtained with the parameters of the case (1), the small alteration of the barrier height, that is, $U_0 - E_0 = 3$ MeV, leads to the agreement with the empirical value. On the other hand, in order to reproduce the experimental gap energy of 5.5 MeV in ^{20}Ne , we have to choose the parameter set corresponding to the case (2), where $U_0 \simeq 0$ with the appreciably large value of $(a_1 + a_2)/2$.

The quantitative results discussed above seem to allow an interpretation, as was expected, that for the case of ^{16}O , the positive parity band still has the molecule-like structure dominantly in spite of the mixing with the symmetric configuration but that for the case of ^{20}Ne , the intrinsic structure of the positive parity band has the transient character in the wide region from the asymmetric configuration with the molecule-like structure to the symmetric configurations with the shell-like structure.

3.3 Microscopic studies on the gap energy

It is interesting to understand from the microscopic point of view the transient character indicated in the gap energy for ^{20}Ne . For this purpose we apply the generator coordinate method³⁶⁾ by choosing a suitable parameter set which can describe not only the molecular configuration but also the configurations along the inversion path. We denote the parameters by ξ and the intrinsic wave function by $\phi(\mathbf{x}, \xi)$. The total wave function $\psi(\mathbf{x})$ which includes the inversion motion in itself is given by superposing $\phi(\mathbf{x}, \xi)$ with the unknown amplitude $f(\xi)$ as follows,

$$\begin{aligned}\psi^\pm(\mathbf{x}) &= \int d\xi f^\pm(\xi) \phi^\pm(\mathbf{x}, \xi), \\ \phi^\pm(\mathbf{x}, \xi) &= \phi(\mathbf{x}, \xi) \pm \phi(-\mathbf{x}, \xi).\end{aligned}\tag{3.6}$$

As is well known, the equation of motion for this amplitude $f(\xi)$ is given by the variational principle to minimize the expectation value of the total Hamiltonian, \mathcal{H} ;

$$\begin{aligned}\int d\xi' \{ \langle \phi^\pm(\mathbf{x}, \xi) | \mathcal{H} | \phi^\pm(\mathbf{x}, \xi') \rangle \\ - E^\pm \langle \phi^\pm(\mathbf{x}, \xi) | \phi^\pm(\mathbf{x}, \xi') \rangle \} f^\pm(\xi') = 0.\end{aligned}\tag{3.7}$$

If we assume that the solution of $f^\pm(\xi)$ is obtained as a localized function at ξ_0^\pm as $f^\pm(\xi) = \delta(\xi - \xi_0^\pm)$, the total energy E^\pm is given by

$$E^\pm(\xi_0^\pm) = \frac{\langle \phi^\pm(\mathbf{x}, \xi_0^\pm) | \mathcal{H} | \phi^\pm(\mathbf{x}, \xi_0^\pm) \rangle}{\langle \phi^\pm(\mathbf{x}, \xi_0^\pm) | \phi^\pm(\mathbf{x}, \xi_0^\pm) \rangle}. \quad (3.8)$$

We now calculate the energy surfaces for the positive and negative parity intrinsic states using the above equation and investigate the dependence of $E^\pm(\xi)$ upon the parameters ξ . To do this we set up a model for the intrinsic wave function $\phi^\pm(\mathbf{x}, \xi)$ adopting the Bloch-Brink α -particle model function. This model wave function contains a set of parameters, $(\mathbf{R}_i, \nu_i; i = 1 \sim A/4)$, but we use in practice minimum number of parameters among them (fixing the remainder constant appropriately) which are necessary at least to specify the path of inversion. They are a set of three parameters, for example, $\mathbf{R}_1, \mathbf{R}_0, \mathbf{R}_2$ which correspond to the dynamical variables $\mathbf{r}_1, \mathbf{r}_0, \mathbf{r}_2$ used in §3.2, and are expressed as

$$\mathbf{R}_1 = \mathbf{R}_1, \mathbf{R}_2 = \mathbf{R}_2 \text{ and } \mathbf{R}_0 = -\frac{4}{A-8} \sum_{i=3}^{A/4} \mathbf{R}_i. \quad (3.9)$$

Then these parameters are transformed into the parameters \mathbf{R}_α and \mathbf{R}_β which correspond to \mathbf{r}_α and \mathbf{r}_β of Eq. (3.2) as follows,

$$\begin{aligned} \mathbf{R}_\alpha &= \mathbf{R}_1 - \mathbf{R}_2, \\ \mathbf{R}_\beta &= \mathbf{R}_0 - (\mathbf{R}_1 + \mathbf{R}_2)/2. \end{aligned} \quad (3.10)$$

For the convenience of later discussions, we express the relative distance parameter, \mathbf{R} , between an alpha cluster and the residual cluster in terms of the parameters \mathbf{R}_α and \mathbf{R}_β ;

$$\mathbf{R} = \mathbf{R}_1 - \frac{4}{A-4} \left(\mathbf{R}_2 + \frac{A-8}{4} \mathbf{R}_0 \right) = \frac{A}{2(A-4)} \mathbf{R}_\alpha - \frac{A-8}{A-4} \mathbf{R}_\beta. \quad (3.11)$$

In Fig. 3.7, the energy surfaces of $E_0^\pm(\xi)$ with $\xi = (\mathbf{R}_\alpha, \mathbf{R}_\beta)$ are drawn for the case of ^{20}Ne . Here we use the effective interactions given by Volkov²³⁾ with the Coulomb interactions.

In the figures of the energy surface, we first note that the energy minimum of the negative parity intrinsic state locates nearly on the \mathbf{R} line with large R value, and that the direction with small curvature is almost parallel to \mathbf{R} . This means that the negative parity band has a molecule-like intrinsic structure strongly polarized into the two-body clusters, and that the relative distance parameter, \mathbf{R} , is considered to be an approximate

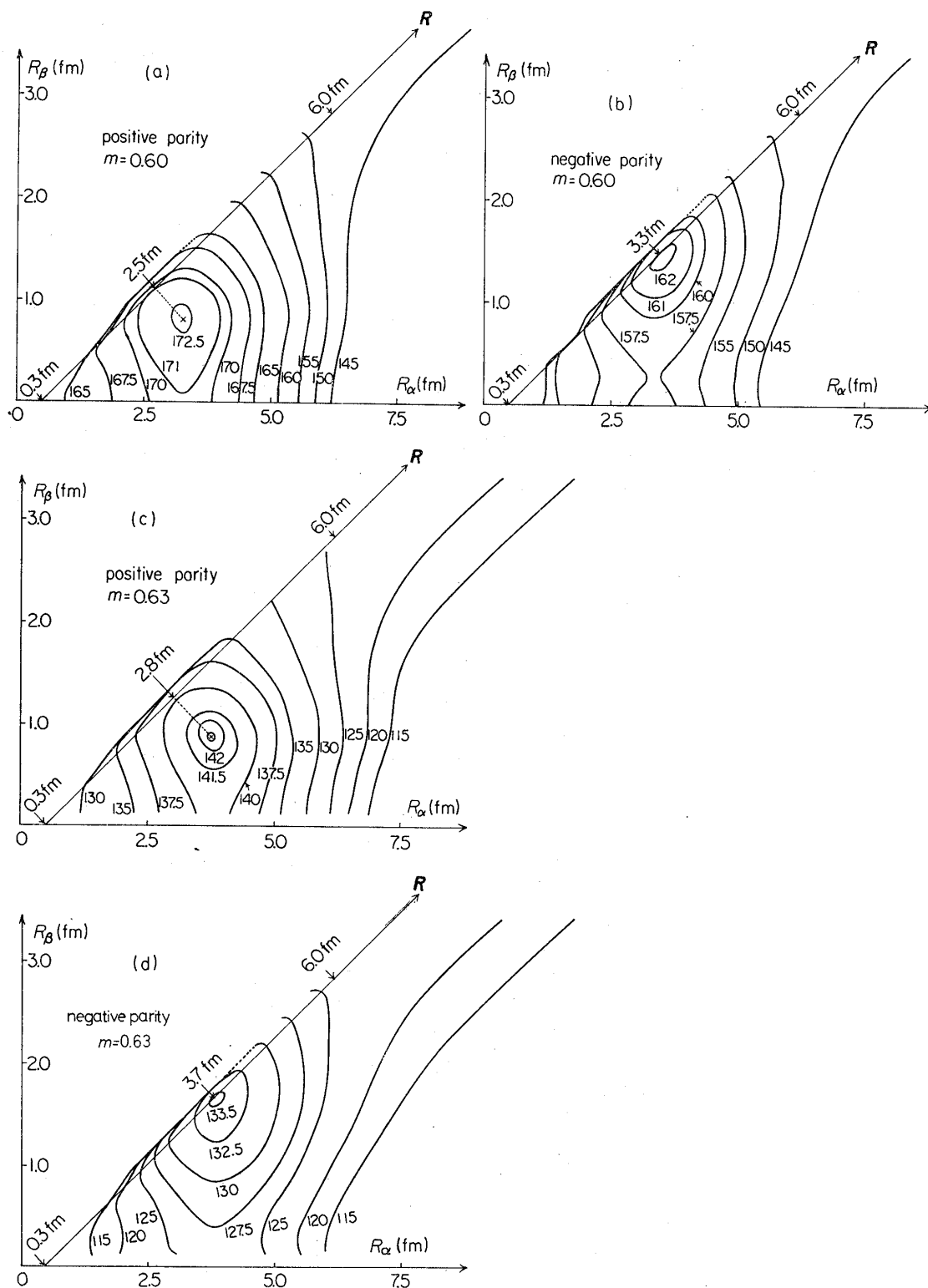


Fig. 3-7. Energy surfaces of $E^\pm(\mathbf{R}_\alpha, \mathbf{R}_\beta)$ for ^{20}Ne case, where the tetrahedron configuration of 4 α -particles with the small inter- α distance of 0.3 fm is identified as the subunit nucleus of ^{16}O . The oscillator parameters of the five α -particles are taken to be of the same value of $\nu_\alpha = 0.238 \text{ fm}^{-2}$. The numerical values in the figure are the binding energies in unit of MeV, and the value of m means the Majorana exchange mixture.

normal coordinate. As for the positive parity intrinsic state, the energy surface has a local minimum at the point with nearly the same R_α but small R_β in comparison with the negative parity case. Unlike the negative parity case, the curvature along the R_β direction is very small, which means that the motion along the inversion path takes place very easily and so there arises a strong mixing between the asymmetric configuration (which is nearly the di-molecular one) and the symmetric one. These results indicate that although the $K=0^-$ band may be well described by the pure di-molecular model, for the $K=0^+$ band there is a large deviation from the pure di-molecular configuration. Therefore, the results obtained here are found to correspond to the case (2) in the schematic model of §3.2, and then the gap energy is expected to be larger than that obtained by the pure inversion doublet picture based on the di-molecular model.

3.4 Summary and further problem

i) Based on the molecular picture, we have calculated the gap energy of the inversion doublet for α -C and α -O. When the di-molecule-like structure is good both for $K=0^-$ and $K=0^+$, the gap energy ΔE_0 is estimated to be 1~3 MeV. This value is known to be small but not very small compared with the frequency of the collective vibration in this mass region. This is a matter of course, because the nuclei under considerations are the light ones whose sizes are only 2~3 times larger than the range of the nuclear force.

ii) In the case of ^{16}O , the experimental gap energy is about 3.4 MeV, from which we can understand that the molecular picture for the structure of the $K=0^+$ band is not so bad. As for ^{20}Ne , since ΔE_0 is 5.2 MeV, we may conclude that the deviation from the molecule-like structure is fairly large. One can take two different viewpoints for the interpretation on this deviation. The first is to regard that the structure is of the deformed shell-like one to which the molecule-like structure dissolves. The second is the viewpoint that the molecular structure still persists in spite of the non-small deviation. We here have made the investigations from the second viewpoint considering the fact that the $K=0^-$ bands in ^{16}O and ^{20}Ne have the molecule-like structure as is seen in §2 and in this section. To represent this viewpoint, we considered the variation of the structure in the wide domain of the configuration space which includes both the asymmetric and symmetric ones. As a result of the studies we have shown that the large value of ΔE_0 can be obtained by the strong mixing of the symmetric configuration with the asymmetric one (molecular configuration) in the intrinsic structure for $K=0^+$ band. This result corresponds to the case (2) in the schematic model of §3.2, where the path length is not small but the central barrier is vanishingly small.

We discussed here the transient character only in the ground rotational

band of ^{20}Ne . However, such a transient character may be also reflected in the excited rotational bands. The comprehensive studies for the ground band states together with these excited states will bring the deep understanding about the interplay of the molecule-like and shell-like structures.

§4. Alpha-chain structures in nuclei

In the Ikeda diagram, the molecule-like structure composed of many α -particles is expected to have the highest excitation energy in each self-conjugate $4n$ -nucleus. The aggregations of $n\alpha$ -particles which couple weakly with each other may have many different configurations. An extreme one of them is the alpha-chain configuration of which the idea was proposed at very early time.⁷⁾ The linear chain structure is generally expected to have a high possibility of existence, because the Coulomb interaction favours energetically the linear chain configuration and the chance of alpha-particle collapse is least for such a configuration. The linear chain structures of 3α -particles have been candidated⁸⁾ for the second excited 0^+ (7.65 MeV) and 2^+ (10.3 MeV) states in ^{12}C . However, these levels have been found to have the properties which are inconsistent with the assumption of the chain structures. Since the rotational band in ^{16}O are experimentally observed,⁹⁾ which may have 4α -chain structures, theoretical considerations on α -chain structures are required again. First of all, we must obtain the systematic understanding of the properties for these levels in ^{12}C and ^{16}O . Then it is possible to understand why the alpha-chain structure is not realized in 3α system but may appear in 4α system. We study this problem by using the semi-classical alpha-particle model, which is also applied to the more general cases of $n\alpha$ -chain structures.

The purpose of this section is to summarize the theoretical studies on the α -chain structures. The first part (§§4.1 and 4.2) is devoted to the problems of 3α - and 4α -particle system whose properties are already known experimentally to some extent. We first discuss the meaning of the experimental facts (especially the decay widths) and show that the pure linear chain structure is inappropriate to explain the main properties of the levels in ^{12}C and that on the other hand the properties of the rotation band in ^{16}O is not inconsistent with the assumption of the linear chain structure¹⁰⁾ (§4.1). Next, in order to obtain the deep understanding of the noted levels we investigate the energetic properties and stabilities of 3α - and 4α -chain structures by using the effective α - α interaction which reproduces the properties of ^8Be (§4.2). In the second part (§4.3), similar theoretical treatments based on the α -particle model are made on the chain structures of $n\alpha$ -particles ($n \geq 5$), and we predict the energies of the $n\alpha$ -chain structures and discuss the possibility of the existence as the quasi-bound states.

In particular, we examine in detail the cases of 5α - and 6α -chain structures which might be of actual interests.

4.1 Characteristic properties of the noted levels in ^{12}C and ^{16}O

The second excited 0^+ state at 7.65 MeV in ^{12}C lies near the threshold for the α decay (7.37 MeV) and has about two times larger α decay width than the Wigner limit.³⁷⁾ Furthermore, a broad level was found around 10.3 MeV which has the same characters as the 0^+ state.³⁸⁾ If this state is assigned to be $J^\pi=2^+, ^8)$ the α reduced width is also very large (about seven times as large as the Wigner limit). If these two levels are the members of the same rotational band, the moment of inertia is found to be small ($\hbar^2/2\mathcal{J}=0.44$ MeV). This small value is quite impossible to be expected from the rotational band of the linear chain configuration of 3α -particles; if the distance between two α -particles is assumed to be 4.0 fm, the moment of inertia is obtained to be $\hbar^2/2\mathcal{J}_{\text{rig}}=0.16$ MeV.

In the case of ^{16}O , the rotational band starting from about 16.8 MeV was found through the $^{12}\text{C}(\alpha, ^8\text{Be})^8\text{Be}$ reaction⁹⁾ and has a very large moment of inertia just expected from the 4α -chain configuration with the mean α - α distance equal to 4.1 fm. However, the partial decay widths to the $^8\text{Be}+^8\text{Be}$ channel is very small, compared with the ^{12}C case where the decay widths to the $^8\text{Be}+\alpha$ channel is very large. Table IV-1 is given to exhibit the clear differences between the properties of $^{12}\text{C}^*$ and $^{16}\text{O}^*$.

It has been examined¹⁰⁾ whether the small ^8Be decay widths of the levels in ^{16}O can be compatible with the 4α -chain assumption which is supported from the energetic properties. The results of the analyses have demonstrated that the decays from such a peculiar configuration as the linear α -chain are mainly limited to the characteristic channels ($\alpha+3\alpha$ chain, $^8\text{Be}+^8\text{Be}$) and the spectroscopic factors for the decays to these channels are, however, greatly reduced. Thus the small ^8Be widths can be obtained under the assumption of the α -chain structure. The analyses have also

Table IV-1. Characteristic properties of $^{12}\text{C}^*$ and $^{16}\text{O}^*$, together with ^8Be ; E_{exc} being the band head energy, and E_{th} the threshold energy for the decay into alpha-particles.

	^8Be	$^{12}\text{C}^*$	$^{16}\text{O}^*$
E_{exc} (MeV)	0.0	7.65	16.75
E_{th} (MeV)	-0.095	7.27	14.44
$E_{\text{exc}}-E_{\text{th}}$ (MeV)	0.095	0.38	2.31
rotational band	confirmed	indistinct	distinct
$\frac{\hbar^2}{2\mathcal{J}_{\text{exp}}}$ (MeV)	0.5	(0.4)	0.06
reduced width	large	large	small

served us to interpret the experimental facts for $^{12}\text{C}^*$. That is, the large α decay widths of $^{12}\text{C}^*$ cannot be expected from the pure α -chain configuration and require large deviations from it. The deviations are also required to spread the energy spacing of the 0^+ and 2^+ states. It seems that 3α -particles do not possess a specified geometrical configuration but rather move freely in a weakly coupled systems. The reasonings which lead to these conclusions are made in detail in Ref. 10). Here, the outline and main results are briefly summarized.

(A) *The two anomalous levels in ^{12}C*

As well known, the second excited 0^+ state is a peculiar level with a large α decay width. The broad level at 10.3 MeV has been assigned to 2^+ and also has properties similar to the 0^+ state. Their decay scheme is shown in Fig. 4-1. The experimental α decay widths are cited in Table IV-2, where the reduced widths θ_α^2 are defined by Eq. (2.1) in §2, and the channel radius is taken as about 5 fm. Although the value of θ_α^2 depends on the channel radius, the dependence is found to be very weak for the present case; there occurs the difference by the factor less than two as long as the channel radius is changed in the range from 4 fm to 6 fm. We can see that the experimental reduced widths of both the 0^+ and 2^+ states are several times larger than the Wigner limit.

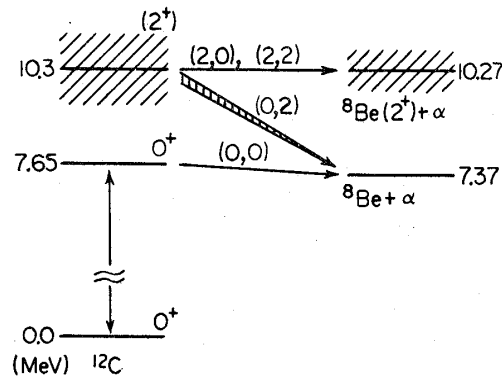


Fig. 4-1. Energetically possible decay modes from $^{12}\text{C}^*$ to $^8\text{Be} + \alpha$, where (L_1, L_2) denotes the angular momenta of ^8Be (L_1), and of the relative motion between ^8Be and α (L_2).

Table IV-2. Experimental values of the α decay widths of the two levels at 7.656 MeV (0^+) and 10.3 MeV (2^+ or 0^+) in ^{12}C .

Ex (MeV)	J^π	Γ_α	θ_α^2
7.656	0^+	9.7 ± 3.3 eV	2 Ref. 37)
10.3	2^+ 0^+	3.0 ± 0.7 MeV	7.5 1.5 Ref. 38)

To understand the large reduced widths of these levels we calculate the spectroscopic factors for the configurations specified by the angle β in Fig. 4.2. The calculated results are shown in Fig. 4.3, where the Bloch-Brink wave function, $\Phi(\beta)$, is used to represent the intrinsic states. For the linear chain configuration ($\beta=0$), the spectroscopic factor is found to be about 1/3 which is very small compared with the experimental one. It should be noted that the spectroscopic factor for the case near the triangular configuration ($\beta=\pi/3$) is about 2 which is comparable with the experimental one.

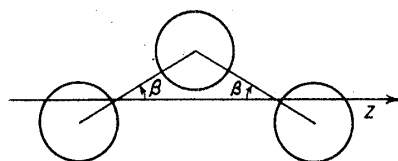


Fig. 4.2. Schematic picture for the configuration of three alpha-particles with the parameter β being the angle of the deviation from the linear arrangement along the z -axis.

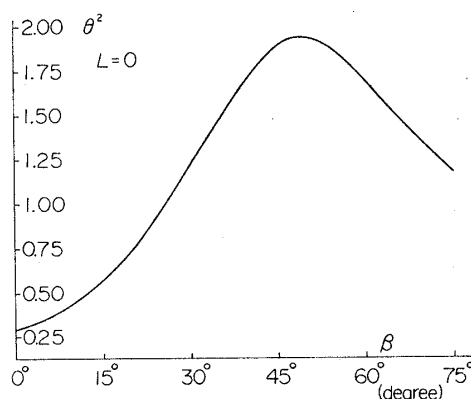


Fig. 4.3. Dependence of the spectroscopic factors on the configuration of three alpha-particles specified by the angle parameter, β .

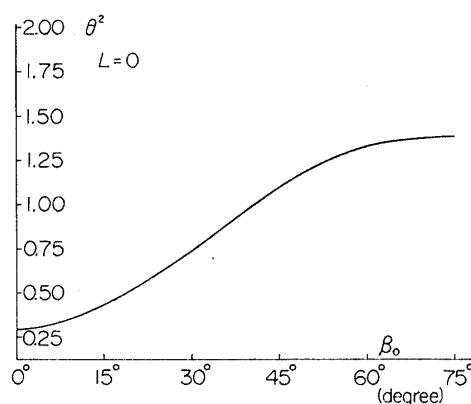


Fig. 4.4. The spectroscopic factors for the 3α -chain-like structures with the bending motion, shown as a function of the parameter β_0 which denotes the maximum amplitude of the bending motion, where the value at the point of $\beta_0=0$ is the one for the pure linear chain.

If we insist on the linear chain configuration, the effect of the zero-point motion, i. e., the bending motion with the large amplitude should be taken into account for getting the large reduced width. Now taking the maximum amplitude as β_0 , we show in Fig. 4.4 the dependence of the spectroscopic factor on β_0 , where the wave function which represents the bending motion is

$$\psi(\text{Bending}; \beta_0) = N \int_{-\beta_0}^{\beta_0} d\beta \phi(\beta). \quad (4.1)$$

Figure 4.4 shows that for small β_0 ($0 < \beta_0 < \pi/8$) the reduced width is small ($0.3 < \theta_\alpha^2 < 0.5$); it increases rapidly when β_0 exceeds $\pi/8$ and it is larger than 1 for $\beta_0 > \pi/5$. Therefore if we start from the linear chain configuration, the large mixing with the configuration around the triangular shape is needed to get the reduced width much larger than unity. Such a bending motion with extremely large amplitude is rather better understood in terms of the weak coupling of an alpha-particle with ^8Be which includes the triangular configuration dominantly.

Thus we conclude that the two levels in ^{12}C are not of the chain configuration but rather of the weak coupling of an alpha-particle with ^8Be or of the weak coupling of three alpha-particles.

(B) The anomalous rotational band in ^{16}O

The decay modes from the rotational levels are shown in Fig. 4.5. When the alpha-chain structure is assumed to be the intrinsic structure, the dominant decay channels are the channels of (chain+chain) and (α +chain), due to the peculiar character of its structure. In Fig. 4.6 we exhibit those special decay modes from $^{16}\text{O}^*$. As is displayed in the figure, the actual decays from the 4α -chain states in ^{16}O are energetically allowed to the

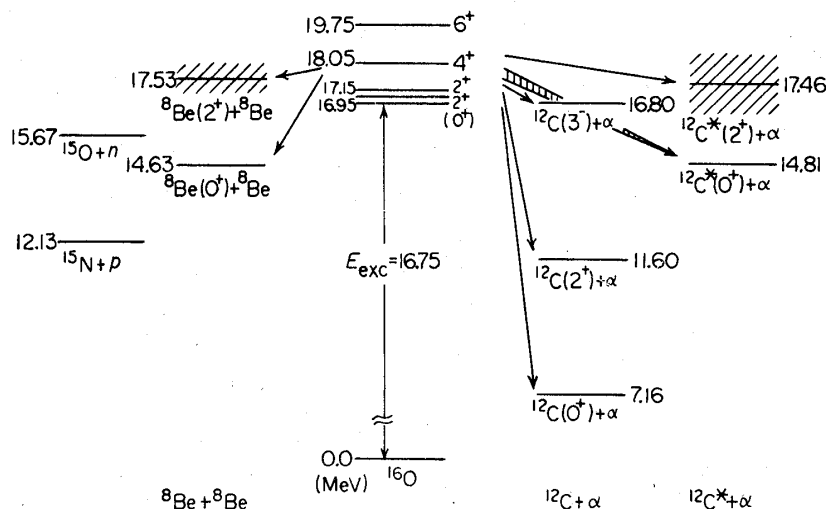
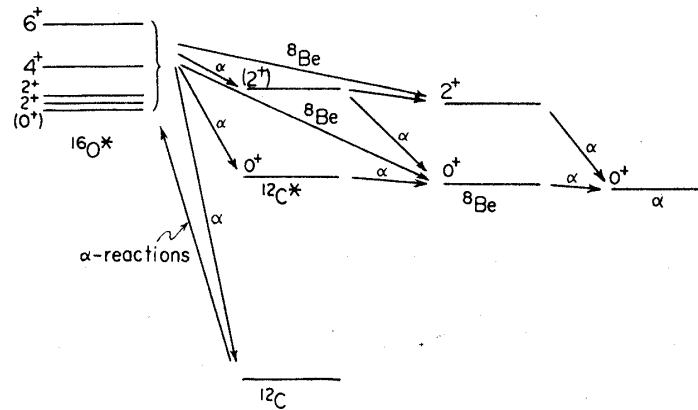


Fig. 4.5. Schematic diagram of the various kinds of decay modes of $^{16}\text{O}^*$.

Fig. 4-6. Schematic diagram of main decay series from $^{16}\text{O}^*$ to α .

channels of the $^8\text{Be} + ^8\text{Be}$ and $\alpha + ^{12}\text{C}^*$. Although $^{12}\text{C}^*$ is not of the pure 3α -chain structure as discussed above, it has surely the character as an aggregation of 3α -particles and then contains the fairly not small component of the 3α -chain configuration. Besides the $^8\text{Be} + ^8\text{Be}$ and $^{12}\text{C}^* + \alpha$, there contributes the $^{12}\text{C} + \alpha$ channel to the total width. For this channel, the Q -value for the decay is larger than the height of the Coulomb plus centrifugal barrier, yielding the large value of penetrability. Then even if the reduced width of this channel is very small, the partial width of this channel is possible to become appreciable. If we assume the reduced width of $^{12}\text{C} + \alpha$ channel to be about 1/100 times one of $^{12}\text{C}^* + \alpha$ channel, the partial width is surely obtained not to be small.

Now we evaluate the reduced widths of $^8\text{Be} + ^8\text{Be}$ and $^{12}\text{C}^* + \alpha$ and show the calculated results in Table IV-3. We see that the values of θ^2 (which is the reduced width in unit of the Wigner limit value, γ_w^2 , as shown in Eq.

Table IV-3. Dependence of the spectroscopic factors θ_L^2 on the distance parameter $R_{4\alpha}$ for the linear chain of 4α -particles.(a) $^8\text{Be}(0^+) + ^8\text{Be}(0^+)$ channel.

$R_{4\alpha}(\text{fm})$	1.0	2.0	3.0	4.0
θ_0^2	0.0083	0.020	0.026	0.014
θ_2^2	0.0076	0.020	0.025	0.014
θ_4^2	0.0069	0.019	0.025	0.013
θ_6^2	0.0057	0.017	0.023	0.013

(b) $^{12}\text{C}^*$ (3α chain, 0^+) + α channel.

$R_{4\alpha}(\text{fm})$	1.0	2.0	3.0	4.0
θ_0^2	0.108	0.122	0.121	0.087
θ_2^2	0.093	0.115	0.116	0.085
θ_4^2	0.074	0.099	0.107	0.081
θ_6^2	0.050	0.079	0.095	0.075

(2·1) of §2) are very small compared with unity. The reason for this smallness can be explained in connection with the geometrical shape of the linear configuration: The linear arrangement of the 4α -particles means to put the very strong constraint on the coupling scheme between the two fragment clusters ${}^8\text{Be} + {}^8\text{Be}$ or $\alpha + 3\alpha$ -chain and then it is necessary for the formation of the linear chain configuration to superpose suitably the many relative angular momentum states from zero to high value, while only a few components with the low angular momentum contribute to the actual decays.

We compare in Table VI-4 the experimental values of Γ_{total} and $\Gamma_{\alpha_0}\Gamma_{8\text{Be}}/\Gamma_{\text{total}}^2$ with the theoretical results. (Here the theoretical Γ_{total} is the sum of the partial widths given in Table IV-3.) As is seen from the Table, the order of magnitude of the experimental values for the 4^+ and 6^+ levels

Table IV-4. Comparison of the theoretical results with the experimental values of Γ_{total} and $\Gamma_{\alpha_0}\Gamma_{8\text{Be}}/\Gamma_{\text{total}}^2$ written in parentheses.

J^π	Γ_{total} (keV)	$\Gamma_{\alpha_0}\Gamma_{8\text{Be}}/\Gamma_{\text{total}}^2$
0^+	29	0.008
2^+	28 (370) (260)	0.010 (0.016) (0.027)
4^+	23 (20)	0.014 (0.025)
6^+	17 (70)	0.015 (0.011)

is obtained by theory. However, for the two 2^+ levels the experimental values of Γ_{total} are one order larger than those of 4^+ and 6^+ , and so large Γ_{total} value cannot be obtained theoretically. We gave in Ref. 10) an interpretation for this discrepancy that the existence of the two 2^+ levels might be the result of the coupling of a single level of the 4α -chain structure with a background compound level which has a total width about a few hundred keV, because they are separated by only a little energy and have similar characters to each other.

We can conclude from the above analyses of the decay properties that it is possible to interpret the decay properties without contradiction under the assumption of the 4α -chain structure. However, the present amounts of the experimental informations on the decay properties are scarce and we are forced to introduce some assumptions in the course of the theoretical estimations, for example, about the values of Γ_{α_0} . It is desirable to get more experimental informations by which we can more deeply understand the structure of these peculiar levels.

4.2 Study of the energetic properties with the alpha-particle model

The alpha-particle model has been known to work very well for the explanation of the main properties of the ground rotational band in ${}^8\text{Be}$.³⁹⁾

The approximations, which are necessary for treating the system of ${}^8\text{Be}$ as the di-molecule-like structure of two alpha-particles, are assured under the following conditions:

$$\frac{\hbar^2}{2\mathcal{J}} < E_{\text{vib}} < E_{\text{int}}, \quad (4.2)$$

where E_{int} , E_{vib} and $\hbar^2/2\mathcal{J}$ are the energies of the intrinsic excitations, of the relative motion and of the rotational motion, respectively. Actually, the condition of Eq. (4.2) is approximately satisfied in the system of ${}^8\text{Be}$; $E_{\text{int}} \gtrsim 16$ MeV, $E_{\text{vib}} \approx 10$ MeV which is the zero-point energy of the relative motion between the two alpha-particles, and $\hbar^2/2\mathcal{J} \approx 0.5$ MeV. Here we use the alpha-particle model for the studies of the alpha-chain structures, considering that the condition of Eq. (4.2) is also approximately valid for the $n\alpha$ -chain structures.

The studies are started with the assumption that the alpha-chain configuration is energetically in local equilibrium. Then the motions of the alpha-particles are represented in terms of the displacements around its equilibrium configuration and the energy of the system can be obtained as the sum of the zero-point energies with respect to all the degrees of freedom for the displacements. For the chain configuration of more than two alpha-particles, the displacements are divided into the two parts, that is, the longitudinal and transverse ones. The restoring forces for the longitudinal displacements may be assumed to be the same interactions between the two alpha-particles as in ${}^8\text{Be}$. However, we have not known the restoring forces for the transverse displacements. If the interactions between the two alpha-particles which are not adjacent are only the Coulomb interactions, the restoring forces for the transverse displacements come only from the Coulomb forces, which are not expected to be strong. Therefore, we anticipate that the other factors, which cannot be taken into account in the semi-classical alpha-particle model, may give the important effects on the transverse motions. So our considerations with the alpha-particle model are limited and then the restoring forces for the transverse displacements are rather regarded as the phenomenological ones. Thus the problems of alpha-chain structures have to be studied under the following conditions;

$$\hbar^2/2\mathcal{J} \lesssim \hbar\omega_0^{(L)} < \hbar\omega_0^{(T)} < E_{\text{int}}, \quad (4.3)$$

where $\hbar\omega_0^{(L)}$ and $\hbar\omega_0^{(T)}$ are the zero-point energies of the longitudinal and transverse vibrations, respectively.

Under the conditions of Eq. (4.3), the following two points are considered to be the main problems for the alpha-chain structure:

i) If the alpha-particle model works well, what amount of the total energy of the chain system can be obtained from the knowledge of the inter-

actions between the two alpha-particles combined with Coulomb interactions?

ii) How large are the amplitudes of the transverse vibrations? Does there arise the inconsistency with the original assumption of the linearity for the chain configuration?

In the following these problems are studied for the 3α - and 4α -chain cases of which experimental informations are at hand to some extent, and we try to obtain the fundamental understanding of these cases, comparing the theoretical results with the experimental properties.

As an effective interaction between the neighbouring two alpha-particles, we assume the local potential with the harmonic oscillator shape which is simplest in reproducing the properties of ^8Be . This effective potential includes the contribution due to the Coulomb forces as well as the nuclear forces. It is assumed for a while that the two alpha-particles not in the immediate vicinity interact with each other only via the Coulomb forces.

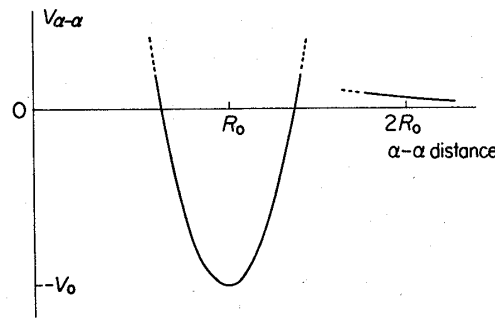


Fig. 4.7. Schematic diagram of the effective potential between two alpha-particles around $R=R_0$ and $R=2R_0$.

Figure 4.7 shows schematically the effective potential between the two alpha-particles. The assumed Hamiltonian for the $n\alpha$ -chain system is now written as

$$\mathcal{H} = -\frac{\hbar^2}{2M_\alpha} \sum_{i=1}^n \nabla_i^2 + \sum_{i=1}^{n-1} \left\{ \frac{1}{2} K_0 (|\mathbf{r}_i - \mathbf{r}_{i+1}| - R_0)^2 - V_0 \right\} + \frac{1}{2} \sum_{|i-j| \neq 0,1}^n \frac{4e^2}{|\mathbf{r}_i - \mathbf{r}_j|}. \quad (4.4)$$

Here the parameters K_0 , V_0 and R_0 can be determined so as to reproduce the properties of ^8Be ; (i. e., the binding energy, the moment of inertia and the extension of the relative wave function between the two α -particles). The extension of the relative wave function is determined with reference to the phenomenological potentials which reproduce the phase shifts for the α - α scattering and also to the analysis based on the resonating group method. The typical values of the potential parameters are taken to be

$$V_0 = 11.7 \text{ MeV}, K_0 = 26.4 \text{ MeV} \cdot \text{fm}^{-2}, R_0 = 4.0 \text{ fm}. \quad (4.5)$$

Under the approximation of the small displacements the Hamiltonian of Eq. (4.4) is transformed into the one consisting of the set of the harmonic oscillators by introducing the normal coordinates. The total binding energy of the $n\alpha$ -chain system is thus given as the sum of the zero-point energies;

$$\begin{aligned} E(n) &= E^{(//)}(n) + E^{(\perp)}(n) + E_c(n), \\ E^{(//)}(n) &= \sum_{i=1}^{n-1} \left(\frac{1}{2} \hbar \omega_i^{(//)} - V_0 \right), \\ E^{(\perp)}(n) &= \sum_{i=1}^{n-2} \hbar \omega_i^{(\perp)}, \\ E_c(n) &= \frac{1}{2} \sum_{|i-j| \neq 0,1}^n \frac{4e^2}{|i-j|R_0}, \end{aligned} \quad (4.6)$$

where $\omega_i^{(//)}$ is the normal frequency of the longitudinal vibration which has the $n-1$ degrees of freedom except for the translation, $\omega_i^{(\perp)}$ is the normal frequency of the transverse vibration which has the twofold degeneracy and the $2(n-2)$ degrees of freedom except for the translation and the rotation, and $E_c(n)$ is the sum of the Coulomb energies between the two alpha-particles which are not adjacent. The calculated energies of Eq. (4.6) are listed in Table IV-5 for the cases of $n=3$ and 4.*) The energy of the 4α -chain structure can be seen to be in good agreement with the experimental band head energy of $^{16}\text{O}^*$. The energy of the 3α -chain structure is known to be a little larger than the energy of the second excited zero plus state by about 0.6 MeV.

Next we study the deviation of the alpha-particles from the linear arrangement. To represent the deviation, we use the angle operator, $\hat{\theta}^2$, which is defined by the following formula;

Table IV-5. Energies of the 3α - and 4α -chain systems calculated with the alpha-particle model.

	3α -chain	4α -chain
$E^{(//)}$	-0.61	-1.51
$E^{(\perp)}$	0.84	1.90
E_c	0.72	1.92
E	0.95	2.31

(unit in MeV)

*) The normal frequencies $\omega_i^{(//)}$ and $\omega_i^{(\perp)}$ are easily obtained analytically. They are given in units of $(K_0/M_\alpha)^{1/2}$ and $(4e^2/M_\alpha R_0^3)^{1/2}$, respectively, as follows;

$$\begin{aligned} \omega_i^{(//)} &= \begin{cases} 1, \sqrt{3} & \text{for } 3\alpha\text{-chain,} \\ \sqrt{2-\sqrt{2}}, \sqrt{2}, \sqrt{2+\sqrt{2}} & \text{for } 4\alpha\text{-chain,} \end{cases} \\ \omega_i^{(\perp)} &= \begin{cases} \sqrt{3/4} & \text{for } 3\alpha\text{-chain,} \\ \sqrt{17/36}, \sqrt{175/108} & \text{for } 4\alpha\text{-chain.} \end{cases} \end{aligned}$$

$$\hat{\theta}^2 = \sum_{k=1}^{n-2} \hat{\theta}_k^2 \approx \frac{1}{(n-2)} \frac{1}{R_0^2} \sum_{i=1}^{n-2} \left(\frac{\mathbf{s}_i + \mathbf{s}_{i+2}}{2} - \mathbf{s}_{i+1} \right)^2, \quad (4.7)$$

where $\hat{\theta}_k$ is the angle variable which represents the normal coordinate as is indicated in Fig. 4.8, and $\mathbf{s}_i = (x_i, y_i)$ is the transverse displacement of the i -th alpha-particle. The expectation values of $\hat{\theta}^2$ for the ground state are given in Table IV-6. The calculated results are compared with a critical angle, θ_{cr} , at which the three alpha-particles contact with each other. If $\langle \hat{\theta}^2 \rangle > \theta_{cr}^2$, the original assumption of the linear arrangement breaks down. When the restoring forces for the transverse displacements are only due to the Coulomb interactions, the value of $\langle \hat{\theta}^2 \rangle^{1/2}$ for the 3α -chain case is known to become about the same as $\theta_{cr} (= \pi/3)$. Therefore, the 3α -particles deviate from the linear arrangement so considerably that such a 3α -chain overlaps with a triangular configuration. The value of $\langle \hat{\theta}^2 \rangle^{1/2}$ for the 4α -chain case is about $0.9 \cdot \pi/3$. Although this value is a little smaller than the one for the 3α -chain case, the deviation of 4α -particles from the linear arrangement is understood to be appreciably large.

As mentioned before, the obtained energy for the 3α -chain system is larger than the energy of the second excited zero plus state by 0.6 MeV. It seems to be very important that the energy of the 3α -chain system cannot reach the experimental one of this anomalous state, even if the amplitude of the transverse vibration is taken to be so large that there arises

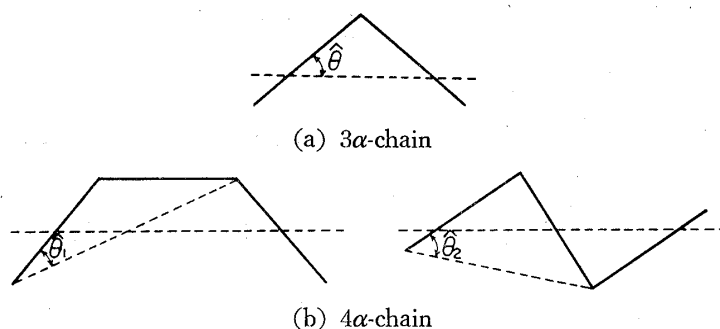


Fig. 4.8. Angle coordinates of the transverse normal vibrational modes; (a) for the 3α -chain and (b) for 4α -chain.

Table IV-6. Expectation values of the mean square amplitude of the transverse vibration for the 3α - and 4α -chain system.

	3α -chain	4α -chain
$\langle \hat{\theta}_k^2 \rangle$	1.17	0.245 0.661
$\langle \hat{\theta}^2 \rangle$	1.17	0.906

the appreciable overlapping with the triangular configuration. Therefore to reproduce the experimental energy, we have to consider that the interacting three alpha-particles move more freely in the system and that the interplays between the triangular and the chain configurations may play an important role. To examine the above interpretation, we calculate the binding energy of the triangular configuration with use of the same potential parameters as adopted for the studies of the alpha-chain system. The energy is obtained to be about -0.23 MeV which corresponds to the excitation energy of 7.0 MeV from the ground state of ^{12}C . Figure 4.9 shows that the anomalous zero plus state lies between the states with the triangular and linear chain configurations within the energy range of about 1.5 MeV. If we also consider the mixings of the triangular configuration in the ground state, the energy of the triangular structure may be pushed up and nearer to the experimental energy. Therefore, we suppose, as a possible interpretation for the anomalous zero plus (and also 2^+) state, that it is rather of the triangular structure with the large fluctuations in which the chain structure is partially involved.

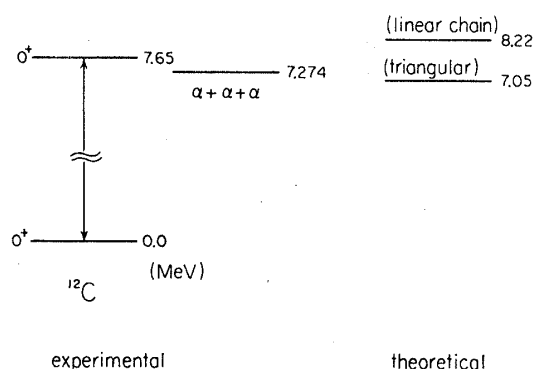


Fig. 4.9. Comparison of the theoretical energies predicted by the alpha-particle model with the experimental energy of the second excited zero plus state in ^{12}C .

As for the 4α -chain structure, the calculated energy is found to agree with the experimental band head energy, but the transverse vibrations have not small amplitudes under the restoring potentials due to the Coulomb forces. In such a case of the large zero-point amplitudes, the rotation-vibration couplings may give the effects on the rotational spectra. However, the experimental rotational band accords to the $I(I+1)$ -rule and has the large moment of inertia which is expected from the 4α -chain structure. If we can assume the small zero-point amplitudes for the transverse vibrations, where the strength of the restoring forces are larger than that of the Coulomb forces, the rotational spectra may be in good agreement with the experiments but the energy of the system may become larger than the experimental one. Here we study the effects of the rotation-vibration coupling on the energy spectra and their dependence on the zero-point amplitudes

of the transverse vibrations.

The rotation-vibration Hamiltonian which includes the coupling between the transverse vibrations and the rotational motion can be given by

$$\begin{aligned}\mathcal{H} &= \mathcal{H}_{\text{rot}}^0 + \mathcal{H}_{\text{vib}} + \mathcal{H}_{\text{rot-vib}}, \\ \mathcal{H}_{\text{rot}}^0 &= \frac{\hbar^2}{2\mathcal{J}_0} (\mathbf{I}_x^2 + \mathbf{I}_y^2), \\ \mathcal{H}_{\text{vib}} &= \sum_{k=1}^{n-2} \left(-\frac{\hbar^2}{2M_\alpha} \frac{d^2}{d\boldsymbol{\xi}_k^2} + \frac{1}{2} C_k \boldsymbol{\xi}_k^2 \right) \\ \mathcal{H}_{\text{rot-vib}} &= \frac{\hbar^2}{2} \left(\frac{1}{\mathcal{J}_x} - \frac{1}{\mathcal{J}_0} \right) \mathbf{I}_x^2 + \frac{\hbar^2}{2} \left(\frac{1}{\mathcal{J}_y} - \frac{1}{\mathcal{J}_0} \right) \mathbf{I}_y^2,\end{aligned}\quad (4.8)$$

where $\mathcal{H}_{\text{rot}}^0$ is the Hamiltonian for the rotation of the linear alpha-chain, \mathcal{H}_{vib} is the Hamiltonian for the transverse vibrations expressed by the normal coordinates, $\boldsymbol{\xi}_k$, and $\mathcal{H}_{\text{rot-vib}}$ is the coupling of the transverse vibrations with the rotational motion. Here, \mathcal{J}_0 is the moment of inertia for the alpha-chain in row which is now assumed to be in equilibrium. And \mathcal{J}_x and \mathcal{J}_y are the moments of inertia for the rotation around the x - and y -axis, respectively, which involve the transverse coordinates. When $\mathcal{H}_{\text{rot-vib}}$ are expanded around the equilibrium point, the first term vanishes and the other terms represent the rotation-vibration couplings. The leading term of $\mathcal{H}_{\text{rot-vib}}$ is conveniently divided into the two parts:

$$\mathcal{H}_{\text{rot-vib}} = \mathcal{H}_{\text{r-v}}^{(1)} + \mathcal{H}_{\text{r-v}}^{(2)}, \quad (4.9)$$

where $\mathcal{H}_{\text{r-v}}^{(1)}$ conserves the z -component of the angular momentum, while $\mathcal{H}_{\text{r-v}}^{(2)}$ does not. Since the effects of $\mathcal{H}_{\text{r-v}}^{(2)}$ on the spectra can be estimated to be far smaller than those of $\mathcal{H}_{\text{r-v}}^{(1)}$, we here discuss only the term of $\mathcal{H}_{\text{r-v}}^{(1)}$. The leading term of $\mathcal{H}_{\text{r-v}}^{(1)}$ can be expressed with use of the angle coordinates, $\hat{\theta}_k$, shown in Fig. 4.8 as

$$\mathcal{H}_{\text{r-v}}^{(1)} = \frac{\hbar^2}{2\mathcal{J}_0} (\mathbf{I}_x^2 + \mathbf{I}_y^2) \sum_{k=1}^{n-2} \eta_k \hat{\theta}_k^2, \quad (4.10)$$

where $\eta_1 = 5/6$ for 3α -chain, and $\eta_1 = 2$ and $\eta_2 = 22/25$ for 4α -chain. When we take into account the effects of $\mathcal{H}_{\text{r-v}}^{(1)}$ on the spectra, the rotational spectra can be given by

$$E_I = \frac{\hbar^2}{2\mathcal{J}_0} I(I+1) + \sum_{k=1}^{n-2} \hbar \omega_k^{(1)} \left\{ \left(1 + \frac{B_k}{\mathcal{J}_0} \langle \hat{\theta}_k^2 \rangle^2 \eta_k I(I+1) \right)^{1/2} - 1 \right\}, \quad (4.11)$$

which can be expanded for small $\langle \hat{\theta}_k^2 \rangle^2 I(I+1)$ as

$$E_I \simeq \frac{\hbar^2}{2\mathcal{J}_0} (1 + \delta_1) I(I+1) - \frac{\hbar^2}{2\mathcal{J}_0} \delta_2 I^2 (I+1)^2, \quad (4.11)'$$

where

$$\delta_1 = \sum_{k=1}^{n-2} \eta_k \langle \hat{\theta}_k^2 \rangle,$$

$$\frac{B_1}{\mathcal{J}_0} = \frac{1}{3} \text{ and } \delta_2 = \frac{1}{12} \langle \hat{\theta}_1^2 \rangle^3 \eta_1^2 \quad \text{for } 3\alpha\text{-chain,}$$

$$\frac{B_1}{\mathcal{J}_0} = \frac{4}{5}, \quad \frac{B_2}{\mathcal{J}_0} = \frac{4}{25} \text{ and } \delta_2 = \frac{1}{5} \langle \hat{\theta}_1^2 \rangle^3 \eta_1^2 + \frac{1}{25} \langle \hat{\theta}_2^2 \rangle^3 \eta_2^2 \quad \text{for } 4\alpha\text{-chain}$$

and $\langle \hat{\theta}_k^2 \rangle$ is the expectation value of $\hat{\theta}_k^2$ with respect to the zero-point transverse vibration.

The values of $\langle \hat{\theta}_k^2 \rangle$ have been shown in Table IV-6 for the case of the Coulomb restoring forces. Then we can obtain that $\delta_1=0.97$, $\delta_2=0.09$ for 3α -chain and $\delta_1=1.07$, $\delta_2=0.02$ for 4α -chain. Therefore, it can be understood that $\mathcal{H}_{r.v}^{(1)}$ tends to broaden the level spacing about two times largely than the unperturbed one of $(\hbar^2/2\mathcal{J}_0)I(I+1)$. The disturbance of the $I(I+1)$ -rule due to $\mathcal{H}_{r.v}^{(1)}$ is also appreciable but not so strong for the 4α -chain case. Next we change somewhat arbitrarily the strength of the restoring forces for the transverse vibrations and study the dependence of

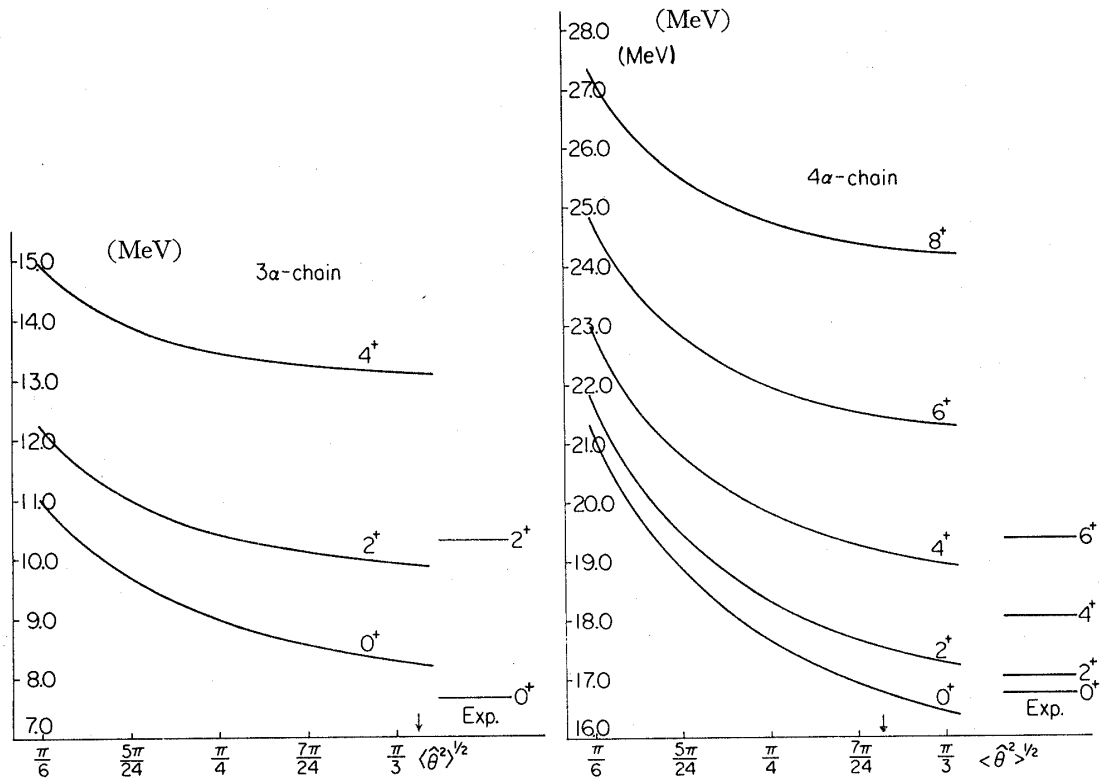


Fig. 4.10. Energy spectra of the 3α - and 4α -chain systems as a function of the root mean square amplitude of the transverse vibrations. The values at arrow point correspond to the case of the Coulomb restoring potential. The ordinates denote the excitation energies in MeV unit.

the energy spectra on the strength or on the root mean square amplitude, $\langle \hat{\theta}^2 \rangle^{1/2}$ of Eq. (4.7). Figure 4.10 displays the calculated energy spectra. It can be seen from the figure that for the 4α -chain case the band head energy shows a good correspondence with the experimental one around the Coulomb restoring forces but the calculated spectra deviate from the observed spectra. As was expected, the experimental spectra are reproduced only when we assume the smaller zero-point amplitude ($\langle \hat{\theta}^2 \rangle^{1/2} \approx \pi/6$) than the one in the case of the Coulomb restoring forces. However, the band head energy is strongly pushed up for the small amplitude. We can also see that for the 3α -chain case the band head energy does not reach to the experimental one, even if $\langle \hat{\theta}^2 \rangle^{1/2} \approx \pi/3$, as was discussed before, but the spectra are fairly improved.

4.3 $n\alpha$ -chain structures

We have studied the experimental properties of $^{12}\text{C}^*$ from the viewpoint of the stability of the 3α -chain configuration and further examined whether the properties observed in ^{16}O are derived under the assumption of the 4α -chain structure. At this stage it is interesting to consider theoretically the possibility of the linear chain structures composed of many α -particles on the basis of the knowledge obtained in the analyses of ^8Be , $^{12}\text{C}^*$ and $^{16}\text{O}^*$. Here we attempt to derive the properties of the $n\alpha$ -chain structures ($n \geq 5$) with use of the alpha-particle model of which the parameters are chosen to be suitable for the case of ^8Be and $^{16}\text{O}^*$.

If we adopt the Hamiltonian given in Eq. (4.4), the energies of the $n\alpha$ -chain states are expressed as the sum of three terms with different characters;

$$E(n) = E^{(//)}(n) + E^{(1)}(n) + E_c(n). \quad (4.6)'$$

The energy of $E^{(//)}(n)$ is the correlation energy of the normal longitudinal vibrations due to the attractive forces acting between the neighbouring α -particles and the energy gain of $E^{(//)}(n)$ is nearly proportional to the number n . The energy of $E^{(1)}(n)$ is a sum of the zero-point energies of the transverse vibrations caused by the restoring forces originated from the Coulomb interactions. $E_c(n)$ is the Coulomb energy of the $n\alpha$ -particles in the equilibrium positions without the contribution between the adjacent α -particles. Both $E^{(1)}(n)$ and $E_c(n)$ are the positive increasing functions of n contrary to the energy gain of $E^{(//)}(n)$.

The normal frequencies for the longitudinal vibrations are easily solved as follows,

$$\hbar\omega_l^{(//)} = 2\hbar \sqrt{\frac{K_0}{M_\alpha}} \sin \frac{l\pi}{2n}. \quad (l=1, 2, \dots, n-1) \quad (4.11)$$

And the correlation energy $E^{(//)}(n)$ can be expressed with the following simple form:

$$\begin{aligned} E^{(//)}(n) &= \sum_{l=1}^{n-1} \left\{ \frac{1}{2} \hbar \omega_l^{(//)} - V_0 \right\} \\ &= \frac{1}{2} \left(\cot \frac{\pi}{2n} - 1 \right) \hbar \sqrt{\frac{K_0}{M_\alpha}} - (n-1) V_0 \\ &\approx \frac{1}{2} \hbar \sqrt{\frac{K_0}{M_\alpha}} \left(\cot \frac{\pi}{2n} - 1 - \sqrt{2} (n-1) \right). \end{aligned} \quad (4.12)$$

The last expression of Eq. (4.12) is obtained by equating the energy of 2α -chain state (${}^8\text{Be}$) to zero; ($V_0 = \hbar \sqrt{K_0/2M_\alpha}$). The restoring potential for the transverse vibrations is assumed to be given by the increase of the Coulomb energy when the $n\alpha$ -particles are displaced under the condition that the distances of the adjacent α -particles are fixed;

$$\delta V^{(1)}(n) = \sum_{i < j} \frac{4e^2}{|\mathbf{r}_i - \mathbf{r}_j|} - \sum_{i < j} \frac{4e^2}{|i-j|R_0} \quad (4.13)$$

with

$$|\mathbf{r}_i - \mathbf{r}_{i+1}| = R_0 \quad \text{for } i=1, \dots, n-1,$$

which is expanded under the approximation of the small displacement as

$$\begin{aligned} \delta V^{(1)}(n) &\sim \frac{4e^2}{R_0} \frac{1}{2R_0^2} \left\{ \sum_{i=1}^{n-1} C_{n,i} (\mathbf{s}_i - \mathbf{s}_{i+1})^2 \right. \\ &\quad \left. - \sum_{i < j} \frac{1}{(j-i)^3} (\mathbf{s}_i - \mathbf{s}_j)^2 \right\} \end{aligned} \quad (4.14)$$

with

$$C_{n,i} = \sum_{k=1}^i \sum_{l=1}^{n-1} \frac{1}{(k+l-1)^2} \quad \text{and} \quad \mathbf{s}_i = (x_i, y_i).$$

Diagonalization of the Hamiltonian with the potential energy $\delta V^{(1)}(n)$ yields

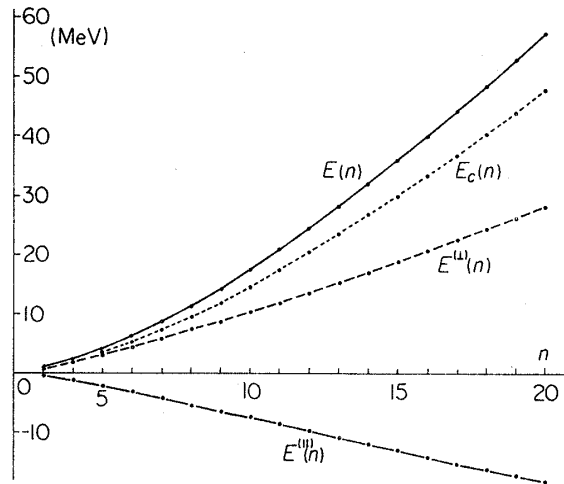


Fig. 4.11. Energies of the $n\alpha$ -chain system calculated with the alpha-particle model.

Table IV-7. Calculated energies of the $n\alpha$ -chain system, where E_{exc} is the excitation energy of the $n\alpha$ -chain from the ground state in the corresponding self-conjugate $4n$ -nucleus.
(unit in MeV)

n	3	4	5	6	7	8	9	10	11
$E(n)$	0.95	2.3	4.1	6.3	8.7	11.4	14.4	17.5	20.8
E_{exc}	8.2	16.7	23.3	34.7	47.2	56.8	66.4	76.6	85.2
n	12	13	14	15	16	17	18	19	20
$E(n)$	24.3	28.0	31.8	35.7	39.8	43.9	48.2	52.6	57.0
E_{exc}	96.5	107.9	119.7	—	—	—	—	—	—

the normal frequencies for the transverse vibrations (degenerate in the x, y directions).

The calculated energies of Eq. (4.6) are shown in Fig. 4.11 and Table IV-7. We see that the correlation energy $E^{(//)}(n)$ approximately cancels the zero-point energies, $E^{(L)}(n)$, of the transverse vibrations in the wide range of n . Thus the energy of $E(n)$ takes the value near the Coulomb energy $E_c(n)$.

To know how the α -particles deviate from the linear chain configuration, we calculate the mean value of the following operator, as defined in Eq. (4.7)

$$\hat{\theta}^2 = \frac{1}{(n-2)} \cdot \frac{1}{R_0^2} \sum_{i=1}^{n-2} \left(\frac{\mathbf{s}_i + \mathbf{s}_{i+2}}{2} - \mathbf{s}_{i+1} \right)^2. \quad (4.15)$$

This operator represents the local deviation from the linearity for the neighbouring three alpha-particles. The value of $\langle \hat{\theta}^2 \rangle^{1/2}$ is shown in Fig. 4.12, where the expectation value is taken with respect to the ground state. We see that $\langle \hat{\theta}^2 \rangle^{1/2}$ decreases with increase of n , which means that the linear arrangement becomes good for the long α -chain. (It should be noted that the value of $\langle \hat{\theta}^2 \rangle^{1/2}$ rapidly decreases at $n \approx 4$.)

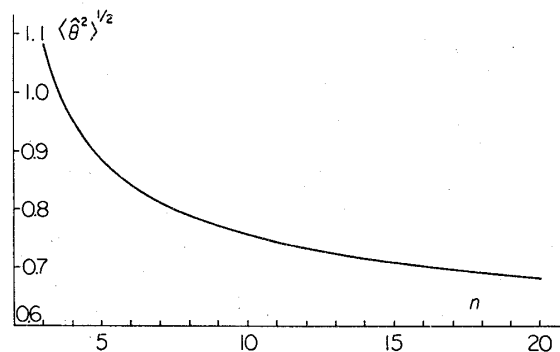


Fig. 4.12. Root mean square amplitude of the transverse vibrations in the $n\alpha$ -chain system.

We have solved the Hamiltonian for the $n\alpha$ -chain under the bound state approximation, assuming that the $n\alpha$ -chain states are quasi-bound. Next we consider whether or not the $n\alpha$ -chain structures exist as the quasi-bound states or resonances. For that purpose it is useful to note that such peculiar states with the α -chain structure decay dominantly into the specific channels where the fragment nuclei are also of chain configurations, as was discussed in §4.1. Here only two-body decays are taken into considerations,

$$n\alpha\text{-chain} \rightarrow (n-k)\alpha\text{-chain} + k\alpha\text{-chain.} \quad (4.16)$$

$$(n-k \geq k)$$

A rough criterion for the existence as the quasi-bound states is given by the comparison of the Q -values with the Coulomb barriers for the various decay modes. The Q -values are estimated by use of the energies for the $n\alpha$ -chain structures, that is, $E(n) - E(n-k) - E(k)$. (Use is made of the experimental values for $n=2, 3$ and 4 , where the energy for $n=3$ is taken as of the second excited zero plus state in ^{12}C .) The Coulomb barrier is roughly estimated by the Coulomb energy between the two fragment chains which contact with each other in row. Table IV-8 displays the Q -values and Coulomb barriers for the various decay modes up to $n=10$.

Table IV-8. Comparison of Q -values with Coulomb barriers for the decay modes of $n\alpha \rightarrow (n-k)\alpha + k\alpha$; Q -value written in the upper and Coulomb barrier in the lower part.

$n \backslash k$	1	2	3	4	5
10	3.15 3.61	6.00 5.91	8.43 7.39	8.94 8.24	9.30 8.51
9	2.94 3.45	5.56 5.58	7.74 6.86	7.95 7.48	
8	2.71 3.28	5.07 5.20	6.94 6.26	6.80 6.60	
7	2.45 3.08	4.51 4.78	6.02 5.56		
6	2.15 2.85	3.85 4.27	5.51 4.71		
5	1.80 2.57	3.64 3.66			
4	1.94 2.24	2.13 2.88			
3	0.28 1.79				

upper- Q -value
lower-Coulomb barrier
unit in MeV

We see that the difference between the Q -values and the Coulomb barriers is small in this region ($n \leq 10$). We thus infer that the $n\alpha$ -chain structures may exist energetically as the quasi-bound states. It is noted here that for the large $n\alpha$ -chain the rotational spectra are condensed, and so, if they exist, the $n\alpha$ -chain structures may be found as the gross resonances rather than the quasi-bound states.

We evaluate semi-quantitatively the decay widths of the 5α - and 6α -chain structures which may most likely be observed experimentally. For these cases, the decay scheme is presented in Fig. 4.13. The partial decay widths defined by Eq. (2.1) for the channels of Eq. (4.16) are calculated with use of the following formula for the spectroscopic factors which are obtained in the α -Boson limit;¹⁰⁾

$$\begin{aligned} & \theta_{L((L_1, L_2)L_3, L_4)}^2 (n\alpha \rightarrow (n-k)\alpha + k\alpha) \\ &= \frac{8}{(1+\delta_{k,1})(1+\delta_{k,n-k} \delta_{L_1, L_2})} \frac{(2L_1+1)(2L_2+1)(2L_4+1)}{(2L+1)} \\ & \times (L_1 0 L_2 0 | L_3 0)^2 (L_3 0 L_4 0 | L 0)^2 \\ & \times \frac{\mathcal{G}_{L_1}(\frac{1}{3}(n-k-1)(n-k)(n-k+1)\lambda) \mathcal{G}_{L_2}(\frac{1}{3}(k-1)k(k+1)\lambda) \mathcal{G}_{L_4}(k(n-k)n\lambda)}{\mathcal{G}_L(\frac{1}{3}(n-1)n(n+1)\lambda)}, \end{aligned} \quad (4.17)$$

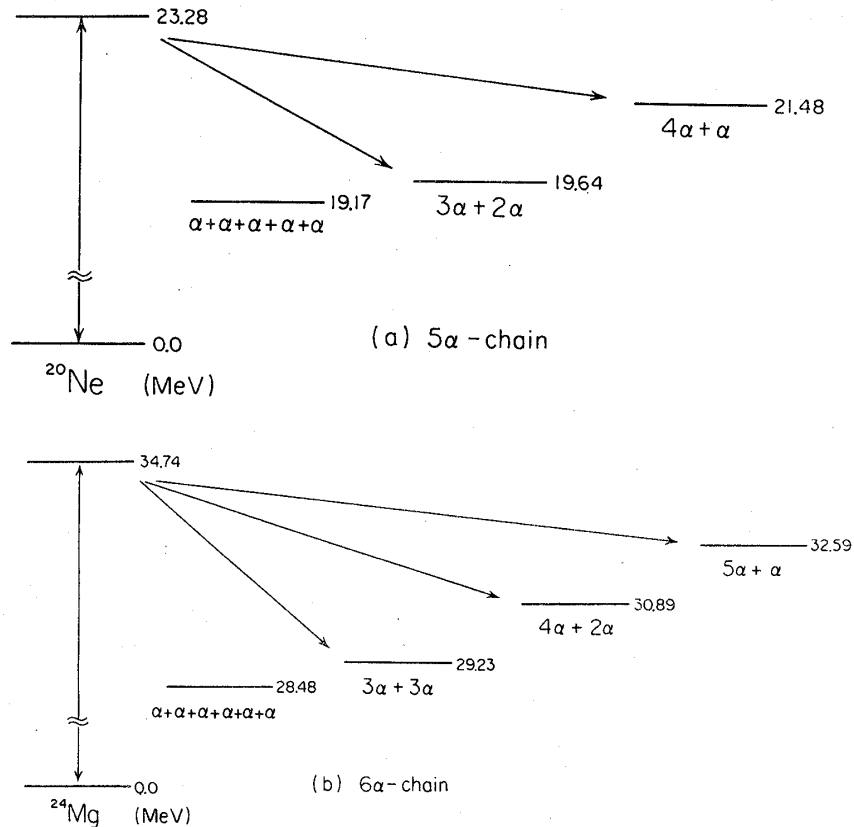


Fig. 4.13. Decay schemes for the states with the 5α - and 6α -chain structures.

Table IV-9. Calculated partial widths for the decays from the states with the 5α - and 6α -chain structures.(a) 5α -chain ($L=0$)

decay channel	$4\alpha(L_1=0) + \alpha$		$4\alpha(L_1=2) + \alpha$		$3\alpha(L_1=0) + 2\alpha(L_2=0)$	
Q -value (MeV)	1.80		1.50		3.64	
L_4	0		2		0	
θ^2	0.0433		0.203		0.00779	
channel radius (fm)	10.0	11.0	10.0	11.0	10.0	11.0
penetrability P_{L_4}	0.830	1.27	0.112	0.234	3.18	4.24
Γ (keV)	14	18	9	15	6	7

(b) 6α -chain ($L=0$)

decay channel	$5\alpha(L_1=0) + \alpha$		$5\alpha(L_1=2) + \alpha$		$5\alpha(L_1=4) + \alpha$	
Q -value (MeV)	2.15		1.95		1.50	
L_4	0		2		4	
θ^2	0.0252		0.121		0.200	
channel radius (fm)	12.0	13.0	12.0	13.0	12.0	13.0
penetrability P_{L_4}	1.61	2.22	0.613	1.02	0.00895	0.0240
Γ (keV)	11	12	19	28	0.5	1

where L , L_1 and L_2 are the angular momenta of the parent and two fragment chains, respectively, L_3 is the vector sum of the angular momenta of the two chains, L_4 is the relative angular momentum between the two chains, λ means νR_0^2 and $\mathcal{J}_L(z)$ is the modified spherical Bessel function defined by $\sqrt{\pi}/2(z/2)^L \sum_{n=0}^{\infty} (z/2)^{2n}/n! \Gamma(L+n+3/2)$. (ν is the size parameter of α -particle.) The calculated partial widths are shown in Table IV-9, where the channels with a very small contribution are omitted. The channel of $(n-1)\alpha + \alpha$ is seen to contribute mainly to the decay and the other channels have very small partial widths because of the smallness of the penetrabilities and/or of the spectroscopic factors. Thus we have obtained the values of a few ten keV as the decay widths for $n=5$ and 6 , which are the same order as the experimental decay widths of the levels (4^+ and 6^+) in the anomalous rotational band of ^{16}O . For the estimation of the decay widths, we used the Q -values given in Table IV-8, although there are some ambiguities

Table IV-10. Dependence of the decay widths on the Q -value around the theoretical one.

δQ (MeV)	5α -chain	6α -chain
-0.25	18	19
0.0	40	41
0.25	78	72

(unit in keV)

in the theoretical study on the energy of the $n\alpha$ -chain system. We examine the dependence of the decay widths on the Q -values around the theoretical ones. Table IV-10 shows that the dependence on the Q -values is not so strong for the case of the alpha-chain structure.

§5. Multi-molecular structures with the linear chain configuration

The studies of the multi-molecular structures with the linear chain configuration have been developed for the cases of the alpha-particles in §4. As a natural extension, we can take up the problems of the other linear chain structures consisting of the alpha-particles and the other constituents with the closed shell nature, like ^{12}C and ^{16}O . For such linear chain structures the direct experimental informations have been scarcely known and then the theoretical considerations are expected to be developed steadily only when the knowledges of the di-molecule-like structures are fully available.

Since we have understood the characteristic natures of α -C and α -O as summarized in §§2 and 3, it will be possible to extend the studies to the linear chain structures which are connected with the bonds of α - α , α -C and α -O. Such kinds of linear chain structures have many varieties of the configurations including the alpha-chain ones, which are listed up for the three-body cases;

$$\begin{aligned} & \text{i) } \alpha\text{-}\alpha\text{-}\alpha, \quad \text{ii) } \alpha\text{-}\alpha\text{-C}, \quad \alpha\text{-}\alpha\text{-O}, \quad \text{iii) } \alpha\text{-C-}\alpha, \quad \alpha\text{-O-}\alpha, \\ & \text{iv) } \text{C-}\alpha\text{-C}, \quad \text{C-}\alpha\text{-O}, \quad \text{O-}\alpha\text{-O} \end{aligned} \quad (5.1)$$

and for the four-body cases;

$$\begin{aligned} & \text{i) } \alpha\text{-}\alpha\text{-}\alpha\text{-}\alpha, \quad \text{ii) } \alpha\text{-}\alpha\text{-}\alpha\text{-C}, \quad \alpha\text{-}\alpha\text{-}\alpha\text{-O}, \\ & \text{iii) } \alpha\text{-}\alpha\text{-C-}\alpha, \quad \alpha\text{-}\alpha\text{-O-}\alpha, \\ & \text{iv) } \text{C-}\alpha\text{-}\alpha\text{-C}, \quad \text{C-}\alpha\text{-}\alpha\text{-O}, \quad \text{O-}\alpha\text{-}\alpha\text{-O}, \\ & \text{v) } \alpha\text{-C-}\alpha\text{-C}, \quad \alpha\text{-C-}\alpha\text{-O}, \quad \alpha\text{-O-}\alpha\text{-C}, \quad \alpha\text{-O-}\alpha\text{-O} \end{aligned} \quad (5.2)$$

and so on.

The studies in this section are mainly devoted to the cases of the three-body as the first step of the considerations for the more general linear chain structures. The actual interests are most strong for the three-body cases, because they will have many chances of the observations through the heavy ion reactions. Especially the case iv) of three-body in which two large subunit nuclei are connected with an intermediate alpha-particle is interesting, since it is one of the most typical examples.

If the cases of C- α -C, C- α -O and O- α -O are compared with the

case of α - α - α , it is easily supposed that an essential difference between them is the increase of the effects due to the Coulomb interactions. We assume that the linear chain configurations are in the local equilibrium. We can easily know the characteristic roles of the Coulomb interaction between the subunit nuclei at both sides by expanding it around the local equilibrium; the zeroth order contributes to the energy shift, the first order for the longitudinal displacements plays the role to separate the subunit nuclei and the second order for the transverse displacements behaves as the restoring force against them. Since the coupling constant of the Coulomb interaction is roughly proportional to $Z_1^2/A_1^{1/3} \propto A_1^{5/3}$, where the subunit nuclei on both sides are assumed to have the same mass, A_1 , and charge number, Z_1 , the roles of the Coulomb interaction increase rapidly with mass number, A_1 . Then the flexibility toward prolongation and the stiffness against bend are understood to increase for the cases of the large subunit nuclei on both sides.

In the case of three alpha-particles, the restoring force due to the Coulomb interactions has been shown in §4 not to be strong enough to confine the zero-point oscillation around the linear chain configuration. However, the rapid increase of the coupling constant with mass number, A_1 , is considered to bring about the stabilization of the three-body linear chain structures like as C- α -C, C- α -O, O- α -O and others. Increase of the flexibility toward prolongation brings us an interesting problem that the molecular structure may appear more clearly in such a linear chain case of three-body than in di-molecular cases; for example, although the di-molecule-like structure is not clearly seen in the ground band of ^{20}Ne , the molecule-like structures of C-Ne and O-Ne are rather expected to be realized as those of C- α -O and O- α -O.

5.1 The interactions between an alpha-particle and a residual core in the contact region

The studies of the alpha-chain structures have been done on the premise that the ground band of ^8Be has the intrinsic structure consisting of two alpha-particles which weakly couple with each other. The energy of the ground state has been therefore utilized as the binding energy of weakly coupled two alpha-particle system, $E_0(2\alpha)$, which is nearly equal to zero. As for the di-molecule-like structures of α -C and α -O, the binding energy of $E_0(\alpha, \text{C})$ and $E_0(\alpha, \text{O})$ can be also obtained from the experimental energies of the rotational bands with these intrinsic structure by using the following formula;

$$\begin{aligned} E_0(\alpha, A) &= \frac{1}{2}(E_0^{(-)}(\alpha, A) + E_0^{(+)}(\alpha, A)) \\ &= E_0^{(-)}(\alpha, A) - \frac{1}{2}\Delta E_0(\alpha, A), \end{aligned} \quad (5.3)$$

where $E_0^{(\pm)}$ are the energies of the negative $(-)$ and positive $(+)$ parity bands measured from the threshold and $\Delta E_0(\alpha, A)$ is the gap energy between them. Since we have clearly identified the di-molecule-like structures in the negative parity bands (as was studied in §2), the empirical energies of these bands can be used as $E_0^{(-)}(\alpha, C)$ and $E_0^{(-)}(\alpha, O)$. However, the empirical energies of the positive parity bands cannot be used straightforwardly because their intrinsic structures are not necessarily the same as the negative parity bands, especially for the case of ^{20}Ne . (See the discussions in §3.) Here we consider that it is rather better for the gap energy, ΔE_0 , between both bands to take the values of $1 \text{ MeV} \lesssim \Delta E_0 \lesssim 3 \text{ MeV}$ obtained theoretically. In the following discussions the gap energy is assumed tentatively to be 3.0 MeV for both cases of α -C and α -O. Then the binding energies are obtained as

$$\begin{aligned} E_0(\alpha, ^{12}\text{C}) &= 0.6 \text{ MeV}, \\ E_0(\alpha, ^{16}\text{O}) &= -0.7 \text{ MeV}, \end{aligned} \quad (5.4)$$

which are also known to be nearly equal to zero.

To study the linear chain structures connected with the bonds of α - α , α -C and α -O, we have to assume the potentials responsible for the relative motion by which the binding energies of Eq. (5.4) are reproduced. As was shown in §§2 and 3, the reduced widths and the moments of inertia of the negative rotational bands indicate that the zero-point oscillation for the relative motion is confined in the region around the contact distance. We assume therefore a simple potential with a harmonic oscillator type;

$$V(R) = \frac{1}{2} K_0 (R - R_0)^2 - V_0. \quad (5.5)$$

The parameter, R_0 , expresses the equilibrium point for the di-molecular configuration and is assumed to be of the contact distance which is now given by

$$R_0 = 1.25 \times (A_1^{1/3} + A_2^{1/3}) \text{ (fm)}. \quad (5.6)$$

The parameter of the restoring force, K_0 , is treated as an unknown parameter. The potential depth, V_0 , can be determined by using the following formula;

$$V_0 = -E_0(A_1, A_2) + \frac{\hbar}{2} \sqrt{\frac{K_0}{M_{12}}}, \quad (5.7)$$

where M_{12} is the reduced mass, $M_1 M_2 / (M_1 + M_2)$. In Table V-1, the potential parameters are given for the cases of α - α , α -C and α -O, where the parameter, K_0 , is assumed to be $20.6 \text{ MeV} \cdot \text{fm}^{-2}$ for all cases.

Table V-1. A typical set of parameters for the effective potentials in the contact region for the cases of α - α , α -C and α -O.

	α - α	α -C	α -O
E_0 (MeV)	0.09	0.6	-0.7
K_0 (MeV·fm ⁻²)	20.6	20.6	20.6
V_0 (MeV)	10.3	7.9	8.9
R_0 (fm)	4.0	4.8	5.1

5.2 The energies of the three- and four-body linear chain structures

To estimate the binding energy for the linear chain structures, we use the same model as for the alpha-chain structure, that is, the interactions between the adjacent subunit nuclei are assumed to be those defined by Eq. (5.5) and the interactions between the other pairs to be the Coulomb interactions. We give the general formula of the binding energies for the three-body cases;

$$E_0(A_1, A_2, A_3) = \left\{ \frac{1}{2} (\hbar\omega_1^{(//)} + \hbar\omega_2^{(//)}) - V_0(A_1, A_2) - V_0(A_2, A_3) \right\} + \hbar\omega^{(1)} + \frac{Z_1 Z_3 e^2}{R_{13}}, \quad (5.8)$$

$$\hbar\omega_{1,2}^{(//)} = \frac{\hbar}{\sqrt{2}} \left\{ \frac{K_{12}}{M_{12}} + \frac{K_{23}}{M_{23}} \pm \sqrt{\left(\frac{K_{12}}{M_{12}} - \frac{K_{23}}{M_{23}} \right)^2 + 4 \frac{K_{12} K_{23}}{M_2^2}} \right\}^{1/2}$$

and

$$\hbar\omega^{(1)} = \hbar \left(\frac{Z_1 Z_3 e^2}{R_{13}^2} \right)^{1/2} \left(\frac{1}{M_1} \frac{R_{23}}{R_{12} R_{13}} + \frac{1}{M_2} \frac{R_{13}}{R_{12} R_{23}} + \frac{1}{M_3} \frac{R_{12}}{R_{23} R_{13}} \right)^{1/2}$$

with

$$M_{ij} = \frac{M_i M_j}{M_i + M_j}, \quad (i, j = 1, 2, 3)$$

where K_{ij} is the coupling constant of the restoring force between the adjacent subunit nuclei (i, j), R_{ij} the distance between the two subunit nuclei and M_i the mass of the i -th subunit nucleus. For the four-body cases, the binding energies can also be given as

$$E_0(A_1, A_2, A_3, A_4) = \sum_{i=1}^3 \left\{ \frac{1}{2} \hbar\omega_i^{(//)} - V_0(A_i, A_{i+1}) \right\} + \sum_{i=1}^2 \hbar\omega_i^{(1)} + \left\{ \frac{Z_1 Z_3 e^2}{R_{13}} + \frac{Z_2 Z_4 e^2}{R_{24}} + \frac{Z_1 Z_4 e^2}{R_{14}} \right\} \quad (5.9)$$

with similar notations as for the three-body cases.

Numerical results of the binding energies are tabulated in Tables V-2

Table V-2. Calculated energies for the three-body linear chain structures connected with the bonds of α - α , α -C and α -O. (unit in MeV)

	α - α - α	α - α -C	α - α -O	α -C- α	α -O- α	C- α -C	C- α -O	O- α -O
$\hbar\omega_{1,2}^{(H)}$	14.67 25.40	11.48 24.19	10.95 24.07	14.67 18.94	14.67 17.97	8.47 22.41	7.91 22.21	7.34 22.00
$E^{(H)}$	-0.52	-0.31	-1.67	1.06	-1.48	-0.30	-1.71	-3.13
$E^{(L)}$	0.85	1.21	1.33	0.47	0.41	1.67	1.83	2.00
E_c	0.73	1.96	2.53	0.59	0.56	5.35	6.93	8.98
E_0	1.06	2.86	2.19	2.12	-0.51	6.72	7.05	7.85
E_{exc}	8.3	14.8	16.2	14.0	13.5	30.6	30.8	31.0

Table V-3. Calculated energies for the four-body linear chain structures connected with the bonds of α - α , α -C and α -O. (unit in MeV)

	α - α - α - α	α - α - α -C	α - α - α -O	α - α -C- α	α - α -O- α	C- α - α -C
$\hbar\omega_{1,2,3}^{(H)}$	11.23 20.74 27.10	8.82 19.03 26.60	8.35 18.84 26.55	10.58 17.34 24.32	10.37 16.68 24.13	6.78 16.94 25.91
$E^{(H)}$	-1.30	-1.20	-2.58	0.11	-2.49	-1.20
$\hbar\omega_{1,2}^{(L)}$	0.67 1.25	0.84 1.67	0.90 1.82	0.47 1.32	0.42 1.42	1.04 2.18
$E^{(L)}$	1.92	2.51	2.72	1.79	1.84	3.22
E_c	1.94	4.04	5.02	2.98	3.50	7.72
E_0	2.56	5.35	5.16	4.88	2.85	9.74
E_{exc}	17.0	26.6	29.2	26.1	26.9	40.6

	C- α - α -O	C- α - α -O	α -C- α -C	α -C- α -O	α -O- α -C	α -O- α -O
$\hbar\omega_{1,2,3}^{(H)}$	6.34 16.67 25.84	5.90 16.40 25.77	7.07 17.57 22.41	6.66 17.36 22.29	6.87 16.94 22.15	6.41 16.78 22.00
$E^{(H)}$	-2.62	-4.04	-0.08	-1.48	-2.69	-4.10
$\hbar\omega_{1,2}^{(L)}$	1.12 2.37	1.21 2.57	0.57 1.82	0.61 1.99	0.51 1.94	0.55 2.13
$E^{(L)}$	3.49	3.78	2.39	2.60	2.45	2.68
E_c	9.45	11.54	7.13	9.07	8.63	11.03
E_0	10.32	11.28	9.44	10.19	8.39	9.61
E_{exc}	40.7	41.5	40.3	40.5	38.7	39.8

and V-3 for the cases of the three-body and four-body linear chain structures, respectively, when we use the parameters, K_{ij} , $V(A_i, A_j)$ and R_{ij} , given in Table V-1. The characteristics for the binding energies are very similar with the α -chain cases: The first term in Eqs. (5·8) and (5·9) is the correlation energy due to the longitudinal vibrations, the second term is the zero-point energy for the transverse vibrations and the energy gain of the first term cancels nearly the loss of the second term. Therefore the binding energies of $E_0(A_1, A_2, A_3)$ and $E_0(A_1, A_2, A_3, A_4)$ become nearly equal

to the Coulomb energies which are the third term of Eqs. (5.8) and (5.9). The model Hamiltonian includes the unknown parameter of K_0 , which is here assumed to be $20.6 \text{ MeV} \cdot \text{fm}^{-2}$. The dependence of the binding energies on these parameters is, however, known to be very small.

5.3 The stabilities of the linear chain structures

The instabilities of the linear chain structures are considered to arise along the direction of the two kinds of displacements, that is, the transverse and longitudinal ones. For the transverse direction the instability occurs due to the mixing of the linear chain structure with the lower order molecular structures. If the amplitudes of the transverse vibrational modes become very large, three subunit nuclei contacts with one another and then the linear chain structure is possibly dispersed in a wide energy region as the results of the mixing due to the nuclear interactions. As for the longitudinal direction, we here take up only the instability due to decays or fissions. If the energy of the linear chain structure is nearer or larger than the top of the Coulomb plus centrifugal barrier for a decay or fission mode, the lifetime of the linear chain structure may become shorter than a periodic time of the zero-point oscillations. If so, the linear chain structure cannot be realized. In the following, the stabilities for such two kinds of displacements are discussed for the three-body cases.

To examine the stability for the transverse displacements, we calculate the mean value of the square of the angle coordinate of $\hat{\theta}$, which represents the deviation from the linear arrangement. The mean value of $\langle \hat{\theta}^2 \rangle^{1/2}$ should be compared with the critical angle, θ_{cr} , defined as the angle at which the three subunit nuclei contact with one another. A parallel comparison can be also done with use of the zero-point energy for the transverse mode instead of $\langle \hat{\theta}^2 \rangle^{1/2}$. In this case the zero-point energy is compared with the critical energy, $\delta V_c(\theta_{\text{cr}})$, which corresponds to the increase of the Coulomb energy at θ_{cr} . The comparisons of the above two quantities are made in Table V-4. The case iv) of Eq. (5.1), i. e., C- α -C, (C- α -O) and O- α -O, is found to satisfy the stability condition of

Table V-4. Comparisons of the energy and of the amplitude for the transverse vibration with the respective critical values in the case of the three-body linear chains.

	α - α - α	α -C- α	α -O- α	C- α -C	O- α -O
$\langle \hat{\theta}^2 \rangle^{1/2}$	1.08	0.89	0.85	0.56	0.47
θ_{cr}	1.05	1.15	1.17	0.94	0.91
$\hbar\omega^{(1)}$ (MeV)	0.85	0.47	0.41	1.67	2.00
$\delta V_c(\theta_{\text{cr}})$ (MeV)	0.73	0.86	0.89	3.71	5.65

$$\langle \hat{\theta}^2 \rangle < \theta_{cr}^2 \text{ and } \hbar\omega^{(1)} < \delta V_c(\theta_{cr}). \quad (5.10)$$

On the contrary the cases i) and iii), that is, α - α - α , α -C- α and α -O- α do not satisfy the condition of Eq. (5.10), namely,

$$\langle \hat{\theta}^2 \rangle \approx \theta_{cr}^2, \quad \hbar\omega^{(1)} \lesssim \delta V_c(\theta_{cr}). \quad (5.10)'$$

To exhibit the characteristics for the energy and the amplitude of the transverse vibration, we show in Fig. 5.1 the dependence of $\hbar\omega^{(1)}$ and $\langle \hat{\theta}^2 \rangle$ on the mass (charge) number for the case of A_1 - α - A_1 according to the formulae;

$$\begin{aligned} \hbar\omega^{(1)} &= \hbar \{ Z_1^2 e^2 (M_\alpha + 2M_1) / 4R_0^3 M_\alpha M_1 \}^{1/2}, \\ \langle \hat{\theta}^2 \rangle &= \hbar \{ (M_\alpha + 2M_1) / Z_1^2 e^2 R_0 M_\alpha M_1 \}^{1/2} \\ &= \hbar\omega^{(1)} / E_c, \end{aligned} \quad (5.11)$$

where E_c is equal to $Z_1^2 e^2 / 2R_0$. For the sake of the comparison, $\theta_{cr} = \cos^{-1}(A_1^{1/3} / (A_1^{1/3} + 4^{1/3}))$ and $\delta V_c(\theta_{cr})$ are also drawn in Fig. 5.1. Equation (5.11) together with Fig. 5.1 shows that the values of $\hbar\omega^{(1)}$ and $\langle \hat{\theta}^2 \rangle$ are nearly proportional to $A_1^{1/2}$ and $A_1^{-7/6}$, respectively and that the stability for the transverse displacements increases with the mass (charge) number of the subunit nuclei on both sides.

As mentioned before, the stability condition for the longitudinal direction

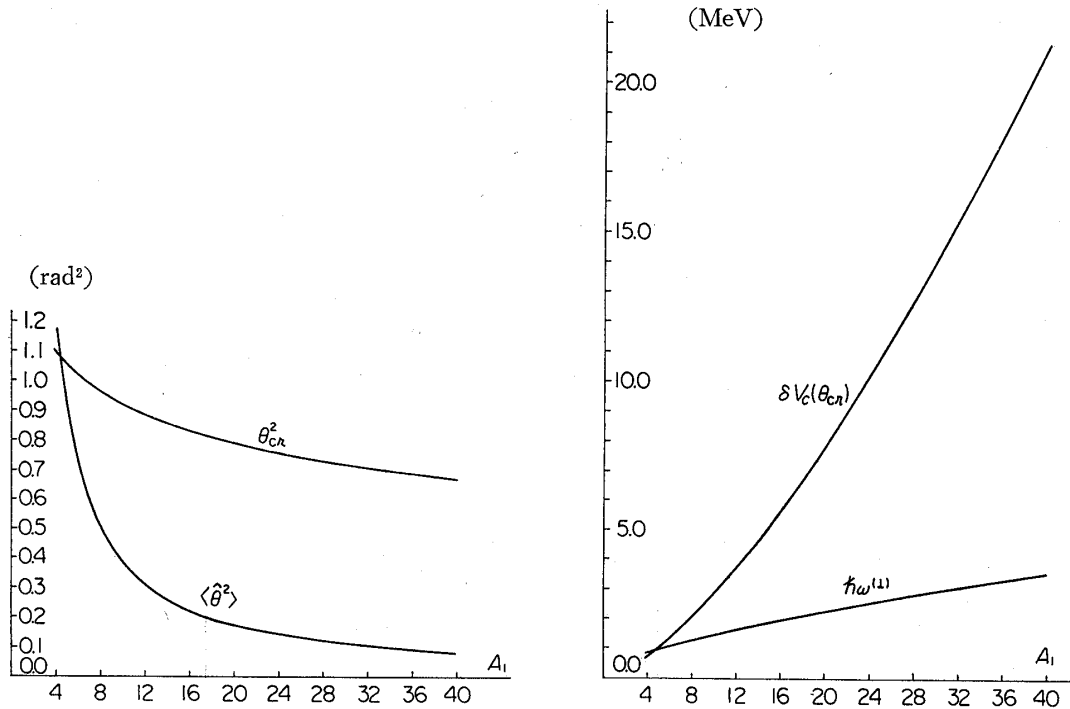


Fig. 5.1. Dependence of the energy and the amplitude of the transverse vibration on the mass number of A_1 for the case of the three-body linear chain of A_1 - α - A_1 .

can be expressed as

$$\frac{1}{\omega^{(1)}} < \frac{\hbar}{\Gamma}, \quad (5.12)$$

where the frequency of the transverse mode, $\omega^{(1)}$, is adopted to represent the periodic time of the zero-point oscillation because of $\omega^{(1)} < \omega^{(//)}$, and Γ is the decay width of the state with the linear chain structure. When the

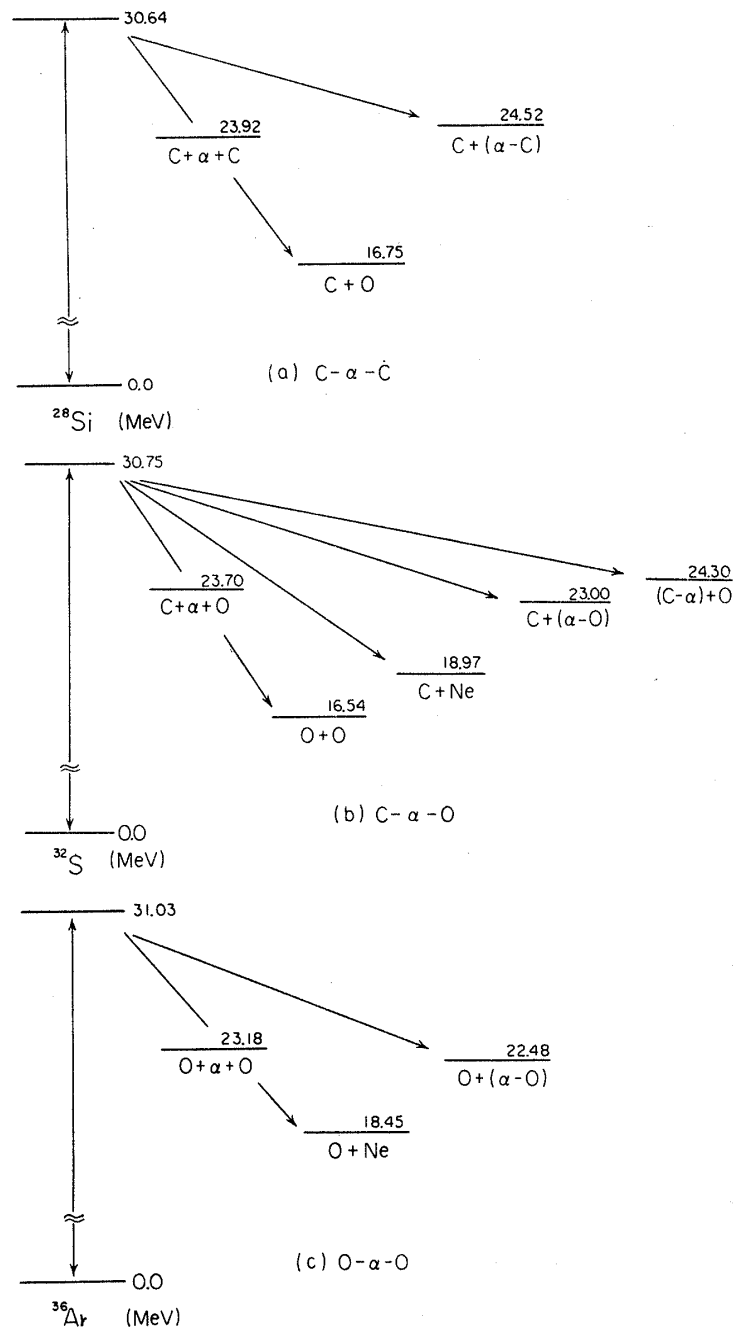


Fig. 5.2. Decay schemes for the cases of the three-body linear chains of $C-\alpha-C$, $C-\alpha-O$ and $O-\alpha-O$.

condition of Eq. (5.12) is satisfied, the state is understood to be the quasi-bound state in which the linear chain structure can be realized within the lifetime of \hbar/Γ .

We discuss here about the decay widths of the states with the three-body linear chain structures, in order to see the stability condition of Eq. (5.12). The total decay widths are obtained as the sum of the partial widths for the various decay channels. Similarly to the alpha-chain case, we assume however that the decays are possible only through the two-body decay channels, $A_1-A_2-A_3 \rightarrow A_1 + (A_2-A_3)$ and $(A_1-A_2) + A_3$. Figure 5.2 displays the decay schemes for the cases of C- α -C, C- α -O and O- α -O.

To know the magnitude of the partial width qualitatively, we compare at first the Q -value with the barrier height for the decay of $A_1-A_2-A_3 \rightarrow A_1 + (A_2-A_3)$. The Q -value is given by

$$\begin{aligned} Q_{L,L_1} &= E_L(A_1, A_2, A_3) - E_{L_1}(A_2, A_3), \\ E_L(A_1, A_2, A_3) &= E_0(A_1, A_2, A_3) + \frac{\hbar^2}{2\mathcal{J}} L(L+1), \\ E_{L_1}(A_2, A_3) &= E_0(A_2, A_3) + \frac{\hbar^2}{2\mathcal{J}_1} L_1(L_1+1), \end{aligned} \quad (5.13)$$

where L is the spin of the parent nucleus and \mathcal{J} its moment of inertia and L_1 and \mathcal{J}_1 are the corresponding quantity of the fragment nucleus, of (A_2-A_3) . The classical moment of inertia is used for \mathcal{J} and \mathcal{J}_1 . The height of the Coulomb plus centrifugal barrier is estimated with the following equation;

$$V_{L_2} = \frac{Z_1 Z_2 e^2}{R_{12} + \delta R} + \frac{Z_1 Z_3 e^2}{R_{12} + R_{23} + \delta R} + \frac{\hbar^2 L_2 (L_2 + 1)}{2\mu \left(R_{12} + \frac{M_3}{M_2 + M_3} R_{23} + \delta R \right)^2}, \quad (5.14)$$

where L_2 and μ are the angular momentum and the reduced mass of the relative motion, respectively and δR is a parameter introduced to represent the indefiniteness of the channel radius (δR is here assumed to be 1.0 fm.). The values of $E_L(A_1, A_2, A_3)$, $E_{L_1}(A_2, A_3)$ and V_{L_2} are shown in Fig. 5.3 for the above three cases. In these cases the Q -value is found to be smaller than the barrier height, especially for the small angular momentum L . It cannot be therefore expected to obtain the large penetrability. However, in the decay of the state with large L the Q -value is known to come near the top of the barrier due to the difference between the moments of inertia for the proportional constants of the rotational energy and for the centrifugal potential near the channel radius. Therefore we can suppose that the high spin state may have appreciably large partial widths.

Next we estimate the partial widths according to Eq. (2.1), where the

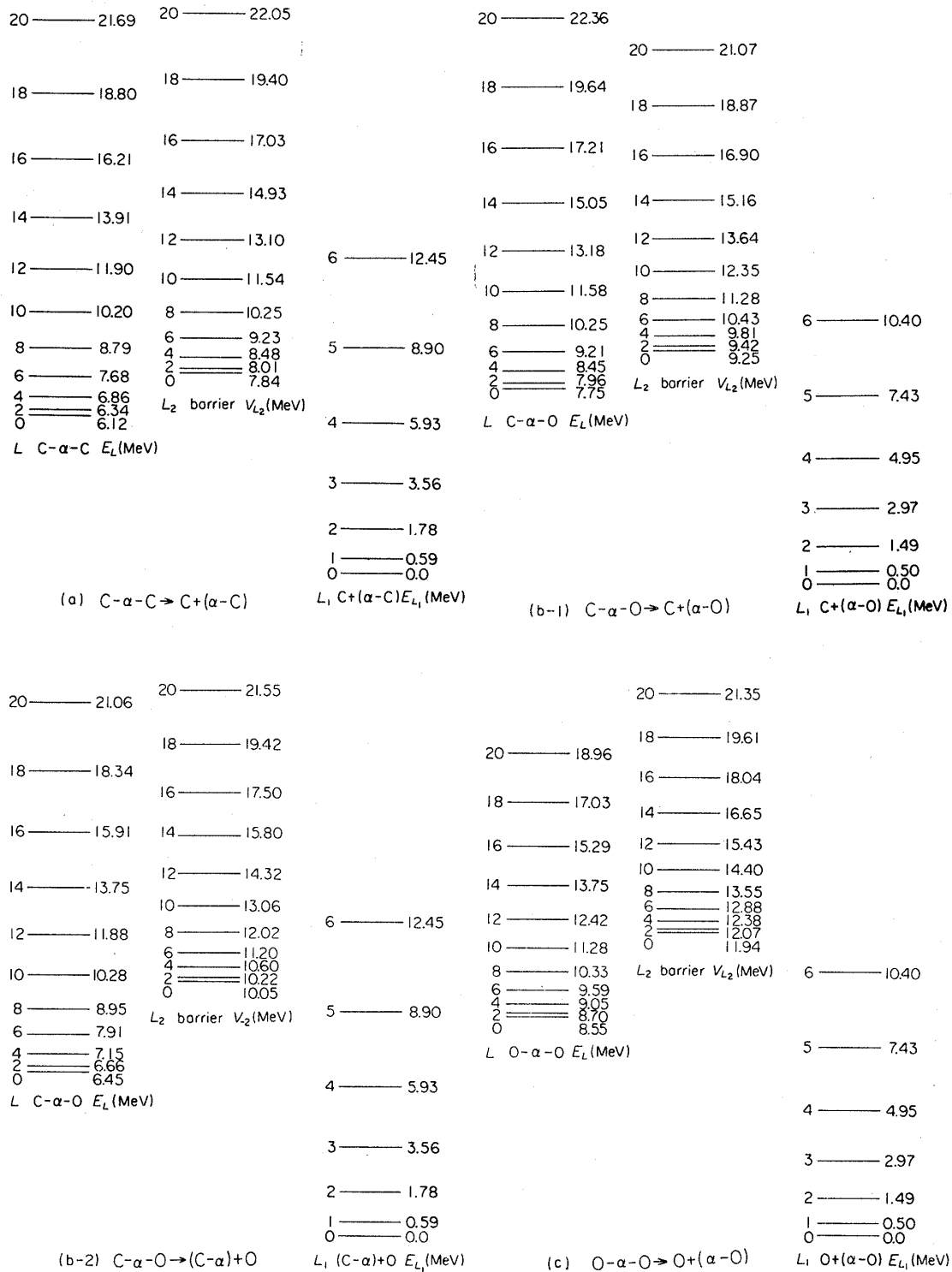


Fig. 5-3. Q -values and Coulomb plus centrifugal barriers for the decays of the three-linear chains of $C-\alpha-C$, $C-\alpha-O$ and $O-\alpha-O$ according to Eqs. (5-13) and (5-14).

spectroscopic factors are given by

$$\begin{aligned}
 & \theta_{L(L_1, L_2)}^2 (A_1 - A_2 - A_1 \rightarrow A_1 + (A_2 - A_1)) \\
 &= 2(1 + \delta_{A_1, A_2}) \frac{(2L_1 + 1)(2L_2 + 1)}{(2L + 1)} (L_1 0 L_2 0 | L 0)^2 \\
 & \times \frac{\mathcal{G}_{L_1} \left(\frac{A_1 A_2}{A_1 + A_2} \lambda \right) \mathcal{G}_{L_2} \left(\frac{A_1 (2A_1 + A_2)}{A_1 + A_2} \lambda \right)}{\mathcal{G}_L (2A_1 \lambda)}. \quad (5.15)
 \end{aligned}$$

Here λ is νR_0^2 and the oscillator parameters for the nuclei of A_1 and A_2 are taken to be a common value of ν for simplicity. We show in Table V-5 the calculated partial widths which have a large contribution to the total decay width. It can be seen from the Table that in the case of C- α -C the high spin states have surely large widths enough to have a possibility of being actually observed, but not so large as to violate the stability condition of Eq. (5.12). Furthermore, we can know that the cases of C- α -O and O- α -O also satisfy the stability condition, in particular the decays of O- α -O are greatly suppressed because of the small penetrability.

We have examined in detail the stability condition of Eqs. (5.10) and (5.12) for the three-body cases and found that almost all the cases, except for α - α - α , satisfy the stability condition. Other cases of the three-

Table V-5. Calculated partial widths for the decays of the three-body linear chain of C- α -C to C+(α -C). The values of L , L_1 and L_2 denote the angular momenta of the parent nucleus, the fragment (α -C) and the relative motion, respectively. The channel radius is taken to be 9.48 fm. The oscillator parameters of α and C are chosen to be a common value of 0.23 fm^{-2} .

L	L_2	L_1	P_{L_2}	θ^2	Γ (keV)
12	12	0	1.6	0.065	20
	11	1	3.6	0.0032	2
14	14	0	2.2	0.063	28
	13	1	1.8	0.0026	1
	12	2	1.4	0.039	11
16	16	0	5.3	0.061	66
	15	1	5.9	0.0021	3
	14	2	6.2	0.038	48
	13	3	1.5	0.046	14
18	18	0	6.0	0.058	72
	17	1	6.8	0.0017	2
	16	2	6.6	0.037	50
	15	3	5.2	0.049	52
	14	4	1.5	0.056	18

body linear chain with the heavy subunit nuclei are expected to be in the similar situations. It is also noted that the four-body cases generally satisfy the above stability conditions.

5.4 Prolongation of the linear molecule-like structure due to the Coulomb interaction

It can be expected that the linear molecule-like structure is prolonged due to the Coulomb interaction. Especially when the subunit nuclei are large, the prolongation effect becomes appreciable. This effect seems to be important for the formation of the linear molecule in nuclear system, because the prolongation is intimately related with the increase of the polarization into the subunit cluster. If the prolongation effect is strong, the nucleus with the indistinct di-molecule-like structure may have the distinct molecule-like structure when it appears as the subunit nucleus in the multi-molecule-like structure. In the following, we discuss qualitatively about the prolongation effect, taking up the three-body case of A_1 - A_2 - A_3 (with $A_3=A_1$) as an example of the multi-molecule-like structures.

For the convenience of the discussion, we express the energy surfaces of three-body linear structure, A_1 - A_2 - A_3 ($A_3=A_1$), and also of di-molecule-like structure, A_1 - A_2 , as a function of the distance parameters between two clusters, i.e., R_{12} and R_{23} for the three-body case and R for the two-body case. The energy surface of the two-body case is represented as

$$E(R) = \langle \Psi(\mathbf{r}_1, \dots, \mathbf{r}_B; R) | \mathcal{H}_0 | \Psi(\mathbf{r}_1, \dots, \mathbf{r}_B; R) \rangle, \quad (5.16)$$

where $\Psi(\mathbf{r}_1, \dots, \mathbf{r}_B; R)$ with $B=A_1+A_2$ is a variational function. If we assume that the energy surface has a local minimum at $R=R_0$, $E(R)$ can be expanded as

$$E(R) = E(R_0) + \frac{1}{2}k_0(R-R_0)^2 + \dots \quad (5.17)$$

The energy surface of the three-body case is conveniently expressed as the sum of the two terms

$$E(R_{12}, R_{23}) = E_0(R_{12}, R_{23}) + \Delta E_c(R_{12}, R_{23}), \quad (5.18)$$

where $E_0(R_{12}, R_{23})$ is the expectation value of the Hamiltonian which includes the Coulomb interaction between the adjacent clusters and $\Delta E_c(R_{12}, R_{23})$ is the Coulomb energy between A_1 and A_3 . The energy function of $E_0(R_{12}, R_{23})$ can be expanded around the equilibrium point of $R_{12}=\tilde{R}_0$ and $R_{23}=\tilde{R}_0$ as

$$\begin{aligned} E_0(R_{12}, R_{23}) = & E_0(\tilde{R}_0, \tilde{R}_0) + \frac{1}{2}k_1(R_{12}-\tilde{R}_0)^2 \\ & + \frac{1}{2}k_1(R_{23}-\tilde{R}_0)^2 + k_2(R_{12}-\tilde{R}_0)(R_{23}-\tilde{R}_0) + \dots \end{aligned} \quad (5.19)$$

Since the distance of $R_{13}=R_{12}+R_{23}$ is large, the Coulomb energy of $\Delta E_c(R_{12}, R_{13})$ can be approximately given as

$$\Delta E_c(R_{12}, R_{13}) = \frac{Z_1^2 e^2}{R_{12} + R_{13}}. \quad (5 \cdot 20)$$

Using Eqs. (5·19) and (5·20), we can obtain the equilibrium point of $R_{12}=\widetilde{\widetilde{R}}_0$ and $R_{23}=\widetilde{\widetilde{R}}_0$ at which the energy surface of Eq. (5·18) has a local minimum. The equilibrium distance between A_1 and A_2 (A_2 and A_3) is found to deviate from \widetilde{R}_0 by

$$\delta R_0 = \widetilde{\widetilde{R}}_0 - \widetilde{R}_0 \approx \frac{Z_1^2 e^2}{(2\widetilde{R}_0)^2 k_1}. \quad (5 \cdot 21)$$

Here, the coefficient of k_2 in Eq. (5·19) is neglected because of $k_2 \ll k_1$. This deviation of δR_0 can be used as a measure of the prolongation due to the Coulomb interaction. If we can assume that the equilibrium distance of \widetilde{R}_0 and the strength of the energy curvature, k_1 , are nearly equal to the parameters (R_0 and k_0) for the di-molecule-like structure, the difference of the equilibrium distances between the three-body and two-body systems can be given by $\delta R_0 (= \widetilde{\widetilde{R}}_0 - \widetilde{R}_0 \approx \widetilde{\widetilde{R}}_0 - R_0)$.

In §3, we have shown the energy surface of the intrinsic structure of O- α by using the phenomenological two-body interactions. The energy curvature is found not to be so large, that is, $k_0 \approx 6 \text{ MeV} \cdot \text{fm}^{-2}$. If this value of k_0 is used as k_1 , the distance between α and O in the O- α -O system increases by $\delta R_0 \approx 0.24 \text{ fm}$. When this increase of δR_0 is compared with the radius of the alpha-particle, it cannot be said to be necessarily small. When the subunit nuclei on both sides become big, the increase of δR_0 is expected to be remarkably large, because of the strong dependence on the mass number as $\delta R_0 \propto A_1^{4/3}$ (Although the curvature constant, k_1 , also depends on the mass number, its dependence is considered to be weak.) If the same value of $k_0 (\approx 6 \text{ MeV} \cdot \text{fm}^{-2})$ is assumed, the value of δR_0 for the case of Ca- α -Ca becomes about one third of the radius of the alpha-particle.

In this section, we have considered the linear multi-molecule-like structures which involve the three and four subunit nuclei on the basis of the knowledge about the di-molecule-like structures of α - α , α -C and α -O and found that these multi-molecule-like structure can be realized with a high possibility as the quasi-bound states near the top of the Coulomb (plus centrifugal) barriers. Among these multi-molecule-like structures, the three-body cases are considered to be most interesting in connection with the actual observations. Further discussions about these cases will be given in the final section.

§6. Summary on the molecule-like structures in nuclei

The change of the structures is considered to be one of the most interesting problems in the nuclear physics. Due to the complexity of the action of the nuclear interaction, the nuclear system has been expected to have many varieties of the structure change. We have proposed that the most typical structure change in the self-conjugate $4n$ -nuclei is induced by the strong α -like four-particle correlation together with the externally weak character of the interaction between nuclei, and as the result of such a structure change the molecule-like structures are expected to be realized systematically near or above the threshold energy for the fission into the constituent subunit nuclei, as shown in Fig. 1.1. In this chapter we have tried to develop the molecular viewpoint in the light nuclei.

The theoretical studies have been done for the nuclei, in the mass region of $8 \leq A \leq 20$, where the typical molecule-like structures have been known to appear at present. The special attention has been paid to extract the physical implications involved in the experimental properties of the states with the molecule-like intrinsic structures. Especially the decay widths and the energetic properties of the anomalous states in ^{12}C , ^{16}O and ^{20}Ne have been carefully studied to assure the molecular viewpoint. Through these studies the concept of the nuclear molecule and the structure change in the light nuclei has been enriched. At first we here summarize the present understanding for the nuclear system obtained by the studies based on the molecular point of view.

The nucleus of ^{12}C has been successfully investigated on the basis of the independent particle model (shell model and Nilsson model), and the intermediate coupling shell model has been known to work very well⁽⁴⁰⁾ in reproducing all the observed levels up to about 17 MeV except the two anomalous levels (the 0^+ level at 7.66 MeV and the broad 2^+ level around 10.3 MeV). The most characteristic properties of the latter two levels show up in the alpha decay widths, of which the reduced widths are several times larger than the Wigner limit. In this chapter (§§ 4.1 and 4.2) we have discussed about the structures of these two levels from the molecular viewpoint. It has been pointed out from the theoretical analysis that the large alpha decay widths can be reproduced only when the two anomalous states have the structure composed of the three alpha-particles which are coupled loosely with each other but not of linear arrangement. This characteristic feature for the structure of the two levels is indicated to appear in the energetic properties. One of them is the magnitude of the level spacing between the two levels, which is not expected from the 3α -particles in a row but rather near that of the ground rotational band in ^8Be . Therefore, the weak coupling of the three alpha-particle system can be also called the weak coupling between an alpha-particle and a Beryllium. Another energetic

property is the binding energy of the 3α system. As was studied in §4.2, even if the transverse vibration is taken to be so large that the 3α -chain extends to the triangular configuration space, the energy of the 3α -chain structure is obtained to be larger than the experimental energy of the second excited zero plus state, while the energy of the 3α system with the triangular configuration is found to be a little smaller than the experimental one.

If we remark that the state with the configuration around the triangular one has a very large reduced width (as shown in §4.1), the anomalous states in ^{12}C may be well described by the aggregation of the three alpha-particles which involve large fluctuations around the triangular configuration. In this sense, the triangular configuration is considered to correspond to the excited anomalous states but not to the ground state. According to this interpretation, the energy of the anomalous states may be explained by taking into account the interplay of the ground configuration, e.g., the interplay of the oblate deformed structure with the molecular one. Thus we can reasonably conclude at present that the two anomalous states in ^{12}C have the structure of the three alpha-particles which are coupled weakly with one another.

The nucleus of ^{16}O has been well known to have the typical closed shell structure and a part of the low-lying states can be interpreted in terms of the excitation modes with a few particle-hole pairs (e.g., $1p-1h$ and $2p-2h$) from the closed core of the ground state. However, the first excited state is the “mysterious zero plus” state upon which the rotational band is formed and cannot be easily understood on the basis of the shell model. When the shell model is applied to interpret the rotational band upon the mysterious zero plus state, the $4p-4h$ configurations have to be adopted as the dominant configurations. We can therefore realize the discontinuity between the structures of the ground state and the first excited zero plus state. This discontinuity is clearly indicated by the success of the interpretation for the positive parity rotational band mentioned above in terms of the weak coupling model, where the level structure is explained to be due to the weak coupling of the correlated four particles with the residual core of ^{12}C . We have chosen the other way of the study for this anomalous rotational band by introducing the molecular aspect as was mentioned in Chap. I and also §1 of this chapter.

One of the most convincing reasons for the necessity of the molecular aspect was provided by the existence of the negative parity rotational band with the di-molecule-like structure of $\alpha\text{-C}$. The quantitative analyses of the alpha decay widths in §2 have clearly shown that the large experimental widths of the levels in the negative parity band can be understood only when the di-molecule-like structure $\alpha\text{-C}$ is assumed to be the intrinsic structure for them. Thus we were led to the interpretation of the rota-

tional band upon the mysterious zero plus state as a part of the inversion doublet with the same di-molecule-like structure of α -C. The semi-quantitative studies in §3 on the gap energy between the two bands with $K=0^\pm$ have confirmed that the interpretation of the positive parity band as the inversion doublet is fairly suitable for ^{16}O case (the interplay of the shell-like symmetric configuration with the di-molecule-like structure is not so large). This interpretation is also supplemented by the fact that the band head deviates from the threshold only by a small amount of energy. Thus we can conclude that the di-molecule-like structure of α -C is surely realized in the negative parity band and that it is also a dominant component of the intrinsic structure for the positive parity band.

The existence of the positive parity band with the structure of α -C in the low excited energy region shows us that the structure change in ^{16}O is very rapid in spite of the nuclear system with the small mass number. We may consider that the rapidness of the structure change is mainly due to the tightly closed shell nature of ^{16}O : If the closed shell nature is strong in ^{16}O , the di-molecule-like structure may be hardly coupled with the shell structure, since the interplay between the two different kinds of structures may arise mainly through the intermediate (deformed-like) structures, of which the energies are, however, expected to be larger than that of the di-molecule-like structure. Such a situation is expressed in the study on the gap energy by the central barrier with a finite height, which reproduces the experimental gap energy.

In the system of ^{16}O , an anomalous rotational band with a very large moment of inertia was found at the excitation energy of about 16.8 MeV. Since the moment of inertia has a magnitude just expected from the 4α -chain in row, the intrinsic structure of this band is considered to be the 4α -chain structure. Through the analysis of the decay properties, we have shown that although the experimental decay data at present are not sufficient to identify the 4α -chain structure for the anomalous band, the present informations are not inconsistent with the assumption of the 4α -chain.

We further tried to explain the energetic properties of the band head and the moment of inertia by using the alpha-particle model. As was shown in §4.2, the energy of the 4α -chain structure was in a good agreement with the experiment but the moment of inertia was obtained to be about a half of the experimental one. However, evidently the pure rotational spectra with the very large moment of inertia cannot be reproduced without assuming such a strongly prolonged intrinsic structure as the 4α -chain. Therefore, in order to understand the experimental moment of inertia, we have to look for any other factors which are not taken into account in our simple alpha-particle model.

The nucleus of ^{20}Ne has been extensively studied on the basis of the

shell model^{41)~43)} and shows a good correspondence with the shell model states in the low excited energy region. A fair part of the levels, especially the ground rotational band has been well explained in terms of the SU_3 scheme. However, it has been known that there are many levels which do not correspond with the shell model states. The experimental facts are considered to indicate that the nucleus of ^{20}Ne has a transient character from the shell-like structure to the molecule-like structure. We here summarize these experimental facts together with the theoretical reasons:

i) One of the most important facts is the existence of the negative parity rotational band, of which all the levels have a very large α widths comparable with the Wigner limit. The quantitative analysis of the α decay widths in §2 confirmed that the intrinsic structure of this band is surely the di-molecule-like structure of $\alpha\text{-O}$.

ii) Another important quantity is the magnitude of the gap energy between both bands, of which empirical value is about 5.2 MeV. The semi-quantitative study in §3 shows that the experimental value is larger than that expected from the di-molecule-like structure by about 2.5 MeV. And also this value is smaller than that expected based on the shell model. In order to reproduce the empirical value, we have to take into account the strong interplay between the symmetric deformed structure and the di-molecule-like structure for the positive parity band.

iii) The ground band head deviates from the threshold of the $\alpha + \text{C}$ channel by -4.7 MeV, which is also an important fact indicating the transient character of ^{20}Ne . This point was discussed in §1 in comparison with the other cases of ^{16}O and ^{12}C and further detailed discussions are made in Chap. IV from the viewpoint of the weak coupling feature.

iv) Next we should note that there are several excited zero plus states in the energy region of 6~10 MeV, upon which the rotation-like spectra are formed. The shell model with $(sd)^4$ configuration can predict only one zero plus state in this energy region.^{42), 43)}

v) These rotation-like bands as well as the ground rotational band are found to be excited selectively by the reactions, e. g., the transfer reactions of an alpha-particle^{34), 35)} and also of Beryllium.⁴⁴⁾

The transient character of ^{20}Ne is in striking contrast to the case of ^{16}O , where the closed shell structure and the molecule-like structure are rather separately realized in the actual states. In other words, this transient character means that the interplay between the different kinds of structures is not weak in the nuclear system of ^{20}Ne . It seems that the strong interplay is mainly due to the existence of the correlated four particles outside the closed core of ^{16}O , because they can be easily clusterized and also dissolved by the nuclear interactions. This feature was represented in the estimation of the gap energy in §3 by the potential with no central barrier and also examined

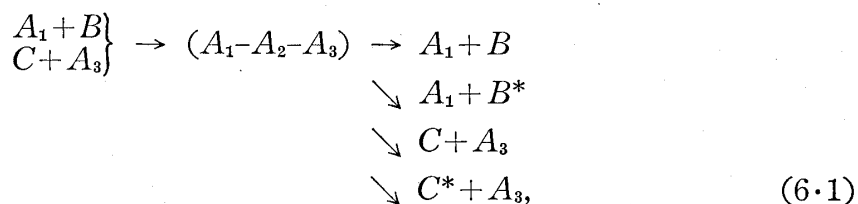
by calculating the energy surfaces from the microscopic point of view. Thus the nucleus of ^{20}Ne can be pointed out to be one of the most interesting nuclear systems for the study on the mechanism of the structure change.

Besides of α - α in ^8Be , we already recognized the di-molecule-like structures of α -C and α -O in ^{16}O and ^{20}Ne , respectively, and also the three and four alpha-particle structures in ^{12}C and ^{16}O , respectively. As the next step of the studies about the molecule-like structures, we intended to develop the theoretical investigations concerning the multi-molecule-like structures, that is, the alpha-chain structures in §4.3 and the linear chain structures connected with the bonds of α - α , α -C and α -O in §5. Although one can consider the other kinds of configurations for the multi-molecule-like structures, the linear chain configuration is generally expected to have a high possibility of the existence by the reason that the Coulomb interaction favours energetically the linear chain configuration and that the interplay of it with the other configurations can be considered to be least.

The series of the alpha-chain structures gives the energetical upper limit of the molecule-like structures in nuclear system. Using the knowledge obtained from the analysis of ^8Be , $^{12}\text{C}^*$ and $^{16}\text{O}^*$, we estimated the energy of the $n\alpha$ -chain structures and studied the stability of its linear arrangement. Due to the weakness of the Coulomb interaction, the stability was known not to be always satisfied, especially for the small number system of the alpha-particles. However, the local deviation from the linearity for the neighbouring three alpha-particles was found to decrease appreciably at about $n \approx 4$. Therefore it can be expected that the $n\alpha$ -chain ($n \geq 5$) structures have a high possibility of the real existence as a quasi-bound state or a resonance. The decay widths were theoretically obtained to be order of several ten keV for $n=5$ and 6. Although there are many difficulties to find experimentally a quasi-bound state with the singular structure, we can only suggest, for example, the reaction of $\text{O}(\alpha, ^8\text{Be})\text{C}^*$ and $\text{C}(\text{C}, \text{C}^*)\text{C}^*$ for the investigation of the alpha-chain structures with $n=5$ and 6.

In §5, we studied the more general multi-molecule-like structures connected with the bonds of α - α , α -C and α -O and found that these kinds of linear chain structures could be realized with a high possibility as the quasi-bound state near the top of the Coulomb (plus centrifugal) barriers. In connection with the actual observation through the heavy ion reactions, we give a few remarks about the three-body cases, e. g., C- α -C, C- α -O and O- α -O in the following.

The state with the tri-molecule-like structure of $(A_1-A_2-A_3)$ is considered to be excited through the heavy ion reactions and to have the various kinds of decay channels as shown schematically below,



where A_1 , A_2 and A_3 are the subunit nuclei, B and C are the nucleus of A_1+A_2 and of A_2+A_3 , respectively, and B^* and C^* are the di-molecule-like structures of (A_1-A_2) and of (A_2-A_3) in the fragment nuclei of B and C , respectively.

We remark at first on the formation process of $A_1+B \rightarrow (A_1-A_2-A_3)$. Since it is the weakly coupled system, the tri-molecule-like structure is considered to be formed through the two-body ion reaction of A_1 with B in the surface region. It is well known that in the surface region the active partial wave with angular momentum J can be determined by the incident energy of E (C.M.) from the relation of $J(J+1) \approx 2\mu R^2 E / \hbar^2$, where μ is the reduced mass for the relative motion and R the contact distance between the two nuclei of A_1 and B . If the energy of the J -state in the rotational band with the molecule-like structure of $(A_1-A_2-A_3)$ matches with the incident energy of E for which the partial wave with the same angular momentum J is active in the surface region, the tri-molecule-like structure has a chance to be favourably formed by the heavy ion reaction. To illustrate the above situation, we show in Fig. 6.1 the relation between the incident energy with the J -th active partial wave and the energy of the rotational band. Since the energy of the tri-molecule-like structure is higher than the threshold energy of the two-body reaction as shown in §5 and the moment of inertia of the tri-molecule-like structure is larger than μR^2 , the energy of the state with low angular momentum cannot match with the incident energy for the corresponding active partial wave but both the energies necessarily cross at a certain high angular momentum.

Next we consider the decay process after the formation of $(A_1-A_2-A_3)$. The decay channels in Eq. (6.1) can be classified into the elastic channel of A_1+B with the exchange channel of $C+A_3$ and the special kinds

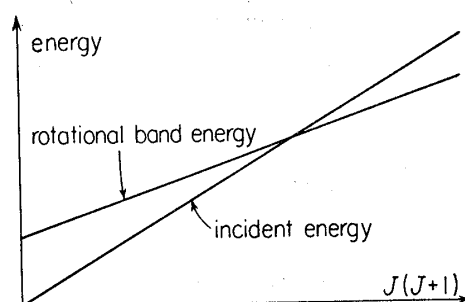


Fig. 6.1. The relation between the incident energy with the J -th active partial wave and the energy of the rotational band with the molecular structure.

of inelastic channel of A_1+B^* with the corresponding exchange channel of C^*+A_3 , where $B^*=(A_2-A_3)$ and $C^*=(A_1-A_2)$. The significant difference in the above two kinds of channels appears in the channel radius at which the nuclear interaction between the daughter nuclei is not effective. If the intermediary subunit nucleus of A_2 is a small element, e. g., an alpha-particle, the difference of the channel radii is considered to be order of a diameter of the subunit of A_2 . Therefore, though the Q -value for the A_1+B^* (or C^*+A_2) channel is in general smaller than that of the elastic A_1+B (or $C+A_2$) channel, the height of the Coulomb plus centrifugal barriers at the respective channel radius becomes nearly equal at a certain angular momentum, as shown schematically in Fig. 6.2. If the tops of the Coulomb (plus centrifugal) barriers for the two channels get nearer, the cross sections for the two channels may be comparable. Thus we can generally expect that the tri-molecule-like structure of $(A_1-A_2-A_3)$ is excited favourably as the high spin state and identified by the correlation between the elastic and the inelastic channels.

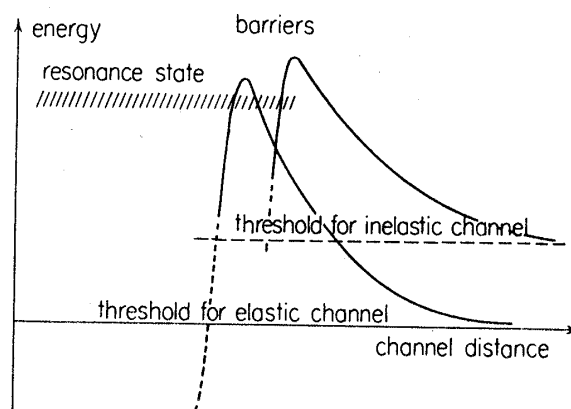


Fig. 6.2. Schematic picture which indicates the characteristic feature of the Coulomb plus centrifugal barriers for the decay of the resonance state with the tri-molecular structure through the elastic and the inelastic channels.

A few molecular resonances have been found through the experimental study on the heavy ion scatterings. For the resonances observed in the $C+C$ scattering, a theoretical explanation was given by Imanishi⁴⁵⁾ as the resonance of $C+C^*(2^+ \text{ state at } 4.42 \text{ MeV})$ with the small coupling of the $C+C$ channel. In the scattering of $O+O$, the quasi-molecular resonances with a gross structure have been also found and interpreted as the doorway states of the molecule-like structure of $O-O$.^{46), 47)}

Unlike these di-molecular resonances, the resonances discussed here are of the tri-molecular structure. An example suggestive of this kind of resonances seems to be found by the recent experiments on the $C(O,O)C$ scattering,⁴⁹⁾ which have shown that the resonance state at 19.7 MeV (C. M.)

has the spin of $J=14$ and that the inelastic scattering of $C(O, O^*)C$ to the first excited 0^+ state in ^{16}O has a strong correlation with the elastic scattering through this resonance. According to our estimation in §5, the energy of the state ($J=14$) with the molecule-like structure of $C-\alpha-C$ is about 22 MeV from the threshold for the $C+O$ channel, which is in good agreement with the experiment. The other example of the tri-molecule-like structures, e. g., $C-\alpha-O$ and $O-\alpha-O$, can be also expected theoretically to appear as the resonances of the heavy ion scattering by $C+Ne$ or $O+O$ and by $O+Ne$. It should be noted that the arguments as stated above concerning the resonance state with the tri-molecule-like structure can be applied in the same manner to the other cases of the more general multi-molecule-like structure, for example, for the four-body cases discussed in §5.

In the study of multi-molecule-like structures we have assumed the simple potential which is attractive only in the contact region as the interaction between the nuclei and chosen the potential parameters so as to fit the binding energy of the molecule-like structure identified by the experiments. This simple picture for the potential is considered to be theoretically tolerable when the molecule-like structure is really formed, where the relative motion between the subunits is the dominant mode. In fact, according to the studies with the resonating group method for the states with the di-molecular structure and the scattering of the two nuclei, if the assumption of the rigidity of the subunit nuclei is valid, we can understand that the relative wave function has the almost energy-independent nodal point as the result of the Pauli principle and has the small amplitude within the nodal point. Therefore in the case that we consider the quasi-bound state with the di-molecule-like intrinsic structure, we can replace the inner region by the hard (or soft) repulsive core at the nodal point.⁵⁰⁾ It is a matter of course that the more extensive studies on the interactions between the complex nuclei have to be theoretically developed in order to obtain the fundamental concept of the interactions and the basis for the understanding of the more complicated molecule-like structures.

We have demonstrated the real and possible existence of the manifold molecule-like structures in nuclear system, though our study is based on the present limited experimental informations. The future development of the molecular aspect is expected to be more extensively made with the accumulation of new systematic data. The theoretical investigations will be developed towards the following two subjects as we emphasized through this chapter: One is to ask what kinds of molecule-like structures will be really able to exist in the nuclear system and then what kinds of motions will be the dominant modes in such structures. The other is to understand the mechanism of the interplay between the different kinds of structures, that is, to know the mechanism of the structure change into the molecule-like

structures, taking into account the interrelation between the nuclear structures and the actions of the nuclear interactions. The problems of the structure change in nuclei can be said to become one of the central subjects in the theoretical and experimental nuclear study.

Acknowledgements

The authors would like to express their hearty thanks to Professors A. Arima, K. Yazaki, M. Nomoto, S. Okai, J. Maki, R. Tamagaki and the members of the Nuclear Theory Laboratories of University of Tokyo, Niigata University and the Research Institute for Fundamental Physics of Kyoto University, for their encouragements and discussions in the course of the works.

One of the authors (K.I.) would also like to express his sincere thanks to Professor A. Bohr and Professor B. R. Mottelson and the members of Niels Bohr Institute for their encouragements and discussions when he stayed there for a 1968 academic year. One of the authors (H.H.) wishes to thank the Sakkokai Foundation for financial aid.

Appendix 1

—*Calculational method of the matrix elements necessary for the evaluation of the reduced width from the model wave function*—

In this Appendix, we give the formulae which are utilized in §2.2 for the calculations of the matrix elements $\langle h_L | Q | \phi_L \rangle$, where $h_L = Y_{L0}(\Omega_r) \phi_0(\alpha) \phi_0(C)$ and Q is either 1 or ΣV_{ij} . The problem is how to execute the integration over the internal coordinates of two clusters (α and the core) and the angle Ω_r of the relative coordinate using the totally antisymmetrized wave function ϕ_L . (This is essentially the same problem in the evaluation of the kernels in the resonating group method.) Our method to calculate these matrix elements is the one given in Ref. 51). We here first explain the method and then, for the case of $Q=1$ in ^{20}Ne , give the convenient formulae executing the procedure indicated in an analytical way.

The aim of our method is to convert the integration over the internal coordinates of two clusters and the angle Ω_r of the relative coordinate to that over the A individual nucleon coordinates and then to make the calculation equivalent to that by the independent particle wave functions. First we include the length r of the relative coordinate in the integration using the delta function technique as follows,

$$\langle h_L | Q | \phi_L \rangle_{r=b} = \frac{1}{Y_{L0}(\Omega_b)} \langle \delta(\mathbf{r}-\mathbf{b}) \phi_0(\alpha) \phi_0(C) | Q | \phi_L \rangle, \quad (\text{A1.1})$$

where the length of \mathbf{b} is fixed to b while the direction of \mathbf{b} can be chosen arbitrarily due to the scalar property of $\phi_0(\alpha)\phi_0(C)$. Next, the total center-of-mass coordinate, \mathbf{X}_G , is included in the integral, by using the following two relations (A1.2) and (A1.3). One is

$$\begin{aligned}\psi_0(\alpha) &= \left(\frac{8\nu_\alpha}{\pi}\right)^{3/4} \exp(-4\nu_\alpha X_\alpha^2) \phi_0(\alpha), \\ \psi_0(C) &= \left(\frac{2C\nu_c}{\pi}\right)^{3/4} \exp(-C\nu_c X_c^2) \phi_0(C), \\ C &= A-4,\end{aligned}\tag{A1.2}$$

where $\psi_0(\alpha)$ and \mathbf{X}_α and $\psi_0(C)$ and \mathbf{X}_c are the Slater determinantal oscillator wave function and the center-of-mass coordinate of α and the core clusters, respectively. Here the oscillator parameters ν_α of α and ν_c of the core are considered to be different in general. The other relation is obtained from the usual supposition that ϕ_{L0} has been obtained from the model wave function ψ_{L0} which includes A individual nucleon coordinates as follows,

$$\psi_{L0} = \phi_G(\mathbf{X}_G) \phi_{L0}, \tag{A1.3}$$

where $\phi_G(\mathbf{X}_G)$ is a scalar function of only \mathbf{X}_G . From (A1.2) and (A1.3) we can get the desired expression for (A1.1), in which the integration is carried over all the A nucleon coordinates;

$$\begin{aligned}\langle \delta(\mathbf{r}-\mathbf{b}) \phi_0(\alpha) \phi_0(C) | Q | \phi_L \rangle \\ = (\pi^2/16C\nu_\alpha\nu_c)^{3/4} [e^{\gamma b^2} / \langle \exp(-\alpha X_G^2 - \beta \mathbf{X}_G \cdot \mathbf{b}) | \phi_G(\mathbf{X}_G) \rangle] \\ \times \langle \delta(\mathbf{r}-\mathbf{b}) \psi_0(\alpha) \psi_0(C) | Q | \psi_L \rangle, \\ \alpha = 4\nu_\alpha + C\nu_c, \quad \beta = \frac{8C}{A}(\nu_\alpha - \nu_c), \\ \gamma = \frac{4C}{A^2}(C\nu_\alpha + 4\nu_c).\end{aligned}\tag{A1.4}$$

Here use is made of the relation,

$$4\nu_\alpha X_\alpha^2 + C\nu_c X_c^2 = \alpha X_G^2 + \beta \mathbf{X}_G \cdot \mathbf{r} + \gamma r^2. \tag{A1.5}$$

Now in the final step, in order to make the calculation of the matrix element in (A1.4) equivalent to those by the Slater determinants, we use the following expression for $\delta(\mathbf{r}-\mathbf{b})$ in (A1.4),

$$\delta(\mathbf{r}-\mathbf{b}) = \frac{1}{(2\pi)^3} \int d\mathbf{k} e^{-i\mathbf{k} \cdot \mathbf{b}} e^{i\mathbf{k} \cdot \mathbf{r}}. \tag{A1.6}$$

The reason to use this expression is due to the separability of the factor $\exp(i\mathbf{k} \cdot \mathbf{r})$ as $\exp(i\mathbf{k} \cdot \mathbf{r}) = \exp(i\mathbf{k} \cdot \mathbf{X}_\alpha) \exp(-i\mathbf{k} \cdot \mathbf{X}_c)$, which enables to incorporate this factor into $\psi_0(\alpha)\psi_0(C)$ as below

$$e^{i\mathbf{k}\cdot\mathbf{r}}\psi_0(\alpha)\psi_0(C) = \exp\left\{-\left(\frac{1}{16\nu_\alpha} + \frac{1}{4C\nu_c}\right)k^2\right\}\psi_0\left(\alpha, -\frac{i\mathbf{k}}{8\nu_\alpha}\right)\psi_0\left(C, \frac{i\mathbf{k}}{2C\nu_c}\right), \quad (\text{A1}\cdot 7)$$

where $\psi_0(\alpha, \mathbf{e})$ ($\psi_0(C, \mathbf{f})$) is entirely the same as $\psi_0(\alpha)$ ($\psi_0(C)$) except that the center-of-mass is located around \mathbf{e} (\mathbf{f}) (namely, each individual nucleon coordinate \mathbf{r} is replaced by $\mathbf{r}-\mathbf{e}$ ($\mathbf{r}-\mathbf{f}$)). Since Ψ_{L_0} 's in §2 are expressed by a Slater determinant or its superposition, we can easily calculate the matrix element $\langle\psi_0(\alpha, \mathbf{e})\psi_0(C, \mathbf{f})|Q|\Psi_L\rangle$ by the usual technique to evaluate the matrix element of a one- or two-body operator with Slater determinantal wave functions. (When Ψ_{L_0} is of the type of the cluster model wave function, we need to apply to Ψ_{L_0} the same procedure by which we have expressed $\delta(r-b)h_L$ by the integral superposition of the products of the single particle wave functions.) When $\psi_0(\alpha)\psi_0(C)$ is scalar as in our case we can reduce the threefold integration to the integration over the single variable $k=|\mathbf{k}|$, giving the general formula of our method for $\langle h_L|Q|\Psi_{L_0}\rangle$ as follows,

$$\begin{aligned} \langle h_L|Q|\Psi_{L_0}\rangle_{r=b} &= \left\{\frac{(\alpha+A\nu)^2}{32CA\pi\nu_\alpha\nu_c\nu}\right\}^{3/4} (2L+1)^{-1/2} i^L \exp\left\{\left(r-\frac{\beta^2}{4(\alpha+A\nu)}\right)b^2\right\} \\ &\times \int_0^\infty dk \cdot k^2 j_L(kb) \langle e^{ikz_r}\psi_0(\alpha)\psi_0(C)|Q|\Psi_L\rangle, \end{aligned} \quad (\text{A1}\cdot 8)$$

where z_r is the z -component of the relative coordinate \mathbf{r} , and we assumed that $\phi_G(\mathbf{X}_G) = (2A\nu/\pi)^{3/4} \exp(-A\nu X_G^2)$.

We below execute in an analytical way the procedure indicated by (A1·8) for the evaluation of $\langle h_L|\Phi_L\rangle$ in the case of the deformed oscillator model wave function of ^{20}Ne which includes SU_3 model wave function as the limiting case of $\nu_\perp = \nu_z$, and give the convenient compact formulae for $\langle h_L|\Phi_L\rangle$. First the matrix element $\langle e^{ikz_r}\psi_0(\alpha)\psi_0(^{16}\text{O})|\Psi_L\rangle$ is put into the form of Eq. (A1·9) using the definition of Ψ_{L_0} as $N_L \int d\Omega D_{00}^L(\Omega) R(\Omega) \Psi((90))$ ($\Psi((90))$ is defined by the intrinsic state of Eq. (2·4) of §3.2 with the one modification of $\nu_z \neq \nu_\perp$);

$$N_L (4\pi^2) \int_0^\pi d\beta \cdot \sin\beta d_{00}^L(\beta) \langle e^{ikz_r}\psi_0(\alpha)\psi_0(^{16}\text{O})|e^{-i\beta L_y}|\Psi((90))\rangle. \quad (\text{A1}\cdot 9)$$

The matrix element in the integrand of the above equation is calculated by the ordinary technique to evaluate the overlap of two Slater determinants as follows,

$$\begin{aligned} &\langle e^{ikz_r}\psi_0(\alpha)\psi_0(^{16}\text{O})|e^{-i\beta L_y}|\Psi((90))\rangle \\ &= \sqrt{4!16!} \langle \hat{\phi}_s^4 \hat{\phi}_s^4 \hat{\phi}_{px}^4 \hat{\phi}_{py}^4 \hat{\phi}_{pz}^4 |\Psi((90))\rangle \\ &= \frac{B}{\sqrt{\binom{20}{4}}} \exp\{-(\tau - \lambda \cos^2\beta)k^2\} \cdot (k \cos\beta) (k^2 \cos^2\beta - 3g) (k^2 \cos^2\beta - g)^3, \end{aligned} \quad (\text{A1}\cdot 10)$$

where

$$\begin{aligned}\hat{\phi}_s &= \left(\frac{2\nu_\alpha}{\pi}\right)^{3/4} \exp\left\{-\nu_\alpha x^2 + \frac{i}{4} \mathbf{k}_\beta \cdot \mathbf{x}\right\}, \\ \phi_s &= \left(\frac{2\nu_0}{\pi}\right)^{3/4} \exp\left\{-\nu_0 x^2 - \frac{i}{16} \mathbf{k}_\beta \cdot \mathbf{x}\right\}, \\ \phi_{px} &= 2\sqrt{\nu_0} x \phi_s, \quad \phi_{py} = 2\sqrt{\nu_0} y \phi_s, \quad \phi_{pz} = 2\sqrt{\nu_0} z \phi_s, \\ \mathbf{k}_\beta &= (-k \cos\beta, 0, k \sin\beta), \\ B, \tau, \lambda, g &: \text{simple functions of } \nu_0, \nu_\alpha, \nu_\perp \text{ and } \nu_z \text{ independent} \\ &\quad \text{of } k \text{ and } \beta \text{ such as}\end{aligned}$$

$$\lambda = \frac{\nu_z - \nu_\perp}{16(\nu_z + \nu_\alpha)(\nu_\perp + \nu_\alpha)} + \frac{\nu_z - \nu_\perp}{64(\nu_z + \nu_0)(\nu_\perp + \nu_0)}.$$

Here ϕ_s^4 stands for $\phi_s^{n+} \phi_s^{n-} \phi_s^{p+} \phi_s^{p-}$ and $n+$ indicates a neutron (p =proton) with spin up etc. The integrations on k and β are done by expanding $\exp\{\lambda k^2 \cos^2\beta\}$ term in (A1.10) as $\sum_{n=0}^{\infty} \lambda^n k^{2n} (\cos\beta)^{2n}/n!$. We give the resulting $y_L = \sqrt{\binom{20}{4}} \langle h_L | \phi_L \rangle$ in the form $\sum_{N \geq L} \hat{C}_L^N R_{NL}(r, 16\nu_B/5)$ with $\nu_B = (5\nu_\alpha \nu_0 + 4\nu_\alpha + \nu_0)/(5\nu + 4\nu_0 + \nu_\alpha)$,

$$\begin{aligned}\hat{C}_L^N &= z_1 \cdot z_2 \sum_{j=0}^4 \theta(N-9+2j) a_j G^j \sum_{n=n_0}^{n_1} E^n F^{n_1-n} z_3(n), \\ z_1 &= \sqrt{S_{(90)}^2} \cdot \hat{n}_L \left\{ \frac{(5\nu + 4\nu_0 + \nu_\alpha)^2}{100\nu_0\nu_\alpha\nu} \nu_B \right\}^{3/4} \cdot \left\{ \frac{2(5\nu_z + 4\nu_0 + \nu_\alpha)}{5(\nu_z + \nu_0)(\nu_z + \nu_\alpha)} \sqrt{\nu_z \nu_B} \right\}^9 \\ &\quad \times \left(\frac{2\sqrt{\nu_\perp \nu_\alpha}}{\nu_\perp + \nu_\alpha} \right)^4 \left(\frac{2\sqrt{\nu_z \nu_\alpha}}{\nu_z + \nu_\alpha} \right)^2 \left(\frac{2\sqrt{\nu_\perp \nu_0}}{\nu_\perp + \nu_0} \right)^{24} \left(\frac{2\sqrt{\nu_z \nu_0}}{\nu_z + \nu_0} \right)^{12}, \\ S_{(90)}^2 &= \left(\frac{5^4 \sqrt{9!!}}{2^{15}} \right)^2 \approx 0.344, \\ z_2 &= \frac{1}{9!} \sqrt{\frac{(N+L+1)!!}{(N-L)!!} (9-L)!! (10+L)!!}, \\ \theta(x) &= \begin{cases} 1 & x \geq 0, \\ 0 & x < 0, \end{cases} \\ a_0 &= 1, \quad a_1 = -6, \quad a_2 = 12, \quad a_3 = -10, \quad a_4 = 3, \\ G &= \frac{40(\nu_z + \nu_0)(\nu_z + \nu_\alpha)(\nu_0 - \nu_\alpha)}{(5\nu_z + 4\nu_0 + \nu_\alpha)^2 \nu_B}, \\ n_1 &= \frac{N-9+2j}{2}, \quad n_0 = \max\left(0, \frac{L-9+2j}{2}\right), \\ E &= \frac{\{4(\nu_z + \nu_0)(\nu_\perp + \nu_0) + (\nu_z + \nu_\alpha)(\nu_\perp + \nu_\alpha)\} \nu_B (\nu_z - \nu_\perp)}{5(\nu_z + \nu_0)(\nu_\perp + \nu_0)(\nu_z + \nu_\alpha)(\nu_\perp + \nu_\alpha)}, \\ F &= 1 - \frac{2(5\nu_\perp + 4\nu_0 + \nu_\alpha) \nu_B}{5(\nu_\perp + \nu_0)(\nu_\perp + \nu_\alpha)}, \\ z_3(n) &= \binom{N-L}{2}_{n_1-n} \cdot \frac{(2n+9-2j)!}{n! (2n+10-2j+L)!!}. \end{aligned} \tag{A1.11}$$

Here \hat{n}_L is $N_L/N_L(\nu_z=\nu_1)$ where $N_L(\nu_z=\nu_1)$ is N_L in the SU_3 limit $\nu_z=\nu_1$, namely, $\sqrt{2L+1}/(8\pi^2) \cdot \sqrt{(9-L)!!(10+L)!!/9!}$ and the factor $S_{(90)}^2$ is s_L^2 value in the case $\nu_\alpha=\nu_0=\nu_1=\nu_z$.

In the SU_3 limit ($\nu_1=\nu_z=\nu$ and therefore $\lambda=0$) the expansion of y_L is compactly done with the choice of oscillator parameter $(16/5)\nu$ rather than $(16/5)\nu_B$ because this choice gives a finite expansion series as follows,

$$y_L(r) = \sum_{\substack{9 \geq N \geq L \\ \text{odd}}} C_{NL} R_{NL} \left(r, \frac{16}{5} \nu \right). \quad (\text{A1.12})$$

The coefficient C_{NL} in this expansion is given by

$$\begin{aligned} C_{NL} = & \sqrt{S_{(90)}^2} \left(\frac{2\sqrt{x_\alpha}}{1+x_\alpha} \right)^{9/2} \left(\frac{2\sqrt{x_0}}{1+x_0} \right)^{69/2} \cdot \sqrt{\frac{(10+L)!!(N-L)!!}{(9-L)!!(N+L+1)!!}} \\ & \times \sum_{j=0}^{(9-N)/2} a_j \left\{ \frac{32(x_0-x_\alpha)}{5(1+x_0)(1+x_\alpha)} \right\}^j \left\{ \frac{2(5+4x_0+x_\alpha)}{5(1+x_0)(1+x_\alpha)} - 1 \right\}^{(9-N)/2-j} \\ & \times \binom{9-2j-L}{2} \cdot \frac{(9-2j)!!(9-L)!!}{9!(9-2j-L)!!}, \\ & x_\alpha = \nu_\alpha/\nu, \quad x_0 = \nu_0/\nu. \end{aligned} \quad (\text{A1.13})$$

Here the definitions of a_j 's are the same as (A1.11).

Appendix 2

—Correction factor for the normalization constant—

Here we give the formula to evaluate the correction factor for the normalization constant of a given model wave function ϕ_L due to the alteration of the tail of $y_L(r)$ of this ϕ_L . We decompose ϕ_L as is shown in the footnote on page 109,

$$\phi_L = \mathcal{A}\{e_L(r) Y_{L0}(\mathcal{Q}_r) \phi_0(\alpha) \phi_0(C)\} + \phi_L^R. \quad (\text{A2.1})$$

Then y_L is given as follows:

$$y_L(r) = \sqrt{q_{AC}} \langle h_L | \phi_L \rangle = \sqrt{q_{AC}} \langle h_L | \mathcal{A}\{e_L(r) h_L\} \rangle, \quad (\text{A2.2})$$

where

$$C = A - 4, \quad q_{AC} = \binom{A}{4} / (1 + \delta_{A-4,4}) \quad \text{and} \quad h_L = Y_{L0}(\mathcal{Q}_r) \phi_0(\alpha) \phi_0(C).$$

From this we see that the modification of y_L (to \hat{y}_L) means that of e_L (to \hat{e}_L) and consequently that of ϕ_L (to $\hat{\phi}_L$) with the following mutual relations,

$$\begin{aligned}\hat{y}_L(r) &= \sqrt{q_{AC}} \langle h_L | \mathcal{A} \{ \hat{e}_L(r) h_L \} \rangle, \\ \hat{\phi}_L &= \mathcal{A} \{ \hat{e}_L(r) h_L \} + \phi_L^R.\end{aligned}\quad (\text{A2}\cdot 3)$$

Here $\hat{\phi}_L$ is no more normalized to unity. We normalize this $\hat{\phi}_L$ by multiplying the correction factor f_L as follows,

$$\hat{\phi}_L^N = f_L \hat{\phi}_L. \quad (\text{A2}\cdot 4)$$

(Accordingly the reduced width is written as $\theta_L^2(a) = (a^3/3) f_L^2 \hat{y}_L^2(a)$.) The factor f_L is evaluated by the following normalization condition:

$$\begin{aligned}1 &= \int_V d\tau (\hat{\phi}_L^N)^2 \\ &= f_L^2 \left\{ \sqrt{q_{AC}} \int_0^a dr \cdot r^2 \hat{e}_L(r) \hat{y}_L(r) + \int_V d\tau (\phi_L^R)^2 \right\},\end{aligned}\quad (\text{A2}\cdot 5)$$

where V denotes the interior region specified by the channel radius a . The term of $\int_V d\tau (\phi_L^R)^2$ is obtained from the normalization condition for the original model function of ϕ_L as

$$1 = \sqrt{q_{AC}} \int_0^a dr \cdot r^2 e_L(r) y_L(r) + \int_V d\tau (\phi_L^R)^2. \quad (\text{A2}\cdot 6)$$

Then we obtain the formula for f_L from Eqs. (A2·5) and (A2·6);

$$f_L = \left\{ 1 + \sqrt{q_{AC}} \int_0^a dr \cdot r^2 (\hat{e}_L(r) \hat{y}_L(r) - e_L(r) y_L(r)) \right\}^{-1/2}. \quad (\text{A2}\cdot 7)$$

If we use the relations that $\hat{y}_L \approx y_L$, $\hat{e}_L \approx e_L$ in the inner region and $\hat{y}_L \approx \sqrt{q_{AB}} \hat{e}_L$, $y_L \approx \sqrt{q_{AC}} e_L$ in the surface region, the correction factor of f_L is approximately given as

$$f_L \approx \left\{ 1 + \int_0^a dr \cdot r^2 (\hat{y}_L^2(r) - y_L^2(r)) \right\}^{-1/2}. \quad (\text{A2}\cdot 8)$$

In the above argument we regarded that the model wave function ϕ_L , is normalized to unity in the internal region specified by the channel radius a . If the model wave function is normalized in a whole space (as we usually do so), it is further needed to multiply the correction factor of g_L to $y_L(r)$ as is explained in the following: In these cases the normalization equation of the original model wave function is written as

$$1 = \sqrt{q_{AC}} \int_0^\infty dr \cdot r^2 e_L(r) y_L(r) + \int_{\text{whole space}} d\tau (\phi_L^R)^2. \quad (\text{A2}\cdot 9)$$

The factor g_L is defined by the required normalization condition of

$$1 = g_L^2 \left\{ \sqrt{q_{AC}} \int_0^a dr \cdot r^2 e_L(r) y_L(r) + \int_V d\tau (\phi_L^R)^2 \right\}. \quad (\text{A2}\cdot 10)$$

When we note the relations $\int_V d\tau (\Phi_L^R)^2 \approx \int_{\text{whole space}} d\tau (\Phi_L^R)^2$ and $\sqrt{q_{AC}} e_L(r) = y_L(r)$ in the outside region ($r \gtrsim a$), we can get the expression for g_L from (A2·9) and (A2·10) as below,

$$\begin{aligned} g_L &= \left\{ 1 - \sqrt{q_{AC}} \int_a^\infty dr \cdot r^2 e_L(r) y_L(r) \right\}^{-1/2} \\ &= \left\{ 1 - \int_a^\infty dr \cdot r^2 y_L^2(r) \right\}^{-1/2}. \end{aligned} \quad (\text{A2} \cdot 11)$$

References

- 1) H. Horiuchi and K. Ikeda, Prog. Theor. Phys. **40** (1968), 277.
- 2) K. Ikeda, N. Takigawa and H. Horiuchi, Prog. Theor. Phys. Suppl. Extra Number (1968), 464.
- 3) R. H. Davis, *Proceedings of the Third Conference on Reactions between Complex Nuclei, Asilomar, 1963* (University of California Press, Berkeley), p. 67.
- 4) W. E. Hunt, M. K. Mehta and R. H. Davis, Phys. Rev. **160** (1967), 782.
- 5) A. E. Litherland, J. A. Kuehner, H. E. Gove, M. A. Clark and E. Almqvist, Phys. Letters **7** (1961), 98.
J. A. Kuehner and E. Almqvist, Can. J. Phys. **45** (1967), 1605.
- 6) A. Arima, H. Horiuchi and T. Sebe, Phys. Letters **24B** (1967), 129.
- 7) H. Morinaga, Phys. Rev. **101** (1956), 254.
- 8) H. Morinaga, Phys. Letters **21** (1966), 78.
- 9) P. Chevallier, F. Scheibling, G. Goldring, I. Plesser and M. W. Sachs, Phys. Rev. **160** (1967), 827.
- 10) Y. Suzuki, H. Horiuchi and K. Ikeda, Prog. Theor. Phys. **47** (1972), 1517.
- 11) T. A. Tombrello and G. C. Phillips, Phys. Rev. **122** (1961), 244.
- 12) A. I. Baz, Adv. in Physics **8** (1959), no. 32, 349.
- 13) B. F. Bayman and A. Bohr, Nucl. Phys. **9** (1958/59), 596.
- 14) H. Horiuchi and Y. Suzuki, Prog. Theor. Phys. **49** (1973), 1974.
- 15) For example, N. K. Glendenning, Phys. Rev. **137** (1965), B102.
- 16) M. Kawai and K. Yazaki, Prog. Theor. Phys. **38** (1967), 850.
M. Igarashi, M. Kawai and K. Yazaki, Prog. Theor. Phys. **42** (1969), 245.
- 17) A. N. Boyarkina, Izv. Akad. Nauk SSSR (ser. fiz.) **28** (1964), 337.
F. C. Barker, Nucl. Phys. **83** (1966), 418.
- 18) J. P. Elliott, in *Selected Topics in Nuclear Theory*, ed. F. Janouch (IAEA, Vienna, 1963).
- 19) T. Lauritsen and F. Ajzenberg-Selove, Nucl. Phys. **78** (1966), 1.
- 20) D. M. Brink, Proc. Int. Sch. Phys. Enrico Fermi Course **36** (1966), p. 247.
- 21) J. L. Russell, Jr., G. C. Phillips and C. W. Reich, Phys. Rev. **104** (1956), 135.
- 22) F. Ajzenberg-Selove, Nucl. Phys. **A166** (1971), 1.
- 23) A. B. Volkov, Nucl. Phys. **74** (1965), 33.
- 24) D. M. Brink and E. Boeker, Nucl. Phys. **A91** (1967), 1.
- 25) E. Boeker, Nucl. Phys. **A91** (1967), 27.
- 26) Y. Abgrall, G. Baron, E. Caurier and G. Monsonego, Nucl. Phys. **A131** (1969), 609.
- 27) For example, G. Herzberg, *Molecular Spectra and Molecular Structure III* (D. Van Nostrand Company Inc., 1945).
- 28) A. Bohr and B. R. Mottelson, Nuclear News 1962.
- 29) S. Gorodetzky, P. Mennrath, P. Chevallier, F. Scheibling and G. Sutter, Phys. Letters **1** (1962), 14.
E. B. Carter, G. E. Mitchell and R. H. Davis, Phys. Rev. **133B** (1964), 1421, 1434.
- 30) W. H. Bassichis and G. Ripka, Phys. Letters **15** (1965), 320.

- 31) G.E. Brown and A.M. Green, Nucl. Phys. **75** (1966), 401.
- 32) J. Eichler and T. Marumori, Kgl. Danske Videnskab. Selskab. Mat.-fys. Medd. **35** (1966), No. 7.
- 33) J. Hiura, Y. Abe, S. Saito and O. Endo, Prog. Theor. Phys. **42** (1969), 555.
- 34) K. Bethge, Ann. Rev. Nucl. Sci. **19** (1969), 255.
- 35) R. Middleton, *Proceedings of the International Conference on Nuclear Reaction Induced by Heavy Ions* (Heidelberg, 1969), p. 263.
A.A. Ogloblin, *ibid.*, p. 231.
- 36) D.L. Hill and J.A. Wheeler, Phys. Rev. **89** (1952), 1102.
J.J. Griffin and J.A. Wheeler, Phys. Rev. **108** (1957), 312.
- 37) V.V. Balashov and I. Rotter, Nucl. Phys. **61** (1965), 138.
- 38) C.W. Cook, W.A. Fowler, C.C. Lauritsen and T. Lauritsen, Phys. Rev. **111** (1958), 567.
D.H. Wilkinson, D.E. Alburger and A. Gallmann, Phys. Rev. **130** (1963), 1953.
- 39) See Chapters I and II, and also for example S. A. Afzal, A.A.Z. Ahmad and S. Ali, Rev. Mod. Phys. **41** (1967), 247.
- 40) S. Cohen and D. Kurath, Nucl. Phys. **73** (1965), 1.
- 41) M. Harvey, *Advances in Nuclear Physics*, M. Baranger and E. Vogt, eds. (Plenum Press, New York, 1968), Vol. 1, p. 67.
G. Ripka, *ibid.*, p. 183.
- 42) Y. Akiyama, A. Arima and T. Sebe, Nucl. Phys. **138** (1970), 273.
- 43) E. C. Halbert, J. B. McGrory, B. H. Wildenthal and S. P. Pandya, *Advances in Nuclear Physics*, M. Baranger and E. Vogt, eds. (Plenum Press, New York, 1971) Vol. 4, p. 316.
- 44) R. Middleton, J.D. Garrett and H.T. Fortune, Phys. Rev. Lett. **27** (1971), 950.
K. Nagatani, M.J. Le Vine, T.A. Belote and A. Arima, *ibid.*, 1071.
- 45) B. Imanishi, Phys. Letters **27B** (1968), 267.
B. Imanishi, Nucl. Phys. **A125** (1969), 33.
- 46) D.A. Bromley, *Proc. Int. Sch. Phys. Enrico Fermi Course 40*, edited by M. Jean (Academic Press, 1969).
- 47) A. Tohsaki, F. Tanabe and R. Tamagaki, Prog. Theor. Phys. **45** (1971), 980.
- 48) E.W. Vogt, *Proceedings of the International Conference on Properties of Nuclear States* (Montreal, 1969), p. 5.
- 49) R.E. Malmin, R.H. Siemssen, D.A. Sink and P.P. Singh, Phys. Rev. Lett. **28** (1972), 1590.
R. Stokstad, D. Shapira, L. Chua, P. Parker, M.W. Sachs, R. Wieland and D.A. Bromley, *ibid.*, 1523.
- 50) See Chapter II and also
R. Tamagaki and H. Tanaka, Prog. Theor. Phys. **34** (1965), 191.
S. Okai and S.C. Park, Phys. Rev. **145** (1966), 787.
- 51) H. Horiuchi, Prog. Theor. Phys. **47** (1972), 1058.